JPRS L/9444

15 December 1980

USSR Report

ELECTRONICS AND ELECTRICAL ENGINEERING

(FOUO 16/80)

FBIS FOREIGN BROADCAST INFORMATION SERVICE

NOTE

JPRS publications contain information primarily from foreign
newspapers, periodicals and books, but also from news agency
transmissions and broadcasts. Materials from foreign-language
sources are translated; those from English-language sources
are transcribed or reprinted, with the original phrasing and
other characteristics retained.

Headlines, editorial reports, and material enclosed in brackets
[] are supplied by JPRS. Processing indicators such as [Text]
or [Excerpt] in the first line of each item, or following the
last line of a brief, indicate how the original information was
processed. Where no processing indicator is given, the infor-
mation was summarized or extracted.

Unfamiliar names rendered phonetically or transliterated are
enclosed in parentheses. Words or names preceded by a ques-
tion mark and enclosed in parentheses were not clear in the
original but have been supplied as appropriate in context.
Other unattributed parenthetical notes within the body of an
item originate with the source. Times within items are as
given by source.

The contents of this publication in no way represent the poli-
cies, views or attitudes of the U.S. Government.

FOR OFFICIAL USE ONLY

USSR REPORT

ELECTRONICS AND ELECTRICAL ENGINEERING

(FOUO 16/80)

CONTENTS

- a -   [III - USSR - 21E S&T FOUO]

FOR OFFICIAL USE ONLY

ANTENNAS

REDUCTION OF NONLINEAR DISTORTIONS IN RECEPTION OF FM SIGNALS BY USING A
TWO-RING TRACKING FILTER CIRCUIT

[Article by G. L. de-Ribas]

[Text] An analysis is made of the operation of a two-
ring tracking filter that is a kind of threshold-
reducing circuit for FM reception. A system of non-
linear differential equations is derived that describes
the operation of the circuit. It is shown on the basis
of solution of this system that the proposed circuit
reduces nonlinear distortions of the received signal
as compared with conventional tracking filters.

One way to improve interference immunity in reception of FM signals is
to include a tracking filter in the i-f channel of the receiver [Ref. 1].
The tracking filter is usually an isolated tank circuit K (Fig. 1) with
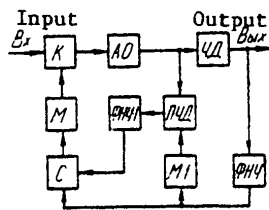
Fig. 1

a central frequency that is tuned by a feedback
circuit consisting of amplitude limiter AO,
frequency detector ЧД, low-frequency filter
ФНЧ, modulator M and adder C. The passband of
the tracking filter tank is narrower than the
spectrum of the received FM signal, which im-
proves the threshold characteristics of the
receiver. However, because of the mismatch
between the instantaneous signal frequency and
the central frequency of tank K that is inherent
in tracking filters, there may be considerable
nonlinear distortions of the received signal.

Such distortions can be reduced by supplementing the tracking filter with
another feedback ring [Ref. 2] that includes a tunable frequency detector
ПЧД with central frequency tuned by modulator Ml and [low-frequency fil-
ter] ФНЧl. The main conditions of effective operation of the two-ring
tracking filter are identical laws for tuning of the central frequencies

1

FOR OFFICIAL USE ONLY

of the tunable frequency detector and tank circuit, and also fast action of the supplementary feedback ring. The first condition is met with the relatively small tuning band relative to the central frequency of the tank which is the case for the proposed circuit. The second condition is satisfied by the wide band of the resonant system of the tunable frequency detector and extra low-frequency filter [ФНЧ]. In virtue of the identity of laws of tuning of the middle frequency of the tunable frequency detector and the central frequency of the tank circuit, the voltage across the output of the tunable frequency detector is proportional to the mismatch between the instantaneous signal frequency and the central frequency of the tank circuit. In the adder, this voltage is combined with the main control voltage, reducing the mismatch, and hence reducing the nonlinear distortions of the received signal.

To analyze the two-ring tracking filter by the method of reduced coordinates [Ref. 1], the tunable tank circuit of the tracking filter must be replaced by a conditional equivalent circuit comprising two mixers, between which is a fixed tank circuit with passband and tuning frequency respectively equal to the passband and central frequency of the tunable tank circuit. In the first mixer, the phase of the tank control voltage Θ_y is subtracted from the phase of the output signal, and in the second mixer the control voltage phase Θ_y is added to the phase of the signal passing through the tank. When FM signal $U(t) = U_m \cos(\omega_0 t + \Theta(t))$ acts on a fixed tank circuit with passband $2\alpha_H$ and tuning frequency ω_0, the following system of nonlinear differential equations [Ref. 3] is valid for phase $\phi_H(t)$ and amplitude $V(t)$ of the voltage at the output of the tank circuit:

$$\left. \begin{aligned} \varphi_\kappa' &= \frac{U_m \alpha_\kappa}{V} \sin(\Theta - \Theta_y - \varphi_\kappa) \\ V' + \alpha_\kappa V &= \alpha_\kappa U_m \cos(\Theta - \Theta_y - \varphi_\kappa) \end{aligned} \right\} . \tag{1}$$

The phase of the signal at the output of the tunable tank circuit is

$$\varphi_\phi = \varphi_\kappa + \Theta_y. \tag{2}$$

If it is assumed that the amplitude limiter does not introduce phase-frequency distortions, then the phase of the signal on the inputs of the frequency detectors ЧД and ПЧД is also described by expression (2). Then we can write the following relations for the elements of the feedback rings that describe their operation:

the voltage at the output of low-frequency filter ФНЧ with complex propagation ratio K(p) equal to $U_\phi(t) = S_{ЧД}\phi_\phi'(t)K(p)$, where $S_{ЧД}$ is the discrimination of frequency detector ЧД;

the tuning frequency of detector ПЧД varies in accordance with the law $f_{ПЧД}(t) = S_{ПЧ}S_M\phi_\phi'(t)K(p)$, where S_M is the discrimination of modulator M1;

2

the voltage at the output of the tunable frequency detector is proportional to the difference between the instantaneous frequency of the signal and the instantaneous tuning frequency of the tunable frequency detector: $U_{\text{ПЧД}}(t) = S_{\text{ПЧД}}(\phi_\phi^I(t) - S_M S_{\text{ЧД}}\phi_\phi^I(t)K(p))$, where $S_{\text{ПЧД}}$ is the discrimination of the tunable frequency detector;

the voltage at the output of filter ФНЧ1 with complex propagation ratio $K_1(p)$: $U_{\phi 1}(t) = S_{\text{ПЧД}}K_1(p)(\phi_\phi^I(t) - S_M S_{\text{ЧД}}\phi_\phi^I(t)K(p))$.

Since the control voltage consists of the sum of the voltages on the outputs of filters ФНЧ and ФНЧ1, the tuning frequency of the two-ring tracking filters varies in accordance with the law

$$f(t) = S_M[S_{\text{ЧД}}\phi_\phi^I(t)K(p) + S_{\text{ПЧД}}\phi_\phi^I(t)(1 - S_M S_{\text{ЧД}}K(p))K_1(p)],$$

where S_M is the discrimination of modulator M, which is equal to the discrimination of modulator M1 under condition of identity of the laws of tuning of the central frequency of tank circuit K and the middle frequency of detector ПЧД.

Accordingly, the control phase is

$$\Theta_y = \int_0^t f(\tau)\,d\tau = S_{\text{м}}\varphi_\phi(t)\,[S_{\text{чд}}K(p) + S_{\text{пчд}}K_1(p)(1 - S_{\text{м}}S_{\text{чд}}K(p))]. \tag{3}$$

When the $\phi_{\text{н}}$ found from (2) is substituted in (1) with consideration of (3), system of equations (1) takes the form

$$\left.\begin{aligned}
&\varphi'_\phi - S_{\text{м}}\varphi'_\phi\,[S_{\text{чд}}K(p) + S_{\text{пчд}}K_1(p)(1 - S_{\text{м}}S_{\text{чд}}K(p)) = \\
&= (U_m\alpha_\kappa/V)\sin(\Theta - \varphi_\phi) \\
&V' + \alpha_\kappa V = \alpha_\kappa U_m\cos(\Theta - \varphi_\phi)
\end{aligned}\right\}. \tag{4}$$

Introducing the notation for the phase difference of signals at the input and output of the two-ring tracking filter

$$\Theta - \varphi_\phi = \varphi \tag{5}$$

and substituting (5) in (4), we get

$$\left.\begin{aligned}
&\varphi' + \frac{U_m\alpha_\kappa\sin\varphi}{V\{1 - S_{\text{м}}[S_{\text{чд}}K(p) + S_{\text{пчд}}K_1(p)(1 - S_{\text{м}}S_{\text{пчд}}K(p))]\}} = \Theta' \\
&V' + \alpha_\kappa V = \alpha_\kappa U_m\cos\varphi
\end{aligned}\right\}. \tag{6}$$

Thus the operation of the two-ring tracking filter circuit is described by a system of nonlinear differential equations analogous to the system that describes the operation of the tracking filter in Ref. 3. A comparative analysis of these circuits can be made with respect to the form

3

of their equivalent frequency responses. The equivalent frequency re-
sponse is the ratio with which the circuit propagates the frequency
deviations of the input signal $K_\text{ч}(p)$, and is defined as the ratio of the
amplitudes of frequency deviation of the voltage at the tank output $\phi_\text{ф}$
and the frequency deviation of the FM signal at its input Θ [Ref. 1].
The equivalent frequency response of the two-ring tracking filter is
found from solution of equations (6) in the linear steady state, i. e.
under the conditions that $\sin\phi = \phi$, $\cos\phi 1$ [sic], $V' = 0$. In this case,
the solution of (6) takes the form

$$\varphi = \frac{\Theta}{1 + \{(\alpha_\text{к}/p)/[1 - KK(p) - K_1 K_1(p) + KK_1 K(p) K_1(p)]\}},\qquad(7)$$

where $S_\text{M} S_\text{чд} = K$ and $S_\text{M} S_\text{пчд} = K_1$.

Coefficient $K_\text{ч}(p)$ is found by transformation of expressions (5) and (7):

$$K_\text{ч}(p) = \frac{\varphi_\text{ф}}{\Theta} = \frac{1}{1 + \{p/\alpha_\text{к}[1 - K_y(p)]\}},\qquad(8)$$

where $K_y(p)$ is the propagation ratio of the controlling circuit:

$$K_y(p) = KK(p) + K_1 K_1(p) - KK_1 K(p) K_1(p).\qquad(9)$$

Expression (8) is analyzed under condition that filters ФНЧ and ФНЧ1 are
integrating links with respective propagation ratios

$$K(p) = \alpha/(\alpha + p);\qquad(10)\qquad K_1(p) = \alpha_1/(\alpha_1 + p);\qquad(11)$$

After substituting (10) and (11) in (8) and making simple but cumbersome
transformations, we arrive at the following expressions for the modulus
and phase of the propagation ratio respectively:

$$|K_\text{ч}| = \sqrt{\overline{A^2 + B^2}}/(C^2 + D^2),\qquad(12)\qquad \psi = -\arctan B/A,\qquad(13)$$

$$\text{where } A = \alpha_\text{к}[\alpha^2\alpha_1^2\alpha_\text{к} + \omega^2\alpha^2(\alpha_\text{к} - \alpha_1 K_1 + \alpha_1 KK_1) +$$

$$+ \omega^2\alpha_1^2(\alpha_\text{к} - \alpha K + \alpha KK_1) + \omega^4(\alpha_\text{к} - \alpha K - \alpha_1 K_1)];$$

$$B = \omega\alpha_\text{к}\{\alpha^2\alpha_1(1 - K - K_1 + KK_1) -$$

$$- \omega^2[\alpha\alpha_1 KK_1 - \omega^2 - \alpha^2(1 - K) - \alpha_1^2(1 - K_1)]\};$$

$$C = \alpha\alpha_\text{к} - \omega^2;\qquad D = \omega(\alpha_\text{к} + \alpha - K\alpha).$$

based on the known relation for the equivalent frequency response of a
tracking filter

$$K_\text{чсф}(p) = \frac{1}{1 + \{p/\alpha_\text{к}[1 - K_y(p)]\}},\qquad(14)$$

$$\text{where } K_y(p) = KK(p),\qquad(15)$$

4

and substituting (10) in (14), after appropriate transformations, we can get expressions analogous to (12) and (13) for the modulus and phase of the propagation ratio of frequency deviations of the tracking filter, where

$$A = \alpha_\kappa (\alpha^2 \alpha_\kappa + \omega^2 \alpha_\kappa - \omega^2 \alpha K); \qquad B = \omega \alpha_\kappa (\omega^2 + \alpha^2 - \alpha^2 K);$$

$$C = \alpha \alpha_\kappa - \omega^2; \qquad D = \omega (\alpha_\kappa + \alpha - K\alpha); \qquad (16)$$

Shown in Fig. 2 are the moduli and phases of the propagation ratios of frequency deviations of the two-ring tracking filter and the conventional tracking filter as calculated from formulas (12), (13) and (16) for different circuit parameters.
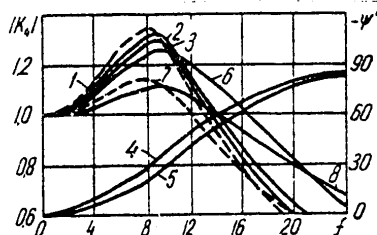
Fig. 2

Curve 1 is the modulus of K_u of the tracking filter computed at $K = 0.9$, $\alpha = \alpha_H = 10$ kHz. Curves 2 and 3 are the same for the two-ring tracking filter at $\alpha_1 = 50$ kHz and $\alpha_2 = 5$ MHz respectively. The addition of the supplementary feedback ring, as can be seen from Fig. 2, ensures more exact reproduction of the frequency deviation (less than the spread of the modulus of K_u), and introduces smaller phase shifts (curve 5 for the two-ring circuit as compared with curve 4 for the conventional tracking filter). However, in this case there is an expansion of the band of the equivalent frequency response of the two-ring tracking filter, i. e. the interference immunity of the circuit is impaired.

Variation of α_1 over a wide range (50 kHz–5 MHz) has little influence on the band of the equivalent frequency response at the same K_1, whereas an increase in K_1 leads to appreciable expansion of the equivalent frequency response (curve 6, where $K_1 = 0.3$, $\alpha_1 = 5$ MHz). A reduction in K at constant K_1 leads to impairment of the effectiveness of the additional ring. For example curve 7, plotted for the conventional tracking filter at $K = 0.7$, practically coincides with the curve for the two-ring filter calculated at $K_1 = 0.1$. Greater effectiveness of the two-ring tracking filter can be realized by increasing K_1, but in doing this, as can be seen from curve 8 plotted for $K_1 = 0.3$, the band of the equivalent frequency response is considerably expanded. The influence of the additional feedback ring on operation of the two-ring filter circuit shows up in improvement of the control coefficient $K_y(p)$, i. e. in an approach of $K_y(p)$ to unity.

5

After making simplifying assumptions about the frequency independence of
the feedback rings, i. e. setting $K(p) = 1$ and $K_1(p) = 1$, and from the
condition of circuit stability assuming $K < 1$ and $K_1 < 1$, we can draw the
following simple conclusions by studying the expression for the control
coefficient $K_y = K + K_1 - KK_1$ at the maximum:

The maxima of K_y at different K are reached when the condition $K + K_1 = 1$
is met; the absolute maximum of K_y is reached as K approaches unity, and
as K_1 correspondingly approaches zero. Hence it is clear that one cannot
realize equally good characteristics of the circuit by reducing the propa-
gation ratio in the main ring and increasing it in the supplementary ring.
It makes sense to introduce a supplementary ring only in a sufficiently
effective tracking filter circuit ($K = 0.9$ or more), where even a low
$K_1 = 0.05-0.1$ can produce a gain with respect to nonlinear distortions.
One can determine this gain by comparing the two-ring tracking filter
with the conventional tracking filter that is equivalent in interference
immunity, i. e. a tracking filter in which the band of the equivalent
frequency response is equal to that of the two-ring tracking filter.
In the equivalent tracking filter the initial equivalent band of the
tank circuit $2\alpha_{H\ \ni HB}$ is not equal to the actual band $2\alpha_H$, but is wider,
and is found from (16) by substituting the band of the equivalent fre-
quency response with respect to a level of 0.7 taken from the curves of
Fig. 2 for the two-ring tracking filter. The use of such a computa-
tional model is convenient for illustrating the physical processes in the
circuit since nonlinear distortions are determined mainly by the width
of the passband of the tank circuit.

To define the nonlinear distortions, we use a method [Ref. 4] according
to which the following expression is derived for the phase difference of
signals at the input and output of the conventional and two-ring tracking
filters:

$$\varphi = \frac{\Delta\omega \sin \omega t}{p + L(p)} - \frac{1}{6}\frac{L(p)}{p + L(p)}\left[\frac{p + \frac{1}{2}\alpha_{\kappa}}{p + \alpha_{\kappa}}\right]\frac{\Delta\omega^3 \sin^3 \omega t}{[p + L(p)]^3}, \tag{17}$$

where $L(p) = \alpha_H/[1 - K_y(p)]$, and $\Delta\omega$ is the maximum frequency deviation.

To calculate the nonlinear distortions with respect to the third harmonic
the amplitudes of the third and first harmonics are respectively factored
out of (17) and divided; the calculation for conventional tracking fil-
ters was based on on $\alpha_{H\ \ni HB}$, while the nonlinear distortions for two-
ring tracking filters were calculated from α_H. The K_y for conventional
filters was found from (15), and for two-ring filters was found from (9).

Fig. 3 shows the results of calculation of nonlinear distortions. Curve
1 is the percent ratio of linear distortions in the conventional filter
to those in the two-ring filter on different frequencies, and shows the

6
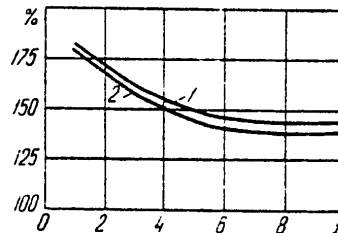
Fig. 3

improvement in nonlinear distortions with introduction of an additional feedback ring by 150-180% on frequencies below 5 kHz and about 150% on high frequencies. The effectiveness of a properly designed two-ring tracking filter (K fairly high, and $K + K_1 = 1$) with various other parameters of the circuit is approximately the same as in the given computational example.

Measurements of nonlinear distortions of an FM signal (carrier frequency 6 MHz, upper modulating frequency 10 kHz, maximum frequency deviation 20, 50, 200 kHz) done on a pilot model of a two-ring tracking filter with the same circuit parameters as used in the calculations without and with activation of the supplementary feedback ring showed good agreement with the calculated data (curve 2).

REFERENCES

1. A. S. Vinitskiy, "Modulirovannyye fil'try i sledyashchiy priyem ChM" [Modulated Filters and Tracking FM Reception], Moscow, Sovetskoye radio, 1969.

2. B. S. Troitskiy, G. L. De-Ribas, "A Receiver of Frequency-Modulated Signals" Soviet Patent No 493925, Patent Bulletin No 44, 1975.

3. V. A. Dorofeyev, "Analysis of Filterless Systems for Tracking FM Reception," Trudy NIIR [Proceedings of the Scientific Research Institute of Radio], Moscow, No 4, 1968, pp 18-21.

4. V. M. Dorofeyev, "Nonlinear Distortions in Tracking FM Demodulators," Trudy NIIR, Moscow, No 3, 1973, pp 5-12.

6610
CSO: 1860

7

I

COMMENT ON THE ARTICLE 'ACCURACY OF MEASURING THE FREQUENCY AND ANGLE OF ARRIVAL OF SIGNALS RECEIVED BY AN ANTENNA ARRAY AGAINST A BACKGROUND OF INTERFERENCE WITH ACOUSTIC-OPTOELECTRONIC PROCESSING'

[Letter to the editors by G. S. Nakhmanson]

[Text] In Ref. 1 in an analysis of the correlation function of distribution of intensities of the light field in the output plane of an acoustico-optical processor when a linear antenna array receives a narrow-band normal random process against a background of white noise (expression (12)), a number of terms were left out, which in some cases leads to inexact results.

With consideration of corrections, the expression for the correlation function of distribution of the light field in the output plane of the acoustico-optical processor (formula (12) [Ref. 1]) takes the form

$$\langle I_n(u_1, \vartheta_1, t_1) I_n(u_2, \vartheta_2, t_2)\rangle - \langle I_n(u_1, \vartheta_1, t_1)\rangle \langle I_n(u_2, \vartheta_2, t_2)\rangle =$$

$$= A_{np}^2 \operatorname{sinc}^2 \frac{\vartheta_1 H}{2} \operatorname{sinc}^2 \frac{\vartheta_2 H}{2} \left\{ \frac{1}{4} \left[(\mu_2^+)^2 (X_2^-)^2 + (\mu_2^-)^2 (X_2^+)^2 \right] \left[(\mu_1^+)^2 (X_1^-)^2 + \right. \right.$$

$$+ (\mu_1^-)^2 (X_1^+)^2] + (\mu_1^-)(\mu_1^+)(\mu_2^-)(\mu_2^+)(X_1^+)(X_1^-)(X_2^+)(X_2^-) \cos 2\omega_0 T_{st} \gamma +$$

$$+ \frac{1}{2Q} \left[(\mu_1^-)(X_1^+)(\mu_2^+)(X_2^-) + (\mu_1^+)(X_1^-)(\mu_2^-)(X_1^+) \right] (Z^+) \operatorname{sinc} \frac{\alpha}{2} +$$

$$+ \frac{1}{2Q} \left[(\mu_1^-)(X_1^+)(\mu_2^-)(X_2^+) + (\mu_1^+)(X_1^-)(\mu_2^+)(X_2^-) \right] (Z^-) \operatorname{sinc} \frac{\beta}{2} +$$

$$+ \frac{1}{4Q^2} \left[(Z^+)^2 \operatorname{sinc}^2 \frac{\alpha}{2} + (Z^-)^2 \operatorname{sinc}^2 \frac{\beta}{2} \right] \right\}. \tag{1}$$

where all notation in (1) coincides with Ref. 1.

Use of the corrected expression (1) in analyzing the statistical characteristics of estimates of the frequency and angle of arrival of the received normal random process in Ref. 1 leads to the following results: the probability that the threshold will be exceeded at the output of the

8

channel of the optoelectronic system (i. e. the threshold corresponding to the parameters of the random process to be analyzed) decreases monotonically from 0.94 to 0.58 as the normalized threshold γ changes from 0.2 to 0.9.

Graphs for the relative shift in the frequency estimate $<f - f_0>/f_0$ as a function of γ are slightly higher than curves according to the results given in Ref. 1.

It should be noted that the corrections that have been introduced do not influence the variances of the estimates of frequencies and angles of arrival of narrow-band normal random processes.

<div align="center">REFERENCE</div>

1. G. S. Nakhmanson, "Accuracy of Measuring the Frequency and Angle of Arrival of Signals Received by an Antenna Array Against a Background of Interference with Acoustic-Optoelectronic Processing," IZVESTIYA VUZov: RADIOELEKTRONIKA, Vol 23, No 1, 1980 p 3.

6610
CSO: 1860

COMMUNICATIONS, COMMUNICATION EQUIPMENT,
RECEIVERS AND TRANSMITTERS, NETWORKS, RADIO
PHYSICS, DATA TRANSMISSION AND PROCESSING,
INFORMATION THEORY

A STUDY OF THE STABILITY OF AN ALGORITHM FOR THE FILTERING OF A
PSEUDORANDOM SIGNAL SUBJECT TO THE ACTION OF SIMILAR CAPTURING
INTERFERENCE

[Article by V.P. Ponomarenko]

[Text] The stability of a two circuit synchronization
system which realizes an optimum filtering algorithm
for a pseudorandom radio signal subject to the action
of a similar capturing interference is studied. The
dynamic characteristics which make it possible to esti-
mate algorithm stability with a change in the system
and interference parameters are determined.

1. Introduction. Formulation of the Problem

The solution of the problem of synthesizing an optimum filtering algo-
rithm for wideband pseudorandom phase keyed signals (ShPS) for a broad
class of cases where the processes of change in the information para-
meters of the signal are that the phases $\Theta(t)$ and delays $T(t)$ are modul-
ated [1, 2] by Wiener and gaussian exponentially correlated random
processes respectively, leads to the following equations [1, 2] for
estimates $\Theta*$ and $T*$ of the parameters Θ and T:

$$\Theta^{\cdot} = \frac{k_1}{p}[R(T-T^{\cdot})\sin(\Theta-\Theta^{\cdot})+n_1(t)],$$

(1)

$$T^{\cdot}-\tau_0 = \frac{k_2}{1+T_i p}[D(T-T^{\cdot})\cos(\Theta-\Theta^{\cdot})+n_2(t)].$$

10

Here, $p \equiv d/dt$; $R(T - T^*)$ is the autocorrelation function of the signal; $D(T - T^*)$ is a nonlinear characteristic defined by an algorithm for generating the error $\varepsilon = T - T^*$; τ_0 is the known constant value of the delay T; T_1 is a time constant; k_1 and k_2 are parameters; $n_1(t)$ and $n_2(t)$ are the noise components of the signal.

The technical realization of algorithm (1) is realized [1] in a two-circuit tracking system with crossed feedback loops, consisting of a filter-free automatic phase tuning system (FAP) [PLL – phase locked loop] and an inertial static delay tracking system (SSZ) with a first order integrating filter. Complicating the models of the information parameters θ and T, as is well known [1, 2] influences only the type of filters in the PLL and static delay tracking subsystems, without changing the fundamental structure of the optimum filtering system.

A study of the quality of algorithm (1) without taking into account the action of interference ($n_1(t) = n_2(t) = 0$) for the purpose of estimating the stability in a large two-circuit filtering system which realizes this algorithm was made in paper [3]. One of the important problems which come up in studying the noise immunity of systems for tracking signal parameters is protection against intentional simulating interference [4, 5] which is intended to disort the useful information and make automatic tracking of the signal parameters impossible. A widespread type of such jamming in ShPS [wideband pseudorandom phase-keyed signal] systems is a capturing ShPS similar to the useful signal, but differing from it in amplitude, frequency offset with respect to the carrier frequency and having a time shift which changes monotonically with the course of time.

Under conditions of exposure to similar interference, along with the problem of filtering algorithm optimization, which leads to more complex correlational compensation processing algorithms, there also arises in connection wi. the problem of realizing these algorithms that problem of estimating the stability of algorithm (1) with respect to the similar interference. The property of stability is understood to here to be the capability of algorthim (1) of maintaining its own characteristics within a specfied range when the interference parameters change (intensity, frequency and time differences).

A characteristic feature of ShPS filtering algorithms is the presence of aperiodic nonlinearities $R(T - T^*)$ and $D(T - T^*)$. Under conditions of exposure to capturing interference, this leads to the fact that the stability of algorithm (1) depends on whether the system is synchronized or not at the point in time when the interference arrives. In the case of simultaneous arrival of the useful and interfering ShPS's, the interfering signal influences the process of locking the system into synchronization. In this case, the stability of algorithm (1) can be disrupted at certain values of the interference parameters because of

11

the impossibility of establishing the signal tracking mode for these
values of the parameters. In a number of situations [5], the inter-
ference can lag the signal so much that at the moment of its arrival,
the search can be completed and the useful ShPS parameter tracking mode
established in the filtering system. The impact of the interfering
ShPS can lead here to a break in the tracking, which also entails a
loss of stability for algorithm (1).

The solution of the problem of the immunity of algorithm (1) is compli-
cated by the substantial nonlinearity of equations (1) and the presence
of the noise components $n_1(t)$ and $n_2(t)$ in them. For this reason, to
ascertain the general laws governing the influence of similar inter-
ference on the stability of algorithm (1), it is expedient to limit
ourselves to the simplest case where the noise components $n_1(t) =$
$= n_2(t) = 0$ are absent. The results of a study of the stability of
algorithm (1) with exposure to similar capturing interference are
given in this paper, which were obtained by means of studying the oper-
ational modes of a model of (1), and determining the regions for the
preservation and loss of tracking as well as the capture range.

2. A Mathematical Model of the System

In accordance with the problem posed here, we shall assume that the
input signal has the form:

(2) $$y(t) = A_s f[t - T_s(t)] \cos \Theta_s(t) + A_n f[t - T_n(t)] \cos \Theta_n(t),$$

where A_s, T_s, Θ_s and A_n, T_n, Θ_n are the amplitudes, time delays and
phase angles of the useful and interfering ShPS's respectively; $f[\cdot]$
is a function which defines the law governing the phase keying and
assumes only two values: 1 and −1. We shall consider the amplitudes
A_s and A_n to be constant. We shall adopt the following linear function
as the model for the change in the delay T_n of the interference:

(3) $$T_n(t) = T_s(t) + T_0 + \alpha t,$$

where T_0 is the initial difference between the delays T_n and T_s;
α is the rate of change in the delay T_n. With the assumptions made
here, the equations for the estimates Θ_s^* and T_s^* of the parameters of
the useful ShPS are written in the form:

12

(4)

$$\Theta = \frac{k_1}{p}[R(T-T^{\cdot})\sin(\Theta_{\cdot}-\Theta_{\cdot}^{\cdot})+\mu R(T_{\cdot}-T_{\cdot}^{\cdot})\sin(\Theta_{\cdot}-\Theta_{\cdot}^{\cdot})],$$

$$T_{\cdot}^{\cdot}-\tau_{\cdot}=\frac{k_2}{1+T_{\cdot}p}[D(T_{\cdot}-T_{\cdot}^{\cdot})\cos(\Theta_{\cdot}-\Theta_{\cdot}^{\cdot})+$$

$$+\mu D(T_{\cdot}-T_{\cdot}^{\cdot})\cos(\Theta_{\cdot}-\Theta_{\cdot}^{\cdot})],$$

where $\mu = A_n A_s^{-1}$. By introducing the instantaneous phase tracking error $\phi = \Theta_s - \Theta_s^*$ and delay tracking error $x = \Delta^{-1}(T_s - T^*)$, where Δ is the width of one element of the ShPS code sequence, and taking (3) into account, we derive the following equations for algorithm (1) when subjected to similar capturing interference:

(5)

$$\frac{d\varphi}{d\tau}=\gamma-R(x)\sin\varphi-\mu R(x+x_0+\delta\tau)\sin(\varphi+\psi+q\tau),$$

$$\frac{dx}{d\tau}=b[\beta-x-\alpha D(x)\cos\varphi-\mu\alpha D(x+x_0+\delta\tau)\cos(\varphi+\psi+q\tau)],$$

where $\tau = k_1 t$; $\gamma = p\Theta_s/k_1$ and $\beta = \Delta^{-1}(T_s - \tau_0 P$ are the relative initial frequency and delay differences; $x_0 = T_0\Delta^{-1}$; $b = (k_1 T_1)^{-1}$; $\delta = \alpha k_1^{-1}$; $q = \Omega k_1^{-1}$; Ω and ψ are the frequency difference and the initial difference in the phases of the interference and the signal respectively; $\alpha = k_2\Delta^{-1}$ is the maximum relative delay selected by the SSZ [inertial static delay tracking system]. The nonlinear characteristics R(v) and D(v) for one period of the change in v are determined in the following fashion [3]:

$$R(v)=\begin{cases}1-v, & 0\leqslant v\leqslant 1,\\ 1+v, & -1\leqslant v\leqslant 0,\\ 0, & 1\leqslant |v|\leqslant M-1,\end{cases}$$

(6)

$$D(v)=\begin{cases}v, & |v|\leqslant 1,\\ 2-v, & 1\leqslant v\leqslant 2,\\ -(2+v), & -2\leqslant v\leqslant -1,\\ 0, & 2\leqslant |v|\leqslant M-2,\end{cases}$$

where M is the number of elements of the code sequence in one signal period. The case where M >> 1 is the most practical real case; then it can be assumed that R(v) = 0 for $|v| \geq 1$, D(v) = 0 for $|v| \geq 2$, i.e., one can assume the nonlinearities R(v) and D(v) are aperiodic with

13

respect to v. Then the right sides of equations (5) are aperiodic with respect to the variables x and τ. Thus, algorithm (1) with the assumptions considered here is written in the form of a nonautonomous system of nonlinear differential equations (5) in the phase space φ, x, τ.

3. Steady-State Modes

To solve the problem posed in this paper, it is necessary to first of all ascertain what steady-state modes of the filtering system are determined by the established motions of the model (5). In the absence of interference ($\mu = 0$), the dynamics of the system are described by the autonomous system of equations:

(7)

$$\frac{d\varphi}{d\tau} = \gamma - R(x)\sin\varphi,$$

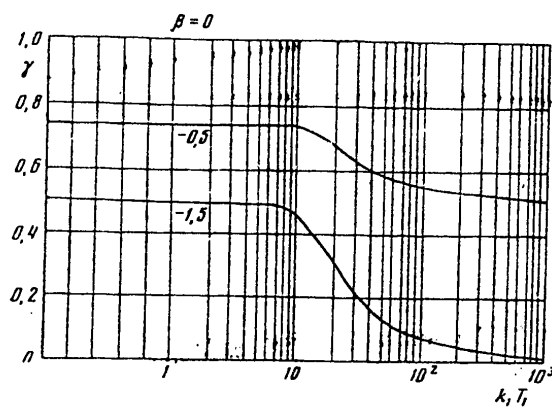$$\frac{dx}{d\tau} = b[\beta - x - \alpha D(x)\cos\varphi].$$

Figure 1.

In this case, the steady-state synchronization mode with a constant phase difference ϕ_S and difference in the delays x_S is determined by

14

the stable equilibrium state [3] of $A_1(\phi_s, x_s)$ on the cylindrical phase surface ϕ, x. For value of the parameters from the capture range of D_s: $\gamma < \gamma*(\beta, b, \alpha)$, the onset of the synchronization mode occurs for any intial values of the phase difference ϕ_{ini} and initial values of the delay difference $x_{ini} = \beta$. The curves for $\gamma = \gamma*(\beta, b, \alpha)$ are shown in Figure 1 in parameters of γ, k_1T_1 where $\alpha = 5$ for values of the initial delay difference of $\beta = 0$, -0.5 and -1.5. It can be seen that size of the capture range falls off with an increase in the absolute value of the difference β. Shown in Figure 2 are curves of $\beta = \beta*(\gamma, b, \alpha)$ where $\alpha = 5$ for a number of values of the dimensionless time constant k_1T_1 of the system, which define the region $|\beta| < \beta*(\gamma, b, \alpha)$ of permissible values of the initial difference β, for which synchronization begins at any initial values of the phase difference ϕ.
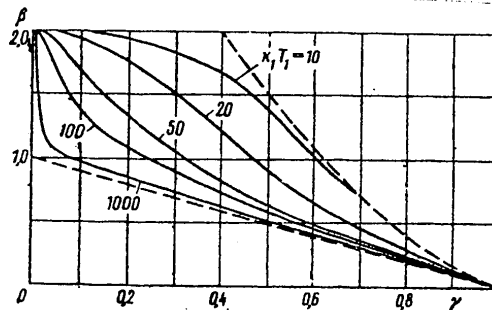
Figure 2.

For values of $\gamma < \gamma*(\beta, b, \alpha)$, the phase picture of the system when $\beta < 0$ is shown in Figure 3a; with these values of the parameters, there is stability on the whole for the equilibrium state A_1 on the phase cylinder ϕ, x. For value of $\gamma > \gamma*(\beta, b, \alpha)$ on the phase surface ϕ, x, in the case of the presence of a stable state of equilibrium A_1, there is a stable ultimate cycle of the second kind (Figure 3b); with these values of the parameters, a beat frequency mode of the second kind can also be established in the system besides the steady-state synchronization mode, where the phase difference ϕ increases without limit, while the difference in the delays x varies periodically about a certain value.

It follows from the results presented here that when $\mu = 0$, the stability range of algorithm (1) with respect to deviations from the steady-state

15

is governed by the values of the parameters γ, β, b and α which belong to the capture range D_S.
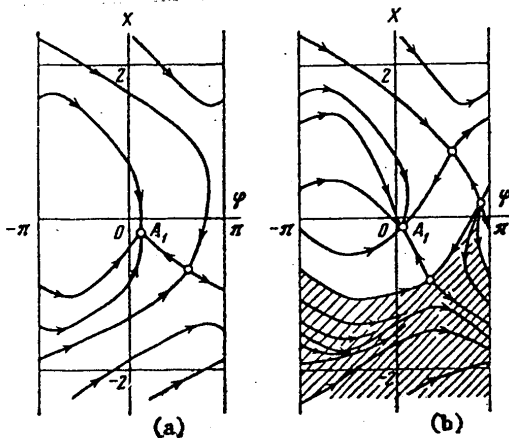
Figure 3.

When $\mu \neq 0$, by virtue of the aperiodicity of the right sides of system (5) with respect to x and τ, the steady-state modes of the filtering system are determined by the limited steady-state motions of system (5) in the phase space ϕ, x, τ, i.e., by those motions during which the mapping point where $-\infty < \tau < \infty$ does not go outside the specified region of the phase space. In accordance with (6), system (5) in the phase space region $|x + x_0 + \Delta\tau| \geq 2$ is an autonomous system (7) with a known picture for the behavior of the phase trajectories. A stable trajectory L_S, which is bounded with respect to the phase coordinates ϕ and x when $-\infty < \tau < \infty$, corresponds to the delay tracking mode for T_S of the useful ShPS (to the P_S mode). The trajectory L_S when $\delta > 0$ (or $\delta < 0$) coincides in the region $x + x_0 + \delta\tau \leq -2$ (or $x + x_0 + \delta\tau \geq 2$) of the phase space ϕ, x, τ with the ray $R_S^-:\phi = \phi_S$, $x = x_S$, and when $\tau \to \infty$, it tends to the ray $R_S^+:\phi = \phi_S$, $x = x_S$ in the region $x + x_0 + \Delta\tau \geq 2$ (or $x + x_0 + \delta\tau \leq -2$). The half-lines R_S^+ and R_{-S}^+ are stable equilibrium states (ϕ_S, x_S) of the autonomous system (7) in the regions of $|x + x_0 + \delta\tau| \geq 2$ in the phase space ϕ, x, τ. The quantities ϕ_S and x_S are found as roots of the equations:

16

(8) $\qquad \gamma - (1-x)\sin \varphi = 0, \ \beta - (1+\alpha \cos \varphi)x = 0.$

System (7) can have [3] either two or four equilibrium states, one of which is always stable, while the remaining are unstable. For the case where system (7) has two equilibrium states (a stable node and a saddle), the qualitative nature of the behavior of the trajectories of system (5) are shown in the phase space ϕ, x, τ in Figure 4 for values of the parameters of the system and interference ($\beta < 0$, $\delta < 0$), for which the trajectory L_s is asymptotically stable through the entire phase space, with the exception of the saddle trajectory Γ_s with its stable manifolds S^+.

In accordance with (6), system (5) in the phase space region $|x| \geq 2$ is equivalent to the following system:

(9)
$$\frac{d\Theta}{d\tau_1} = \gamma_1 - R(z)\sin \Theta,$$
$$\frac{dz}{d\tau_1} = b_1[\beta_1 + \delta_1\tau_1 - z - kD(z)\cos \Theta],$$

where $\Theta = \phi + \psi + q\tau$ and $z = x + x_0 + \delta\tau$ are respectively the phase difference and the difference in the delays of the interference and reference signal; $\gamma_1 = (\gamma + q)\mu^{-1}$; $\beta_1 = \beta + x_0 + \delta b^{-1}$; $b_1 = b\mu^{-1}$; $\delta_1 = \delta\mu^{-1}$; $k = \mu\alpha$; $\tau_1 = \mu\tau$. The trajectories of system (9), when the time τ_1 increases, enter inside the phase space regions $\beta_1^- + \delta_1\tau_1 \leq$ $\leq z \leq \beta_1^+ + \delta_1\tau_1$, where $\beta_1^- = \beta_1 - \delta_1 b^{-1} - k$ and $\beta_1^+ = \beta_1 - \delta_1 b^{-1} + k$. It follows from this that all of the solutions of system (9) are not bounded. By virtue of the absence of bounded solutions for system (9), system (5) does not have any steady-state motions which are bounded with respect to the variables v and Θ when $-\infty < \tau < \infty$. This means that a steady-state interference tracking mode is impossible in the system considered here.

From what has been presented, it is clear that the problem of the stability of algorithm (1) for the case of exposure to similar capturing interference consists in determining a stable trajectory L_s, finding the range of its existence in the space and interference parameters and in finding the region of attraction of the trajectory L_s in the phase space ϕ, x, τ. This problem is solved in this paper by means of a numerical investigation of system (5) using a computer. The results of the study of the stability of algorithm (1) are given below for two different situations, where the interference acts on a locked-on

17

filtering system, and when the signal and interference arrive at the system input simultaneously.
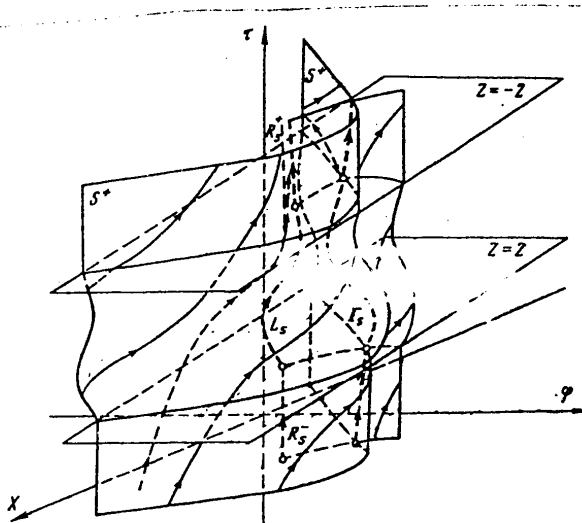
Figure 4.

4. The Stability of Algorithm (1) where Interference Acts on a Locked-
   -On System

Interference has an impact on a locked-on system in those cases where he interference lags the signal in time. Such cases arise, for example, when the law governing the generation of the useful ShPS is unknown to the jamming party [5], and the expenditure of time is needed to ascertain this law and generate similar interference. In this case, the inter-ference can lag the signals so much that at the point in time $\tau_0 =$
$= (2 - x_0 - x_s)\delta^{-1}$ of its arrival (x_s is the system error when $\tau = \tau_0$), the tracking mode is established in the system for the useful ShPS.

We shall assume in accordance with the situation considered here that the initial difference between the interference and signal delays is $x_0 \geq$
≥ 4, the parameter δ is less than zero and the initial phase difference

18

ψ varies in a range of $[0, 2\pi]$; the parameters of the system γ, b, β and α belong to the capture region D_g of the autonomous model (7), while the initial state of the system at the point in time $\tau = \tau_0$ is determined in the phase space by the point on the straight line R_g^-, i.e., by the equilibrium states (ϕ_s, x_s) of model (7). Then when $\tau > \tau_0$, with the influence of interference, the mapping point in moving in the phase space along the trajectory L_s is deflected from the steady-state status (ϕ_s, x_s), however, with the course of time moves out into the region of $x + x_0 + \delta\tau \le -2$ of the phase space and falls in the region of attraction of the half-line R_g^+.

The amount of the deflection of the mapping point from the steady-state status (ϕ_s, x_s) and the time of its arrival in the small vicinity of the half-line R_g^+ depend substantially on the parameters of the jamming. Starting at certain values of the jamming parameters, the peak-to-peak value of the steady-state motion of L_s and the time needed to establish P_S mode can become impermissibly large. For this reason, we conventionally assume that if the trajectory L_s exists, and when $-\infty < \tau < \infty$, it does not leave the region V: $|x| \le 2$ of the phase space, then with these values of the interference parameters, the P_S mode is not disrupted by the interference. In this case, the difference x in the delays of the useful and reference signals is kept within the bounds of the discrimination characteristic $D(x)$. The exiting of the trajectory L_s beyond the limits of the region V will then mean that, in the system, with these values of the interference parameters, the disruption of the tracking begins. Thus, a break in the tracking in the system considered here, subject to the action of similar capturing interference, we shall conditionally consider as the difference in the delays x going beyond the limits of the discrimination characteristic $D(x)$.

We shall estimate the stability of algorithm (1) in this case from the size of the region G_S for maintaining tracking (i.e., the range of signal retention). The region G_S is the range of values of the system and interference parameters for which there exists a stable trajectory L_S in system (5), which is located entirely in the region V of the phase space ϕ, x, τ.

By virtue of the fact that the initial phase difference ψ between the interference and the signal is a random quantity, the stability of algorithm (1) can be estimated based on the probability of maintaining the tracking. For this, we specify the function $F(\psi)$ for the distribution of the random initial values of ψ such that $\int F(\psi)d\psi = 1$. Let

U_S be the set of values of ψ from the range $[0, 2\pi]$, for which the trajectory L_S does not go outside the bounds of the region V. Then the probability p_S of maintaining tracking and the probability p_0 of the loss of tracking are defined in a manner similar to [6, 7] by the expressions:

19

$$(10) \qquad p_s = \int_{v_s} F(\psi)\,d\psi, \qquad p_s = 1 - p_s.$$

In those cases where ψ is uniformly distributed [8, 9] in the range $[0, 2\pi]$, $F(\psi) = $ const., and then $p_s = U_s/2\pi$ and $p_0 = 1 - U_s/2\pi$.
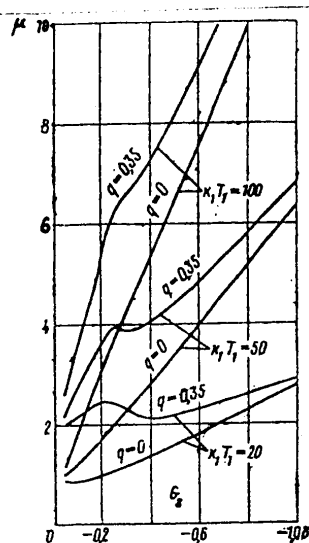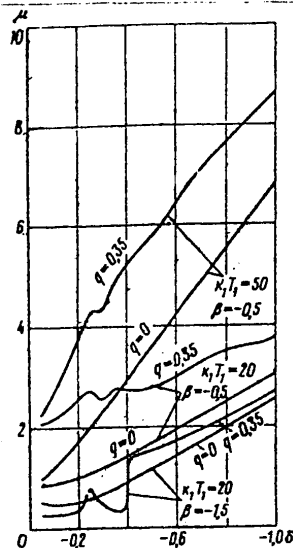
Figure 5.   Figure 6.

By specifying definite values of the probability p_s, one can determine the size of the region G_s for a specified probability of signal retention. Shown in Figure 5 are curves for $\mu = \mu_s(\delta)$, which define the region G_s in the parameters of the interference δ and μ: $\mu < \mu_s(\delta)$ for the maintenance of tracking with a probability of $p_s = 1$, computed for values of the parameters $\gamma = 0.2$, $\beta = -0.5$, $\alpha = 5.0$, $k_1 T_1 = 20$, 50, and 100, and $q = 0$ and 0.35. It follows from the results obtained that the most dangerous interference occurs in the region of small absolute values of the rate of change δ in the delay of the interference, where a break in tracking occurs when the ratio of the amplitudes of the interference

20

and the signal μ is on the order of 1. With a reduction in the initial frequency q between the interference and the signal, the efficiency of the interference increases, while the size of the region G_s falls off so that a break in tracking for the same values of δ occurs at lower values of μ. The interference has the greatest jamming effect when the carriers of the frequencies coincide, i.e., when q = 0. Increasing the response time of the SSZ, i.e., reducing the parameter b, leads to an increase in the range of stability G_s.

5. The Stability of Algorithm (1) with the Simultaneous Action of the Signal and Interference

In this case, the initial timewise x_0 and phase ψ shifts of the interference and signal vary respectively in ranges of $x_0 \in [-2-\beta, 2 - \beta]$ and $\psi \in [0, 2\pi]$. A change in the parameter x_0 in the indicated range corresponds to a change in the initial difference in the delays z between the interference and the reference signal in a range of $z \in [-2, 2]$. We shall assume that the system parameters γ, β, b and α belong to the region D_s (in order for capture to be possible). Then when $\tau = 0$, the initial value of the difference $x = x_{ini}$ should satisfy the condition $|x_{ini}| < \beta^*(\gamma, b, \alpha)$ (Figure 2); the initial phase difference ϕ takes on arbitrary values from the range $[0, 2\pi]$. Thus, when $\tau = 0$ the initial state of the system in the phase space ϕ, x, τ is defined by the set of points of the segment L_0: $\{\tau = 0, x = \beta, 0 \le \phi \le 2 \pi\}$.

We conventionally assume that the establishing of the synchronous mode P_s at values of the system parameters which satisfy the condition $\gamma < \gamma$ $\gamma < \gamma^*(\beta, b, \alpha)$, takes place in the case where for all values of the interference parameters x_0 and ψ from the range V_p: $\{0 \le \psi \le 2\pi, -2 -$ $- \beta \le x_0 \le -2 + \beta\}$, all trajectories starting at $\tau = 0$ in the segment L_0 fall in the region of attraction of the half-line R_s^+ when the time τ increases, without leaving the region V: $|x| \le 2$ of the phase space. We shall call the range of value of the parameters γ, β, α, μ, δ, b and q for which this occurs the capture range Ω_s. The stability of algorithm (1) is estimated in this case based on the size of the region Ω_s for which, despite the action of interference, the mode P_s is established. For values of the parameters outside the range of Ω_s, the difference in the delays x takes on values which go beyond the limits of $x = \pm 2$ during the process of establishing the synchronization mode P_s. Moreover, if in this case the system parameters satisfy the condition $\gamma > \gamma^*(\beta, b, \alpha)$, then the mode P_s may not start at all because of the onset of the steady-state beat frequency mode of the second kind.

Since the initial values of the difference in the phases ϕ and the parameters x_0 and ψ are random quantities, the stability of algorithm (1)

can be estimated on the basis of the lock-on probability. We shall consider the system parameters from the region D_S. We introduce the function $F(\phi, \psi, x_0)$ for the distribution of the random initial values of ϕ, ψ and x_0 in the region of V_0: $\{0 \leq \phi \leq 2\pi; \ 0 \leq \psi \leq 2\pi; \ -2 - \beta \leq \ \leq x_0 \leq 2 - \beta\}$, which satisfies the condition $\iiint\limits_{V_0} F(\varphi, \psi, x_0)\,d\varphi d\psi dx_0 = 1.$

Let $V_S \subseteq V_0$ be the region of initial values of ϕ, ψ and x_0 for which the P_S mode is established without the frequency difference x going beyond the limits of the region V: $|x| \leq 2$. Then the capture probability q_S is defined in a manner similar to [7] by the expression:

(11)
$$q_s = \iiint\limits_{V_s} F(\varphi, \psi, x_0)\,d\varphi d\psi dx_0.$$

In the case where ϕ, ψ and x_0 are uniformly distributed [9] in the region V_0, $F(\phi, \psi, x_0)$ = const., then we derive from (11) $q_S = V_S/16\pi^2$. By specifying values of the probability q_S, one can determine the size of a capture region having a specified probability.

Curves of $\mu = \mu_S^*(\delta)$ are shown in Figure 6 where these curves define the region Ω_S in terms of the interference parameters δ and μ: $\mu < \mu_S^*(\delta)$, computed for system parameter values of $\gamma = 0.2$, $\alpha = 5.0$, $k_1 T_1 = 20$ and 50 and $\beta = -0.5$ and -1.5, which belong to the region D_S for values of the parameter $q = 0$ and 0.35. It follows from a comparison of the results obtained for various values of the initial difference β that as the values of the system parameters approach the boundary of the region D_S, the size of the stability region Ω_S decreases, and a range of values of δ appears and increases, in which the disruption of the stability of algorithm (1) occurs for a ratio of the interference and signal amplitudes of $\mu < 1$; in this case, the oscillating nature of the curves $\mu = \mu_S^*(\delta)$ when $q \neq 0$ is manifest more strongly. With an increase in the dimensionless time constant $k_1 T_1$ the size of the region Ω_S increases. The influence of the frequency difference q on the size of the region Ω_S has a different nature depending on the degree of closeness of the values of the system parameters to the boundary of the region D_S. Thus, by comparing the curves $\mu = \mu_S^*(\delta)$ for $k_1 T_1 = 20$, we see that when $\beta = -0.5$, increasing the difference q leads to an attenuation of the influence of the interference, i.e., to an increase in the region Ω_S. However, when $\beta = 1.5$, the oscillating nature of the curve $\mu = \mu_S^*(\delta)$ when $q \neq 0$, leads to the appearance of ranges of values of the rate δ, in which the interfering effect of the interference is, on the contrary, increased, while the size of the stability region Ω_S decreases with an increase in the difference q.

22

By comparing the curves $\mu = \mu_q(\delta)$ and $\mu = \mu_s^*(\delta)$ which define the boundaries of the regions G_s and Ω_s, we establish the fact that when $\delta < 0$, in a range of small values of $|\delta|$, the sizes of the regions G_s and Ω_s are close, and with an increase in $|\delta|$, the size of the region Ω_s is greater than the region G_s. Such a difference in the stability conditions is related to the different values of the parameter μ at which the exit of the trajectory L_s begins and the trajectories which start in the segment L_0, beyond the bounds of the region V for the same values of the parameter δ. Thus, to estimate the stability of algorithm (1) in both of the situations considered here, one can make use of the curves for $\mu = \mu_s(\delta)$; in this case, with the simultaneous action of signal and interference, these curves define the region of stability of Ω_s with a slight margin of safety.

Conclusion

The results of the study performed here make it possible to come to the following conclusions. In the absence of interference, the stability characteristic of algorithm (1) is the range of values of the parameters D_s: $\gamma < \gamma^*(\beta, b, \alpha)$. It is characteristic that just as in the autonomous model of [7], the stability of the model considered here can be assured only for limited values of the initial delay difference. In this case, for the initial conditions found [2] in the phase space ϕ, x on the circle L_0: $\{\phi \in [-\pi, \pi], x = -2\}$, the system considered here is unstable and the synchronization mode is impossible because of the fact that a periodic mode is established in it, which is defined on the phase cylinder by an ultimate cycle which coincides with the circle L_0. The stricter limitations on the amount of the initial delayed difference follows from this, where this quantity is usually specified [2] by the preliminary coarse synchronization (search mode): for system stability, the condition $|x_{ini}| \le \beta^*(\gamma, b, \alpha)$, where $|\beta^*(\gamma, b, \alpha)| < 2$ should be met. Under conditions where similar capturing interference acts, the stability of algorithm (1) can be estimated on the basis of the size of the tracking retention region G_s: $\mu < \mu_s(\delta)$ and based on the size of the capture region Ω_s: $\mu < \mu_s^*(\delta)$. The quantitative results shown for the regions D_s, G_s and Ω_s make it possible to estimate the impact of the system and interference parameters on the stability of algorithm (1).

BIBLIOGRAPHY

1. A.N. Detinov, RADIOTEKHNIKA I ELEKTRONIKA, 1968, 13, 3, 455.

2. G.I. Tuzov, "Statisticheskaya teoriya priyema slozhnykh signalov" ["The Statistical Theory of the Reception of Complex Signals"], Sovetskoye Radio Publishers, 1977.

23

3. L.N. Belyustina, V.P. Ponomarenko, in the book, "Fazovaya sinkhroniza-tsiya" ["Phase Synchronization"], edited by V.V. Shakhgil'dyan and L.N. Belyustina, Chapter 12, Svyaz' Publishers, 1975.

4. V.M. Svistov, "Radiolokatsionnyye signaly i ikh obrabotka" ["Radar Signals and Their Processing"], Sovetskoye Radio Publishers, 1977.

5. "Shumopodobnyye signaly v sistemakh peredachi informatsii" ["Pseudonoise Signals in Data Transmission Systems"], edited by V.B. Pestryakov, Sovetskoye Radio Publishers, 1973.

6. V.P. Ponomarenko, RADIOTEKHNIKA I ELEKTRONIKA, 1978, 23, 10, 2141.

7. V.P. Ponomarenko, RADIOTEKHNIKA I ELEKTRONIKA, 1979, 24, 9, 1765.

8. A.I. Starikovskiy, D.V. Nezlin, RADIOTEKHNIKA, 1977, 32, 2.

9. Blarkem, Sers, Frimen, "Zarubezhnaya radioelektronika" ["Foreign Radio Electronics"], Sovetskoye Radio Publishers, 1968, No. 1.

8225
CSO: 8144/1711

UDC 621.391.2

NONCOHERENT CORRELATION FILTERING OF COMPLEX SIGNALS

[Article by G.I. Tuzov, V.I. Prytkov and V.V. Spirin]

[Text] Noncoherent receivers for complex signals
are synthesized with a comprehensive use of non-
linear filtering theory in a gaussian approximation
and linear filtering theory for several cases of
practical importance involving the a priori conditions
for the change in the frequency and delay. Expressions
are given for a covariation filtering error matrix.
The operational capability of the derived structures
is confirmed by the results of analog computer modeling.

The synthesis of optimal systems for estimating the frequency of narrow
band signals using nonlinear filtering theory [1, 2] leads to the
necessity of accounting for all of the parameters of the useful signal -
amplitude, phase and frequency - and leads to structures, the basis of
which is a phase locked loop (FAP) [PLL].

However, as regards units with unstable reference generators, when the
signal propagates throught a medium which introduces phase distortions,
as well as in connnection with mobile units, the speed of which fluctu-
ates, the use of receivers with PLL's proves to be ineffective of their
narrow capture band the presence of phase jumps.

In practice, an automatic frequency control circuit (ChAP) [AFC] is
used instead of the PLL circuit, or a combination of these circuits
is used in these cases.

Papers [1, 3 and 4] were devoted to questions of synthesizing optimum
frequency estimation devices. Thus, the aposteriori distribution of

25

---

the probabilities for the frequency was determined in [1, 3] using a modified nonlinear filtering theory, and a differential equation was obtained for the optimum filtering. Nonetheless, the structure modulating this equation is difficult to realize in practice, since a frequency discriminator in explicit form is lacking in it. An equation is given [4] for estimating the frequency, which was derived from a nonlinear filtering equation for a posteriori probability densities of the frequency and phase by means of averaging both sides of the equation with respect to the phase. Such an approach made it possible to substantiate the optimality of an AFC frequency discriminator in explicit form for a signal with a constant frequency. Similarly, the synthesis of optimum filtering systems for complex signals yields the structure of [8], which consists of two coherent mutually coupled circuits: a PLL circuit and a delay tracking circuit (SSZ). However, such a structure has a small synchronization lock-in range with respect to the carrier and the clock frequencies, and consequently, requires a long signal search time. For this reason, structures are proposed in [6, 7] for complex signal receivers, in which the SSZ circuity provides for noncoherent signal processing, while the PLL circuit can be replaced by an AFC circuit.

However, the questions of the optimality of receivers of complex signals which incorporate a noncoherent SSZ and AFC (or PLL) circuitry remain unproved at the present time.

For this reason, an attempt is made in the following to synthesize complex signal receivers with noncoherent discriminators. For this, by using a modified nonlinear filtering theory, the synthesis is carried out for the case of a constant frequency (using a gaussian approximation to obtain the structure), and then by means of linear filtering methods, assuming that the structure of the discriminators is constant, filters are synthesized in the control circuits for the case of variable frequencies.

1. Let the following realization be fed to the input of the system being synthesized:

(1) $$\xi(t) = S(t) + n(t),$$

where
$$M[n(t)] = 0;$$
$$M[n(t_1)n(t_2)] = 0{,}5N_0\delta(t_2 - t_1);$$
$$S(t) = Ag(t - \tau)\cos(\omega t + \varphi)$$

is the useful signal; A is the unknown amplitude of the signal. G(t−τ) is a function which assumes values of ±1 in accordance with the modulation; φ is the random initial phase with a uniform distribution in [0, 2π].

26

The signal parameters, the frequency ω, the phase ϕ and the delay τ are assumed to be constant with time. Then the optimum nonlinear filtering equation for this case will have the form [4]:

(2)

where
$$W_{ps}(t, \omega, \tau, \varphi) = [F(t, \omega, \tau, \varphi) - \langle F(t, \omega, \tau, \varphi) \rangle] W_{ps}(t, \omega, \tau, \varphi),$$

$$F(t, \omega, \tau, \varphi) = \frac{2A}{N_0} \xi(t) g(t-\tau) \cos(\omega t + \varphi).$$

The a posteriori probability density W_{ps} takes the form of the functional [1]:

(3)
$$W_{ps}(t, \omega, \tau, \varphi) = C \exp\left\{ -\frac{A^2 t}{N} \int_0^t g^2(t_1-\tau) \cos^2(\omega t_1 + \varphi) dt_1 + \right.$$

$$\left. + \frac{2A}{N_0} \int_0^t g(t_1-\tau) \xi(t_1) \cos(\omega t_1 + \varphi) dt_1 \right\}.$$

We shall introduce the symbols:

(4)
$$X(t, \omega, \tau) = \int_0^t \xi(t_1) g(t_1-\tau) \cos \omega t_1 \, dt_1,$$

$$Y(t, \omega, \tau) = \int_0^t \xi(t_1) g(t_1-\tau) \sin \omega t_1 \, dt_1,$$

(5)
$$f(t, \omega, \tau, \varphi) = X(t, \omega, \tau) \cos \varphi - Y(t, \omega, \tau) \sin \varphi.$$

Averaging both parts of equation (2) with respect to ϕ for the case of low power parameters reduces to averaging the expression:

(6)
$$F(t, \omega, \tau, \varphi) W_{ps}(t, \omega, \tau, \varphi) = \frac{2AC}{N_0} \xi(t) g(t-\tau) \times$$

$$\times \cos(\omega t + \varphi) \exp\left\{ -\frac{A^2 t}{2N_0} + \frac{2A}{N_0} \int_0^t \xi(t_1) g(t_1-\tau) \cos(\omega t_1 + \varphi) dt_1 \right\},$$

which, taking (4) and (5) into account, can be represented in the form:

(7)

$$F(t, \omega, \tau, \varphi) W_{ps}(t, \omega, \tau, \varphi) =$$

$$= -\frac{2AC}{N_0} \frac{\partial f}{\partial t} \exp \left\{ -\frac{A^2 t}{2N_0} + \frac{2A}{N_0} f(t, \omega, \tau, \varphi) \right\}.$$

Averaging expression (6) with respect to ϕ for the case of a uniform phase distribution in a range of $[0, 2\pi]$, i.e., $W(\phi) = 0.5/\pi$, we obtain:

(8)

$$\frac{1}{2\pi} \int_0^{2\pi} F(t, \omega, \tau, \varphi) W_{ps}(t, \omega, \tau, \varphi) d\varphi =$$

$$= \frac{C}{2\pi} \exp \left\{ -\frac{A^2 t}{2N_0} \right\} \frac{\partial}{\partial t} \left[\int_0^{2\pi} \exp \left\{ \frac{2A}{N_0} f(t, \omega, \tau, \varphi) \right\} d\varphi \right] =$$

$$= C \exp \left\{ -\frac{A^2 t}{2N_0} \right\} \frac{\partial}{\partial t} \left[I_0 \left\{ \frac{2A}{N_0} Z \right\} \right].$$

since

$$W_{ps}(t, \omega, \tau) = C \exp \left\{ -\frac{A^2 t}{2N_0} \right\} I_0 \left\{ \frac{2A}{N_0} Z \right\},$$

while the ratio

$$\frac{\partial}{\partial t} \left[I_0 \left\{ \frac{2A}{N_0} Z \right\} \right] / I_0 \left\{ \frac{2A}{N_0} Z \right\} =$$

$$= \frac{\partial}{\partial t} \ln I_0 \left\{ \frac{2A}{N_0} Z \right\},$$

then

$$W_{ps}(t, \omega, \tau) = C \exp \left\{ -\frac{A^2 t}{2N_0} \right\} \frac{\partial}{\partial t} \left[I_0 \left\{ \frac{2A}{N_0} Z \right\} \right] -$$

$$- \langle F(t, \omega, \tau, \varphi) \rangle W_{ps}(t, \omega, \tau),$$

where $Z^2 = X^2 + Y^2$; I_0 is a Bessel function. By taking $W_{ps}(t, \omega, \tau)$ outside the braces, we obtain the final equation for the combined aposteriori probability density of the frequency and the delay:

(9)

$$W_{ps}(t, \omega, \tau) = \left\{ \frac{\partial}{\partial t} \left[\ln I_0 \left\{ \frac{2A}{N_0} Z(t, \omega, \tau) \right\} \right] - \right.$$

$$\left. - \langle F(t, \omega, \tau, \varphi) \rangle \right\} W_{ps}(t, \omega, \tau).$$

By using a gaussian approximation for (9), we obtain the equations for the estimates of the frequency and delay of a complex signal and for the second central moments of these quantities:

$$\dot{\omega}^* = K_{\omega\omega} \frac{\partial}{\partial\omega^*} \frac{\partial}{\partial t} \left\{ \ln I_0 \left[\frac{2A}{N_0} Z(t, \omega^*, \tau^*) \right] \right\} +$$

$$+ K_{\omega\tau} \frac{\partial}{\partial\tau} \frac{\partial}{\partial t} \left\{ \ln I_0 \left[\frac{2A}{N_0} Z(t, \omega^*, \tau^*) \right] \right\},$$

(10)

$$\tau^* = K_{\tau\tau} \frac{\partial}{\partial\tau} \frac{\partial}{\partial t} \left\{ \ln I_0 \left[\frac{2A}{N_0} Z(t, \omega^*, \tau^*) \right] \right\} +$$

$$+ K_{\omega\tau} \frac{\partial}{\partial\omega} \frac{\partial}{\partial t} \left\{ \ln I_0 \left[\frac{2A}{N_0} Z(t, \omega^*, \tau^*) \right] \right\},$$

(11)

$$dK/dt = -KDK.$$

For the sake of convenience, we introduce the following symbols:

$$F_i(t, \omega, \tau) = \frac{\partial}{\partial t} \ln I_0 \left[\frac{2A}{N_0} Z(t, \omega, \tau) \right],$$

(12)

$$D = \left| \begin{matrix} F_{2\omega\omega} & F_{2\omega\tau} \\ F_{2\omega\tau} & F_{2\tau\tau} \end{matrix} \right| \quad ,$$

$$F_{2ij} = \left\| \frac{\partial^2 F_i}{\partial x_i \partial x_j} \right\|, \quad K = \left| \begin{matrix} K_{\omega\omega} & K_{\omega\tau} \\ K_{\omega\tau} & K_{\tau\tau} \end{matrix} \right|,$$

$$x_1 = \omega, \quad x_2 = \tau; \quad \vec{x}^T = |x_1, x_2| = |\omega, \tau|.$$

In scalar form, the equations for the central correlation moments will have the following form:

$$K_{\omega\omega}^2 F_{\omega\omega} + 2K_{\omega\omega}K_{\omega\tau}F_{\omega\tau} + K_{\omega\tau}^2 F_{\tau\tau} = -\frac{dK_{\omega\omega}}{dt},$$

$$K_{\omega\omega}K_{\omega\tau}F_{\omega\omega} + K_{\omega\tau}^2 F_{\omega\tau} + K_{\omega\omega}K_{\tau\tau}F_{\omega\tau} +$$

(13)

$$+ K_{\omega\tau}K_{\tau\tau}F_{\tau\tau} = -\frac{dK_{\omega\tau}}{dt},$$

$$K_{\omega\tau}^2 F_{\omega\omega} + 2K_{\omega\tau}K_{\tau\tau}F_{\omega\tau} + K_{\tau\tau}^2 F_{\tau\tau} = -\frac{dK_{\tau\tau}}{dt},$$

29

where

$$F_{\tau\tau} = \frac{\partial^2 F_1}{\partial \tau^2} = \frac{\partial}{\partial t}\left[\frac{\partial B(Z)}{\partial Z}\left(\frac{\partial Z}{\partial \tau}\right)^2 + B(Z)\frac{\partial^2 Z}{\partial \tau^2}\right] ;$$

$$F_{\omega\omega} = \frac{\partial^2 F_1}{\partial \omega^2} = \frac{\partial}{\partial t}\left[\frac{\partial B(Z)}{\partial Z}\left(\frac{\partial Z}{\partial \omega}\right)^2 + B(Z)\frac{\partial^2 Z}{\partial \omega^2}\right] ;$$

$$F_{\omega\tau} = \frac{\partial^2 F_1}{\partial \omega\,\partial \tau} = \frac{\partial}{\partial t}\left[\frac{\partial B(Z)}{\partial Z}\frac{\partial Z}{\partial \omega}\frac{\partial Z}{\partial \tau} + B(Z)\frac{\partial^2 Z}{\partial \omega\,\partial \tau}\right] ;$$

$$B(Z) = \frac{\partial}{\partial Z}\left\{\ln I_0\left[\frac{2A}{N_0}Z(t,\omega,\tau)\right]\right\}.$$

The solutions of equations (11) for the central correlation moments will have the form

(13a)
$$K^{-1} = C''t + C',$$

The solutions of these equations for the steady-state case yield zero values of the gain coefficients $K_{\omega\omega}$, $K_{\omega\tau}$ and $K_{\tau\tau}$. This indicates that this way of estimating the quantities K_{ij} is unacceptable in the steady-state mode.

The procedure for deriving the averaged dispersions of the estimates is given in [3] for obtaining an estimate of a signal frequency, where it is shown that:

(14)
$$K_{\omega\omega} = \frac{12N_0}{A^2 t^3}.$$

The precise values of this coefficient and its dependence on time do not play a fundamental role in tracking. Only its order of magnitude is important, while the time function is more important for studying the nature of the nonlinear dynamics of the tracking system.

This is very important since it makes it possible to substantially simplify the problem of designing optimum systems through replacement of a variable gain, for example, let us say (14), with a certain constant gain. Constant gain coefficients are obtained when the expressions for F and K are averaged under the condition where $t/\tau_i \gg 1$, where τ_i is the time during which the i-th parameter remains practically constant, while t is the current time of the estimate [3]. In this case, there is no necessity for using cross-couplings $K_{\omega\tau}$ and $K_{\tau\omega}$

30

between the frequency tracking and the delay tracking circuits, which can be taken into the count in the form of constants added to the averaged constant gains of these circuits. In practice, these coefficients can be obtained as a result of studying the overall dynamics, determined by a solution of the differential equations of motion corresponding to the given system.

Taking this into account, and making a transition from equations in partial derivatives to approximate equations, in which the partial derivaties are replaced by finite differences, one can write:

$$\omega^{\cdot} = \frac{K_{\omega\omega}}{2a} \left\{ \ln I_0 \left[\frac{2A}{N_0} Z(t, \omega^{\cdot}+a, \tau^{\cdot}) \right] - \right.$$
$$\left. - \ln I_0 \left[\frac{2A}{N_0} Z(t, \omega^{\cdot}-a, \tau^{\cdot}) \right] \right\},$$

(15)

$$\tau^{\cdot} = \frac{K_{\tau\tau}}{2b} \left\{ \ln I_0 \left[\frac{2A}{N_0} Z(t, \omega^{\cdot}, \tau^{\cdot}+b) \right] - \right.$$
$$\left. - \ln I_0 \left[\frac{2A}{N_0} Z(t, \omega^{\cdot}, \tau^{\cdot}-b) \right] \right\},$$

where $a = \Delta\omega$ (the frequency increment); $b = \Delta\tau$ (the delay increment).

A filter structure which realizes equations (15) is shown in Figure 1. It was proposed for the first time in [6].

This receiver, just as the coherent one of [5], contains a circuit for frequency estimation and a circuit for delay estimation. In contrast to the coherent configura. on, the frequency estimation is accomplished by an AFC circuit, while the delay tracking circuit contains a discriminator. Such a receiver design provides for stable operation under conditions of large phase and frequency fluctuations, and also has a substantial impact on the nature of the nonlinear dynamics of the receiver, facilitating the solution of signal search and capture problems.

2. We shall consider the case where the signal frequency fluctuates about its constant value of ω_0. In other words:

(16) $$\dot{\omega} = -\alpha(\omega-\omega_0) + \alpha n_\omega(t).$$

Since the solution of the problem of nonlinear system synthesis for frequency estimation is rather complex in this case, we shall assume that the circuit of the discriminator is also specified and smoothing circuits

31

FOR OFFICIAL USE ONLY

are treated as the object of synthesis. This approach is substantiated in [8].

Then, by using the equations for a continuous Kalman filter for the steady-state case with the message model of (16), we obtain the filtering algorithm which will have the form [9]:

(17)
$$\dot{\omega}^* = -\alpha\omega^* + K_\omega(\omega - \omega^*).$$

The difference ($\omega - \omega^*$) is the output signal of the linearized frequency discriminator, the precise algorithm for which is derived from a non-linear synthesis. The filter corresponding to equation (17) is modeled by the structure shown in Figure 3a.

By using this same algorithm, one can derive the structure of the filter in the control loop for any other initial conditions for parameter change. Thus, for the parameters

(18)
$$\dot{\omega} = V, \quad \dot{V} = -\beta V + \beta n_v(t)$$

the filter takes the form of the circuit shown in Figure 3b.
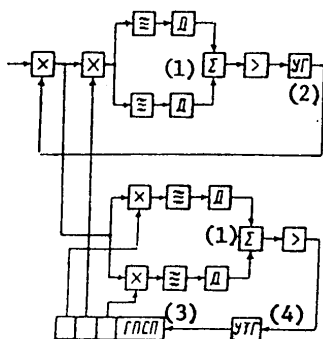
Figure 1. An incoherent complex signal receiver.

Key: 1. D [envelope detector];
2. UG [controlled harmonic signal generator];
3. GPSP [pseudorandom sequence generator];
4. UTG [controlled clock generator];

Σ = adder.

Yet another variant of a complex signal receiver [7], which occupies an intermediate position between the noncoherent receivers can be proposed and easily synthesized using the method presented above. This variant (Figure 2) contains a phase locked loop and a noncoherent delay tracking circuit.

32

FOR OFFICIAL USE ONLY
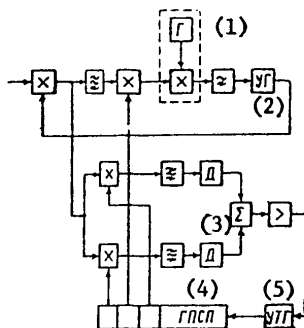
Figure 2. A semi-coherent complex signal receiver.

Key: 1. G [highly stable harmonic generator];
2. UG [controlled harmonic generator];
3. D [envelope detector];
4. GPSP [pseudorandom sequence generator];
5. UTG [controlled clock generator].
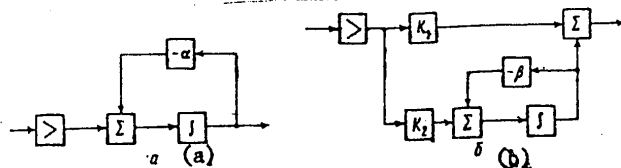
Figure 3. Low pass filters.

Key: Σ = adder;
$\int$ = integrator;
α, β = drift coefficients of the parameters being filtered;
K_1, K_2 = amplifiers.

And finally, we shall make a purely qualitative remark concerning the noise immunity of the noncoherent filtering circuits synthesized here as compared to the coherent filter described in [5].

The noise immunity of correlation filtering circuits, described in [5, 6, 7] will be determined in many respects by the filters (as a rule, the IF amplifiers, inserted after the multipliers, which provide for the filtering of the mixture of received and reference signals. These IF amplifier filters (Figures 1 and 2) increase the signal-to-noise ratio at the input to the amplitude detectors. The passband of these filters, if one works from the conditions for the stability of the systems being studied in the case of identical dynamics of the frequency of the input process, can be made less in the case of AFC than

33

FOR OFFICIAL USE ONLY

in the case of a PLL circuit. For this reason, the noise immunities
of coherent and noncoherent complex signal receivers with correctly
chosen filters (IF amplifiers) prove to be close together. This is
explained by the fact that the noncoherent receivers being analyzed
[6, 7], provide for coherent filtering of the signals in narrow band
IF amplifiers and noncoherent filtering in the low-pass filters of
an AFC circuit and a delay tracking circuit.

BIBLIOGRAPHY

1. V.I. Tikhonov, "Statisticheskaya radiotekhnika" ["Statistical Radio
   Engineering"], Sovetskoye Radio Publishers, 1966.

2. V.I. Tikhonov, V.S. Yefimenko, RADIOTEKHNIKA I ELEKTRONIKA, 1979, 24,
   4, 765.

3. R.L. Stratonovich, RADIOTEKHNIKA I ELEKTRONIKA, 1961, 6, 7, 1063.

4. V.N. Kharisov, V.A. Khodakovskiy, IZV. VUZOV MVSSO SSSR (RADIO-
   ELEKTRONIKA) [PROCEEDINGS OF THE HIGHER EDUCATIONAL INSTITUTES OF
   THE MINISTRY OF SPECIAL AND SECONDARY HIGHER EDUCATION (RADIO
   ENGINEERING)], 1979, 22, 4.

5. G.I. Tuzov, "Sledyashchiy fil'tr s perekrestnoy modulyatsiyey i
   programmnym upravleniyem" ["A Tracking Filter with Cross Modulation
   and Program Control"], Patent No. 259972, OTKRYTIYA, IZOBRETENIYA
   PROMYSHLENNYYE OBRAZTSY, TOVARNYYE ZNAKI [DISCOVERIES, INVENTIONS,
   INDUSTRIAL MODELS, TRADEMARKS], 1970, 3, 51.

6. G.I. Tuzov, P.D. Zhernosek, B.I. Glazov, "Nekogerentnyy sledyashchiy
   fil'tr dlya obrabotki sluchaynogo signala" ["An Incoherent Tracking
   Filter for Random Signal Processing"], Patent No. 596114, OTKRYTIYA,
   IZOBRETENIYA, PROMYSHLENNYYE OBRAZTSY, TOVARNYYE ZNAKI, 1979, 21, 224.

7. G.I. Tuzov, R.D. Zhernosek, M.V. Yegorov, "Sledyashchiy fil'tr dlya
   obrabotki signala s podavlennoy nesushchey" ["A Tracking Filter for
   Processing a Signal with a Suppressed Carrier"], Patent No. 710008,
   OTKRYTIYA, IZOBRETENIYA, PROMYSHLENNYE OBRAZTSY, TOVARNYYE ZNAKI,
   1980, 2, 199.

8. G.I. Tuzov, "Statisticheskaya teoriya priyema slozhnykh signalov"
   ["The Statistical Theory of Complex Signal Reception"], Sovetskoye
   Radio Publishers, 1977.

9. E. Sage, J. Mels, "Teoriya otsenivaniya i yeye primeneniye v svyazi
   i upravlenii" ["Estimation Theory and Its Application to Communica-
   tions and Control"], Svyaz' Publishers, 1976.

8225
CSO: 8144/1711

UDC 621.391.019.4

OPTIMIZATION OF COMMUNICATIONS SYSTEMS WITH NOISE-LIKE SIGNALS AND CORRECTING CODES

Moscow RADIOTEKHNIKA in Russian No 5, 1980 pp 17-22 manuscript received 12 Sep 79

[Article by L. Ye. Varakin and Yu. K. Sal'nikov]

[Text] Introduction. Noise resistance of data transmission systems (SPI) is defined by the signal-to-noise ratio at the output of the matched filter (correlator) which, at limited noise power, equals [1]

$$h_m^2 = \frac{P_c}{P_n} FT,$$ (1)

where P_s/P_p is the ratio of signal power to noise power at the receiver input; F is the spectral width of the noise-like signal (ShPS); T is its duration; FT is the ShPS base; the index m designates the size of the alphabet.

By selecting the ShPS base we can obtain a value of h^2_m at which the desired noise immunity is achieved. This is especially important where the signal-to-noise ratio at the input of the receiver is small (P_s/P is much less than unity). However, at high rates of data transmission, the duration of ShPS is small and to achieve the desired noise immunity there must be a wide frequency band, which is difficult to produce. We know [2, 3] that the use of corrective coding permits enhancement of the noise immunity of SPI, and thus, by using correcting codes we
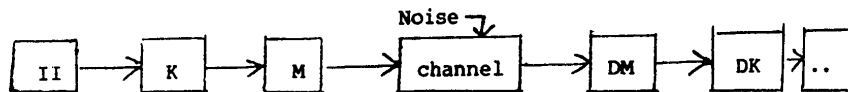

Figure 1

can support the desired noise immunity with lower signal-to-noise ratios as compared to SPI without coding. According to (1) information can be transmitted in a narrower frequency band. Below is examined the noise

36

immunity of SPI with ShPS and correcting codes, and optimum correcting codes are found which minimize the required frequency band. We now know of a large number of varied codes [2, 3], but [4] the most promising from the standpoint of practical utilization are the block codes. Among these codes we shall mention the divisible codes with achievable maximum distance. These contain some Bowes-Choudhury-Hockingham (BChKh) codes and Reed-Solomon (RS) codes. At identical code length and maximum number of corrected errors, these codes have maximum speeds [2, 3] as compared to others. Optimum codes can be found in the class of divisible codes. As we know [1], high noise immunity is found by $\underline{m}$ SPI with ShPS; therefore it is advisable to find optimum codes with respect to these systems.

The arrangement of such an SPI is shown in Figure 1: information from source II reaches encoder input K in the form of a train of $\underline{nu}$ symbols, where these sysmbols are at first grouped in blocks k_0 in length. Each block is the $\underline{m}$ symbol where

$$m = v^{k_0}.$$

(2)

Then $\underline{m}$ symbols are grouped in blocks k in length (Figure 2a), are encoded and at the encoder output, the train of $\underline{m}$ symbols is formed $\underline{n}$ in length (Figure 2b). This is the code sequence. Its symbols acquire values from the field GF (nu^{k_0}). Then in the modulator M, each symbol of the code sequence is modulated by orthogonal ShPS (Figure 2c) and is transmitted along the communications channel where additive noise is generated with uniform spectral power density in the receiver's frequency band. The number of different ShPS (size of alphabet) equals $\underline{m}$.
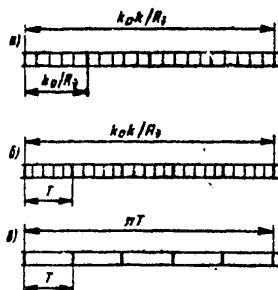
Figure 2

The demodulator DM is an optimum receiver in the sense of maximum likelihood, making a decision on each $\underline{m}$ ShPS separately. From the output of DM the train of $\underline{m}$ symbols enters the decoder DK where a decision is made on each block of m symbols n in length. As a result of decoding at the output of DK is shaped the information sequence $\underline{k}$ in length, which enters the information receiver PI.

37

.

Noise immunity of the cited SPI we shall give in the form of an equivalent probability of error for the nu information symbol R_{nu}. Let us introduce several definitions in order to calculate it.

Definitions

Any correcting code, except the length of the code train n and the number of information symbols k, is characterized by the speed c = k/n. For divisible codes c with a desired n unambiguously defines its correcting properties.

Using the introduced code parameters, let us calculate the length of ShPS necessary for further analysis. Let n symbols enter the input of the encoder at a speed of R_{nu}. If all symbols are equally probable, and the rate of information transmission R is given in binary units, we then have the equation

$$R = R_{\nu} \log_2 \nu.$$

Since the length of the mth signal at the encoder input is k_0/R_{nu} (Figure 2a), and the length of the code train is $k_0 k/R_{nu}$ (Figure 2b), then the length of the mth signal at its output or the length of ShPS at the modualtor output (Figure 2c) equals

$$T = \frac{k_0 c}{R} \log_2 \nu. \qquad (3)$$

Having defined the length of ShPS, let us calculate the probability of R_{nu} in the SPI in question.

Probability of error

The probability of error in incoherent reception of ShPS is defined by the formula [1]

$$p \approx \frac{m-1}{2} e^{-h_m^2/2}, \qquad (4)$$

where m is defined according to (2), $h^2{}_m$ according to (1). Substituting (3) in (1), we find

$$h_m^2 = \frac{P_c}{P_u} \frac{F}{R} k_0 c \log_2 \nu. \qquad (5)$$

38

The resultant probability in this SPI equals the probability of error of reception of the mth symbols of the encoded sequence. In the given system a code is used having the parameters n, k, r: an (n,k,r) code. If errors in the channel originate independently, the encoded sequence will be decoded incorrectly if any r+1 or greater independent errors occur. The probability of error in decoding [2, 3] is

$$P = \sum_{i=r+1}^{n} C_n^i p^i (1 - p)^{n-i},$$

where $C_n^i = n!/i! (n - i)!$; p is defined according to (4). On the other hand, an information sequence $\underline{k}$ in length is received correctly only when all $k_0 k$ of $\underline{nu}^{th}$ symbols are received without error. This means that $1 - R = (1 - R_{nu})^{k_0 k}$, hence where R_{nu} is much less than unity,

$$P_* \approx \frac{1}{k_* k} \sum_{i=r+1}^{n} C_n^i p^i (1 - p)^{n-i}. \tag{6}$$

Relationships of $R_2 = R_{nu}$ as a function of h_2 for the case where information is presented in binary form nu = 2, calculated according to (4), (6), are cited in Figure 3. For each of the four values m = 8, 16, 32, 64 the relationships of R_2 versus h_2 have been calculated for two RS codes. These codes have the respective parameters (7,5,1), (7,3,2), (15,11,2), (17,7,4), (31,25,3), (31,27,2), (63,53,5), (63,49,7). Furthermore, the same figure shows the relationships for the mth SPI without encoding, calculated according to known formula [1]:

$$P_2 \approx \frac{m}{4} e^{-\frac{h_2^2}{2} k_*}. \tag{7}$$

Figure 3 shows that various codes of the same length yield different probabilities of error: for example, SPI with codes (31,25,3) and (15,11,2) have higher noise immunity than SPI with codes (31,27,2) and (15,7,4). Hence it follows that among the codes of identical length there are optimum codes.

Selection of an optimum code

As was noted, a criterion for optimalcy of a code is the minimum required frequency band; thus for further consideration we should introduce the parameter

$$\tau = \frac{P_c}{2 P_a} \frac{F}{R} \log_2 v, \tag{8}$$

which at specified R_s/R_p fully defines the frequency band F. Let us find the optimum codes which minimize $\underline{gamma}$. Substituting (5), (8) in (4), we find that

39

$$p = \frac{m-1}{2} e^{-7k\sigma c}. \tag{9}$$
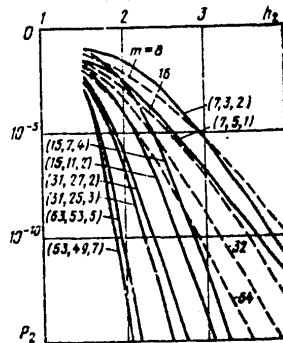
Figure 3

Let us define the relationship of gamma as a function of its parameters to select an optimum code. For this purpose we must find the relationship of p as a function of R_{nu} by means of (6), and then express gamma by p based on relationship (9).

There is no precise analytic expression for the inverse function $p(R_{nu})$, and therefore we shall use the one cited in [2] as an upper estimate for the binominal sum of (6). For this purpose let us designate that

$$\lambda = \frac{r+1}{n}, \qquad \mu = 1 - \lambda.$$

The upper estimate based on (6) appears as follows:

$$P_v \leqslant \frac{1}{k_v k} \lambda^{-\lambda n} \mu^{-\mu n} p^{\lambda n} (1 - p)^{\mu n}, \tag{10}$$

where p is less than lambda. The minimum value of lambda equals 2/n; thus (10) is satisfied for all p less than 2/n. Rejecting the last cofactor in (10), let us write a stricter inequality:

$$P_v < \frac{1}{k_v k} \lambda^{-\lambda n} \mu^{-\mu n} p^{\lambda n}, \tag{11}$$

40

which for p much less than unity differs negligibly from inequality (10). The right side of inequality (11) is a smoothly increasing function of p. We can show that for all values of p such that

$$p \leqslant (k_0 k P_*)^{\frac{1}{r+1}} \lambda_\mu^{\frac{\mu}{\lambda}},$$
(12)

the equivalent probability of error for the nuth informational symbol will not exceed the desired R_{nu}.

Let us now find the relationship of gamma as a function of the parameters of ShPS and the code. For this purpose, we log both parts of equation (9) and find that

$$\gamma \approx \frac{1}{k_* c} \ln \frac{m-1}{p}.$$
(13)

Expressions 912) and (13) clearly show the interrelationship between gamma and the code parameters for a fixed number of ShPS and probability R_{nu}. The parameters k, r, lambda, mu for divisible codes unambiguously are expressed by the code rate c; consequently (13) may be considered a function of the code rate. It appears that as c increases the correcting properties of the code deteriorate and p diminishes. The second cofactor on the right side of (13) increases logarithmically with c. The first cofactor of equation (13) decreases hyperbolically in inverse proportion to c. Hence we may assume that at low code rates gamma acquires greater values and high speed codes will be optimum. In the general case, the relationship of gamma as a function of c is complex in nature, and discovery of the minimum of gamma with respect to c involves certain problems. Let us examine RS codes to find the kind of relationship.

Optimum Reed-Solomon Codes

It follows from (8) for gamma that selection of nu is not critical in this formulation of the problem, so we will assume nu = 2. In this instance, the symbols of the encoded sequence acquire values from the field GF(2^k0). By definition, the length of RS code above the field GF(2^k0) equals [2, 3]

$$n = 2^{k_*} - 1 = m - 1$$
(14)

and selection of the ShPS alphabet volume unambiguously sets the code length. Substituting (14) in (13) we find that

$$\gamma \approx \frac{1}{k_* c} \ln \frac{n}{2p}.$$
(15)

If we select values of p at which the equivalent probability of error for a binary information signal does not exceed the quantity $R_2 = 10^{-4}$, according to precise formula (6), substituted in (15), we find the relationship of gamma as a function of c for all RS codes of lengths n = 7,

41

FOR OFFICIAL USE ONLY

15, 31 and several RS codes of lengths $\underline{n}$ = 63. Values of $\underline{gamma}$ for $R_2 = 10^{-4}$ of calculated codes are shown in the table and in Figure 4. The graphs show that for all $\underline{n}$ there exists an optimum code which permits use of the minimum frequency band of the receiver for desired data transmission rates R and ratio P_s/P_p at its input. As was supposed, optimal codes are high speed ones. At code speeds c greater than or equal to 0.5, the relationship of $\underline{gamma}$ as a function of c is weak; therefore any code can be used if the increase in $\underline{gamma}$, in this case negligible, does not play a substantial role. With low speed codes c less than 0.5, the parameter $\underline{gamma}$ sharply rises since code redundancy is increased.

k_0	(n,k,r)-code	gamma$_{cor.}$	gamma$_m$ code	$\dfrac{gamma_{cor.}}{gamma_m}$	$\dfrac{gamma_{cor.}}{gamma_{cor.opt.}}$
3	(7,5,1)	2.837	3.301	0.859	1
	(7,3,2)	3.702		1.121	1.305
	(7.1.3)	9.910		3.002	3.493
4	(15,13,1)	2.002	2.649	0.756	1.013
	(15,11,2)	1.976		0.746	1
	(15,9,3)	2.138		0.807	1.082
	(15,7,4)	2.504		0.945	1.267
	(15,5,5)	3.253		1.228	1.646
	(15,3,6)	5.128		1.936	2.595
	(15,1,7)	14.929		5.636	7.555
5	(31,29,1)	1.676	2.258	0.742	1.085
	(31,27,2)	1.568		0.694	1.015
	(31,25,3)	1.545		0.684	1
	(31,23,4)	1.563		0.692	1.012
	(31,21,5)	1.616		0.716	1.046
	(31,19,6)	1.719		0.761	1.113
	(31,17,7)	1.849		0.819	1.197
	(31,15,8)	2.027		0.898	1.312
	(31,13,9)	2.262		1.002	1.464
	(31,11,10)	2.596		1.150	1.680
	(31,9,11)	3.089		1. 68	1.999
	(31,7,12)	3.853		1. 97	2.494
	(31,5,13)	5.248		2.324	3.397
	(31,3,14)	8.702		3.854	5.632
	(31,1,15)	25.979		11. 05	16.815
6	(63,61,1)	1.516	1.997	0.759	1.139
	(63,59,2)	1.410		0.706	1.059
	(63,57,3)	1.363		0.683	1.024
	(63,55,4)	1.338		0.670	1.005
	(63,53,5)	1.331		0.666	1
	(63,51,6)	1.335		0.609	1.003
	(63,49,7)	1.349		0.676	1.014
	(63,47,8)	1.371		0.687	1.030
	(63,45,9)	1.394		0.698	1.047
	(63,43,10)	1.428		0.715	1.073
	(63,31,16)	1.739		0.8 6	1.344
	(63,15,24)	3.385		1.695	2.543
	(63,1,31)	48.522		24.297	36.455

Note: Some figures not reproduced in source.
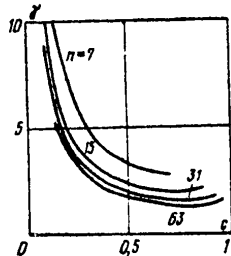
42

FOR OFFICIAL USE ONLY

Figure 4
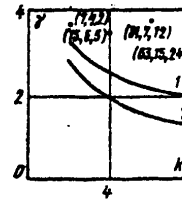
Figure 5

In order to show that the use of corrective encoding yields a gain in the frequency band, let us compare this SPI to a similar system without encoding. In SPIs without encoding, each $\underline{m}^{th}$ symbol is directly modulated by orthogonal ShPS and is transmitted along the communications channel. From (7) we find that

$$\gamma \approx \frac{1}{k_0} \ln \frac{m}{4P_1}.$$

(16)

Values of gamma = $gamma_m$ code calculated according to (16) for $P_2 = 10^{-4}$ are also given in the table. The relationship of gamma as a function of k_0 (number of ShPSs) is represented in Figure 5 by curve 2; curve 1 is the relationship in which optimum codes (7,5,1), (15,11,2), (31,25,3), (63,53,5) are used. As we can see, the use of optimum codes makes it possible to obtain a substantial gain in the frequency band as compared to a similar system without encoding. The tabular data show that not all codes reduce the frequency band. The use of codes with low rates of transmission requires an expansion of the frequency band and therefore is not advantageous in SPI with ShPS. The primary result of this study is the proof of the existence of optimum codes which minimize the frequency band and provide a gain in the frequency band as compared to m^{th} encoding.

References

1. Varakin, L. Ye. Teoriya sistem signalov [Theory of signal systems], Moscow, Sov. radio, 1978.

2. Piterson, U., Ueldon, E. Kody, ispravlyayushchiye oshibki [Error correcting codes], Moscow, Mir, 1976.

3. Kasami, T., Tokura, N., Ivadari, Ye., Inagaki, Ya. Teoriya kod-irovaniya [Coding theory], Moscow, Mir, 1978.

4. Blokh, E.L., Zyablov, V.V., ELEKTROSVYAZ' No 6, 1978.

8617
CSO: 1860

43

FOR OFFICIAL USE ONLY

RESOLUTION AND COMPRESSION OF SPACE-TIME SIGNALS

[Article by A. I. Pogorelov]

[Text] Algorithms are proposed for shaping and pro-
cessing linear-frequency modulated space-time signals,
and circuits for practical implementation of these
algorithms are considered.

An expression is given for the uncertainty function,
and the possibilities for resolution and compression
of such signals are analyzed.

Problems of resolution and compression of space-time signals, despite
their topicality, are not well covered in the literature. For example
Ref. 1 and 2 cover only questions of the resolution of simple space-time
signals, and Ref. 3 and 4 deal with problems of shaping and compression
of complex radiation patterns, while Ref. 5 presents methods of shaping
and processing noise-like discrete-coded space-time signals.

The purpose of this paper is to study the possibilities of shaping,
resolving and compressing linear-frequency modulated space-time signals.

In the general case, a space-time signal treated as a vertical or hori-
zontal component of the electric field intensity with uniform angular
density $s(t;\theta)$, where $\theta = \sin\Theta$, and Θ is the angular coordinate, can be
represented in the form [Ref. 5]

$$s(t;\theta) = s(t) F(\theta; t),\qquad(1)$$

where $F(\theta; t)$ is the radiation pattern:

$$F(\theta; t) = |F(\theta; t)| \exp\{j\varphi(\theta; t)\}.\qquad(2)$$

44

FOR OFFICIAL USE ONLY

Considering that the spatial characteristics of signal (1) are completely determined by radiation pattern (2), we represent the phase characteristic $\phi(\theta;t)$ of the radiation pattern $F(\theta;t) = F(\theta;0)$ in the form $\phi(\theta;0) = b\theta^2$ for realization of a linear-frequency modulated space signal, assuming that the amplitude characteristic of the radiation pattern is constant in the scanning sector $|F(\theta;0)| = F_0$. This will correspond to a linear law of change in the spatial frequency of the signal on its interval of existence $2\theta_M - 1/2\pi \cdot d/d\theta(b\theta^2) = b\theta/\pi$.

Using a linear antenna array and assuming a predetermined width of the space frequency spectrum $2\chi_M = 2X_M/\lambda$, where $2X_M$ is the maximum dimension of the array aperture, and λ is wavelength, we arrive at the following expression for the radiation pattern:

$$F(\theta; 0) = F_0 \exp\left\{ j \frac{\chi_M}{\theta_M} \theta^2 \right\}. \tag{3}$$

The relation given by Fourier transformation between the radiation pattern of the antenna array and the amplitude-phase distribution in the aperture yields the following expression for the amplitude-phase distribution on a fixed value of the aperture $|\chi| \leqslant \chi_M$ with bounded limits of integration $|\theta| \leqslant \theta_M$:

$$I(\chi; 0) = I_0 \exp\left\{ -j\pi \frac{\theta_M}{\chi_M} \chi^2 \right\} [C(Y_1) + jS(Y_1) + C(Y_2) + jS(Y_2)], \tag{4}$$

where I_0 is a constant determined by F_0, θ_M, χ_M, while $C(Y)$ and $S(Y)$ are the Fresnel integrals

$$C(Y) = \int_0^Y \cos\frac{\pi t^2}{2}\, dt; \qquad S(Y) = \int_0^Y \sin\frac{\pi t^2}{2}\, dt;$$

$$C(-Y) = -C(Y); \qquad S(-Y) = -S(Y);$$

$$Y_1 = 1\overline{2\theta_M 2\chi_M} [1 - \chi/\chi_M]; \qquad Y_2 = \sqrt{2\theta_M 2\chi_M}\, [1 + \chi/\chi_M].$$

Representing expression (4) in the form

$$I(\chi; 0) = I_0 \exp\left\{ j\left[-\pi \frac{\theta_M}{\chi_M} \chi^2 + \Phi(\chi; 0) \right] \right\} \times$$

$$\times \{[C(Y_1) + C(Y_2)]^2 + [S(Y_1) + S(Y_2)]^2\}^{1/2}, \tag{5}$$

where $\Phi(\chi; 0) = \operatorname{arc\,tg}\{[S(Y_1) + S(Y_2)][C(Y_1) + C(Y_2)]^{-1}\}$,

we note that in the range of values of the variables that is of interest to us $(2\theta_M 2\chi_M \gg 1)$, the radicand in (5) is equal to approximately 2, and falls off rapidly outside of the interval $|\chi| \leqslant \chi_M$, while $\Phi(\chi;0) = \pi/4$.

45

In accordance with this, we get for (4) with accuracy to a constant coefficient

$$I(\chi; 0) = I_0 \exp\left\{ -j\pi \frac{\theta_M}{\chi_M} \chi^2 \right\}. \tag{6}$$

The approximate form of the functions $|I(\chi;0)|$ and $\Phi(\chi;0)$ is shown in Fig. 1.
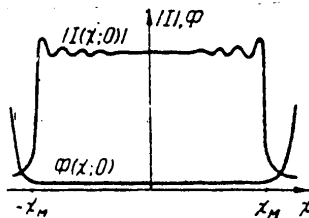
Fig. 1

To shape space-time signal (1), we carry out smooth cyclic scanning of radiation pattern (3) in sector $[-\theta_M; \theta_M]$. To do this, we extend the radiation pattern along axis θ from $-\infty$ to $+\infty$ periodically with period $2\theta_M$ and carry out scanning in such a way that the complete scanning cycle on interval $2\theta_M$ is completed in time $2T$. With consideration of this, we get the following expressions for the radiation pattern, the amplitude-phase distribution that realizes this pattern, and the space-time signal that is shaped respectively:

$$F(\theta; t) = F_0 \sum_{i=-\infty}^{\infty} \Pi\left[\frac{t - \theta T/\theta_M - i2T}{T} \right] \exp\left\{ j\pi \frac{F_M}{T} \left(t - \theta \frac{T}{\theta_M} - i2T \right)^2 \right\}; \tag{7}$$

$$I(\chi; t) = I_0 \sum_{i=-\infty}^{\infty} \Pi\left[\frac{t - \chi T/\chi_M - i2T}{T} \right] \exp\left\{ -j\pi \frac{F_M}{T} \left(t - \chi \frac{T}{\chi_M} - i2T \right)^2 \right\}; \tag{8}$$

$$s(t; \theta) = S_0 F_0 \sum_{i=-\infty}^{\infty} \Pi\left[\frac{t - \theta T/\theta_M - i2T}{T} \right] \times$$

$$\times \exp\left\{ j\left[2\pi f_0 t + \pi \frac{F_M}{T} \left(t - \theta \frac{T}{\theta_M} - i2T \right)^2 + \varphi_0 \right] \right\}. \tag{9}$$

In (7)-(9), $\Pi(x)$ is the following function

$$\Pi(x) = \begin{cases} 1; & |x| \leqslant 1; \\ 0; & |x| > 1; \end{cases} \qquad F_M = \frac{\chi_M \theta_M}{T}.$$

46

As implied by (9), smooth cyclic scanning of radiation pattern (3) with quadratic phase response for predetermined deviation of space frequencies $2\chi_M$ leads to time modulation of the space-time signal with deviation of the "time" frequencies equal to $2F_M$.

Let us consider a system that realizes an algorithm for shaping signal (9) for the case of utilization of a discrete aperture. In this case, we have on the basis of (7)-(9)

$$s(t;\theta) = S_0 I_0 \sum_{i=-\infty}^{\infty} \sum_{k=-m}^{m} \Pi\left[\frac{t-\chi T/\chi_M - i2T}{T}\right] \times$$

$$\times \exp\left\{j\left[2\pi f_0 t + 2\pi k\Delta\chi\theta + \pi\frac{F_M}{T}\left(t-k\Delta\chi\frac{T}{\chi_M}-i2T\right)^2 + \varphi_0\right]\right\}. \tag{10}$$

where $\Delta\chi$ is the distance between elements of the antenna array, and $2m+1$ is the number of elements in the array.
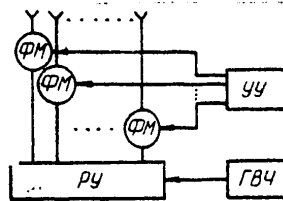
Fig. 2

A block diagram of a system for shaping $s(t;\theta)$ is shown in Fig. 2. Signals $s(t) = S_0 \exp\{j(\omega_0 t + \phi_0)\}$ from rf oscillator _ГВЧ_ are sent to the radiators of the array through distribution device _РУ_ and controllable phase modulators _ФМ_. The controlling voltages for the phase modulators are shaped in accordance with (10) by control device _УУ_.

The signals shaped by the system are uniformly distributed on plane $|t| \leqslant T$; $|\theta| \leqslant \theta_M$ (have a constant amplitude), are linear-frequency modulated with respect to both time and space coordinates, have identical shape in contrast to discrete-coded space-time signals [Ref. 5], and differ for different directions θ_i, θ_j only in the time displacement of $s(t;\theta_i) = s(t+\Delta t; \theta_j)$ by an amount

$$\Delta t = |\theta_i - \theta_j| T/\theta_M.$$

The possibilities for resolution and compression of signal $s(t;\theta)$ and evaluating its parameters are determined by the space-time uncertainty function

47

$$\psi(\tau;\eta) = C \left| \int_{-T}^{T} \int_{-\theta_M}^{\theta_M} s(t;\theta) s^*(t+\tau;\theta+\eta)\, dt\, d\theta \right| = \operatorname{sinc}^2 2\pi F_M \left(\tau - \eta \frac{T}{\theta_M}\right), \quad (11)$$

where C is a normalizing factor such that $\Psi(0;0) = 1$; $\operatorname{sinc} x = \dfrac{\sin x}{x}$. Un-

certainty function (11) has one main lobe and a comparatively low level
of side lobes. Since the uncertainty function describes signal behavior
at the output of an optimum processing system, the width of its main lobe
with respect to axes τ and η will characterize the degree of compression
of the space-time signal. The width of the main lobe with respect to
axes τ and η respectively on the zero level is

$$\Delta\tau = 1/2F_M = 2T/2\chi_M 2\theta_M; \quad \Delta\eta = 1/2\chi_M = 2\theta_M/2\chi_M 2\theta_M.$$

The curtailment factor [Ref. 2] in the given case is determined by the
product of the width of the space frequency spectrum $2\chi_M$ multiplied by
the duration of the space interval $2\theta_M$, which by definition [Ref. 4] is
the spatial base of the signal. The temporal base of the signal, defined
as the product of the width of the time frequency spectrum $2F_M$ multiplied
by signal duration 2T, coincides in the given instance with the spatial
base -- $2F_M 2T = 2\chi_M 2\theta_M$.

Let us proceed to examination of the particulars of optimum processing of
linear-frequency modulated space-time signals. As in Ref. 5, we will
assume that a field $y(t;\chi)$ arrives at the aperture of the reception
antenna system $[-\chi_{M\ прм}; \chi_{M\ прм}]$ on intervals of time $[-T_{прм}; T_{прм}]$ and
space $[-\theta_{M\ прм}; \theta_{M\ прм}]$ with distribution density with respect to angle
coordinate

$$y(t;\theta) = \sum_{i=1}^{n} s_i(t;\theta)\, \delta(\theta - \theta_i) + n(t;\theta),$$

which is a mixture of space-time signals (5) reflected or re-radiated by
objects located in sector $[-\theta_M; \theta_M]$ with thermal additive normal inter-
ferences uniformly distributed in space and described by the correlation
function [Ref. 1]

$$\langle n(t_1;\theta_1)\, n^*(t_2;\theta_2)\rangle = N_0 \delta(t_1 - t_2)\, \delta(\theta_1 - \theta_2).$$

We will consider processing of space-time signals on the same intervals
on which they were formed: $T_{прм} = T_{прд}$; $\theta_{M\ прм} = \theta_{M\ прд}$; $\chi_{M\ прм} = \chi_{M\ прд}$.

We will also assume that the angular spacing of the received signals
exceeds the Rayleigh limit $|\theta_i - \theta_j| \geqslant 1/2\chi_{M прм}$, and taking consideration
of situations that actually occur, we will disregard the influence of
signal envalope delay over the aperture.

In this case the expression for the optimum output effect of the process-
ing system takes the form

48

$$Y(\theta) = \left| \sum_{k=-m}^{m} \text{sinc } 2\pi\chi_{M}(\theta - k\Delta\theta) \times \right.$$

$$\left. \times \int_{-T}^{T} S_0 \exp\left\{-j\left[2\pi f_0 t + \pi\frac{F_M}{T}\left(t - \theta\frac{T}{\theta_M}\right)^2 + \varphi_0\right]\right\} Y(k\Delta\theta; t)\, dt \right|,$$

(12)

$$\text{where } Y(k\Delta\theta; t) = \int_{-\chi_M}^{\chi_M} y(t; \chi) \exp\{j2\pi k\Delta\theta\chi\}\, d\chi;$$

$$2m + 1 = 2\theta_{M\,\text{пр}M} 2\chi_{M\,\text{пр}M}; \quad \Delta\theta = 1/2\chi_{M\,\text{пр}M}.$$

Optimum processing algorithm (12) is realized by the same system (Fig. 3) as in Ref. 5. The system contains an antenna array with pattern shaper, each of the (2m+1) outputs sending waveforms Y(kΔθ;t) to temporal pro-
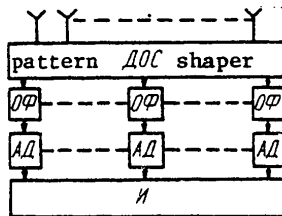
Fig. 3

cessing channels that consist of optimum filters (ОФ) and amplitude detectors (АД). The resultant aggregate of discrete values of Y(kΔθ) of the output effect

$$Y(k\Delta\theta) = \int_{-T}^{T} Y(k\Delta\theta; t) S_0 \exp\left\{-j\left[2\pi f_0 t + \pi\frac{F_M}{T}\left(t - \theta\frac{T}{\theta_M}\right)^2 + \varphi_0\right]\right\} dt$$

goes to the interpolator (И) which shapes output effect (12).

Let us consider the signal component $Y_s(\theta)$ and the interference component $Y_n(\theta)$ separately in output effect (12). In doing so, we will assume that the only significant parameter of the received signal s(t;θ) is the direction of its arrival

$$s(t; \theta) = S_0 \exp\left\{j\left[2\pi f_0 t + \pi\frac{F_M}{T}\left(t - \theta\frac{T}{\theta_M}\right)^2 + \varphi_s\right]\right\} \delta(\theta - \theta_s).$$

(13)

Substituting (13) in (12), we get

49

$$Y_s(\theta) = \left| \sum_{k=-m}^{m} \operatorname{sinc} 2\pi\chi_{_M}(\theta - k\Delta\theta) \int_{-T}^{T} S_0 \exp\left\{ -j\left[2\pi f_0 t + \pi \frac{F_{_M}}{T} \times \right. \right. \right.$$

$$\left. \left. \times\left(t - \theta\frac{T}{\theta_{_M}}\right)^2 + \varphi_0 \right] \right\} dt \int_{-\theta_{_M}}^{\theta_{_M}} s(t;\theta) \operatorname{sinc} 2\pi\chi_{_M}(\theta - k\Delta\theta)\, d\theta \right| \simeq$$

$$\simeq \left| S_0^2 2Te^{j(\varphi_s - \varphi_0)} \operatorname{sinc} 2\pi\chi_{_M\,\text{пр}_M}(\theta - \theta_s)\operatorname{sinc} 2\pi\frac{F_{_M}}{T}\left(t - \theta_s\frac{T}{\theta_{_M}}\right) \times \right.$$

$$\left. \times\left[1 - \frac{|t - \theta_s T/\theta_{_M}|}{T} \right] \right|.$$

(14)

Expression (14) implies that the signal component at the output of the optimum processing system is determined both by the characteristics of the reception system and by those of the space-time signal shaping system. The maximum value of the output effect $Y_{s\ max} = S_0^2 2T$ is formed for the direction that coincides with the direction of arrival of the received signal. In contrast to systems with discrete-coded space-time signals [Ref. 5] where the shape of the signal component of the output effect depends on the direction of arrival of the signals, in the given case no such dependence is observed, and the processing system forms an output effect of identical shape regardless of direction $|\theta| \leqslant \theta_M$. Shown in Fig. 4 is an example of the form of envelope of output effect (14)
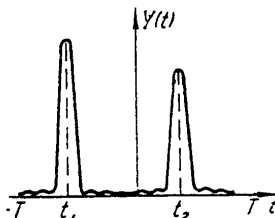
Fig. 4

for the case of reception of two space-time signals arriving from directions θ_1; $\theta_2 \in [-\theta_M;\ \theta_M]$. The time position of each of the pulses at the output of the processing system as read out relative to some fixed time is uniquely related to the direction of signal arrival $t_i = \theta_i T/\theta_M$. In this relation, the spatial distribution of objects in sector $[-\theta_M;\ \theta_M]$ is transformed to temporal distribution on interval $[-T;\ T]$, and curtate (compressed) signals (14) are produced at the output of the processing system. The resolution with respect to the time coordinate $\Delta\tau = 1/2F_M$ corresponds to angular resolution $\Delta\eta = \Delta\tau\theta_M/T = 1/2\chi_M$.

50

The interference component of the output effect is defined analogously to the signal component

$$Y_n(\theta) = \left| \sum_{k=-m}^{m} \text{sinc } 2\pi\chi_{_M}(\theta - k\Delta\theta) \int_{-T}^{T} S_0 \exp\{-j\,[2\pi f_0 t + \right.$$

$$\left. + \pi F_{_M}/T\,(t - \theta T/\theta_{_M})^2 + \varphi_0]\}\,dt \int_{-\theta_{_M}}^{\theta_{_M}} n(t;\theta)\,\text{sinc } 2\pi\chi_{_M}(\theta - k\Delta\theta)\,d\theta \right|$$

and is a normal random process with zero mathematical expectation and with correlation function

$$\langle Y_n(\theta_1)\,Y_n^*(\theta_2)\rangle = \left| \sum_{k=-m}^{m} \sum_{q=-m}^{m} \text{sinc } 2\pi\chi_{_M}(\theta_1 - k\Delta\theta) \times \right.$$

$$\times \text{sinc } 2\pi\chi_{_M}(\theta_2 - q\Delta\theta) \int\!\!\!\int_{-T}^{T} S_0 \exp\left\{-j\left[2\pi f_0(t_1 - t_2) + \pi\frac{F_{_M}}{T}\left[\left(t_1 - \theta_1\frac{T}{\theta_{_M}}\right)^2 - \right.\right.\right.$$

$$\left.\left.\left. - \left(t_2 - \theta_2\frac{T}{\theta_{_M}}\right)^2\right]\right]\right\}\,dt_1\,dt_2 \int\!\!\!\int_{-\theta_{_M}}^{\theta_{_M}} \langle n(t_1;\theta_1)\,n^*(t_2;\theta_2)\rangle \times$$

$$\times \text{sinc } 2\pi\chi_{_M}(\theta_1 - k\Delta\theta)\,\text{sinc } 2\pi\chi_{_M}(\theta_2 - q\Delta\theta)\,d\theta_1 d\theta_2 \right| \simeq$$

(15)

$$\simeq \left| S_0^2 2T\,\frac{N_0}{2\chi_{_M}}\,\text{sinc } 2\pi\chi_{_{M\,\text{прм}}}(\theta_1 - \theta_2)\,\text{sinc } 2\pi\chi_{_{M\,\text{прд}}}(\theta_1 - \theta_2)\left[1 - \frac{|\theta_1 - \theta_2|}{\theta_{_M}}\right]\right|.$$

Analysis of the energy characteristics of processing system (14), (15) shows that despite unification of all processing channels into one, in contrast to systems with complex radiation patterns and simple space-time signals [Ref. 6], the influence of the interference acting at the input of the processing system (Fig. 3) is attenuated by a factor of $2\chi_M 2\theta_M$. And with respect to its energy capabilities, this system is equivalent to an optimum multichannel system that realizes parallel scanning of space. The reason for the reduced action of interference, as in the theory of linear-frequency modulated time signals [Ref. 2], is the increased resolution of the system with respect to angle coordinates.

It should be noted that output effect (14) can be shaped by a system that uses a scanning radiation pattern $F_{CK}(\theta)$ of the type

$$F_{CK}(\theta) = \text{sinc } 2\pi\chi_M(\theta - t\theta_M/T),$$

51

FOR OFFICIAL USE ONLY

which maximizes the output effect when the maximum of the radiation
pattern $F_{CK}(\theta)$ coincides with the direction of signal arrival. However
the throughput of such a system will be limited since at the same instant
of time the signals arriving from other directions of the scanning sector
will not be received by radiation pattern $F_{CK}(\theta)$.

Thus the proposed algorithms for shaping and processing space-time sig-
nals enable shaping and compression of complex linear-frequency modulated
signals with respect to both time and space coordinates, ensuring high
angular resolution by extension of the spectrum of space frequencies
without narrowing the radiation pattern.

The proposed algorithms are distinguished by comparatively simple hard-
ware realization. And in fact the circuit that realizes the algorithm
for shaping linear-frequency modulated space-time signals is even simpler
than the analogous circuit for shaping discrete-coded signals [Ref. 5].
Elimination of the rather complicated and cumbersome pattern shaper in
the given case (Fig. 2) not only simplifies the hardware realization,
but also improves the quality characteristics of the system by reducing
energy losses and signal distortions in the pattern shaper circuits.
As for the circuit used in processing linear-frequency modulated signals
(Fig. 3), it should be noted that this is not the only possible con-
struction of a system for processing space-time signals. Analysis of the
output effect of the space-time processing system [Ref. 1, 5] shows that
with the same constraints as used in deriving (12), space and time pro-
cessing can be accomplished independently, and the design peculiarities
of the system will be determined by the processing sequence. For in-
stance in writing (12), preference was given to carrying out operations
of spatial processing first, which led to the necessity of using a
pattern shaper in realization. On the other hand, carrying out the
temporal processing operations first leads to a system without a pattern
shaper [Ref. 6], which in many cases simplifies the processing system
and improves its characteristics.

REFERENCES

1. S. Ye. Fal'kovich, "Otsenka parametrov signala" [Evaluating Signal
   Parameters], Moscow, "Sovetskoye radio," 1970.

2. Ya. D. Shirman, "Razresheniye i szhatiye signalov" [Resolution and
   Compression of Signals], Moscow, "Sovetskoye radio," 1974.

3. Drabovich, Orbi, Bonnas'ye, "Compression of the Radiation Pattern of
   an Antenna Array by the Method of Space-Time Coding," ZARUBEZHNAYA
   RADIOELEKTRONIKA, No 3, 1971.

4. A. I. Pogorelov, "Using Complex Radiation Patterns in Direction-Finding
   Systems for Resolving Signals in a Broad Scanning Sector" in: "Radio-
   tekhnika" [Radio Engineering], Vishcha shkola, No 37, 1976.

52

FOR OFFICIAL USE ONLY

FOR OFFICIAL USE ONLY

5. A. I. Pogorelov, "On the Theory of Noise-Like Space-Time Signals," IZVESTIYA VUZOV: RADIOELEKTRONIKA, Vol 22, No 7, 1979 p 3.

6. A. I. Pogorelov, "Analysis of Systems with Complex Radiation Patterns" in: "Metrologicheskiye voprosy prikladnoy elektrodinamiki" [Metrological Problems of Applied Electrodynamics], Proc. of Metrological Institutes of the USSR, Leningrad, 1978.

6610
CSO: 1860

FOR OFFICIAL USE ONLY

THREE SCIENTISTS IN FIBER OPTICS AWARDED A. S. POPOV PRIZE

Moscow VESTNIK AKADEMII NAUK SSSR in Russian No 8, 1980 pp 135-6

[Article: "A. S. Popov Prize Awarded to G. G. Devyatykh, Ye. M. Dianov and M. Ye. Zhabotinskiy"]

[Text]
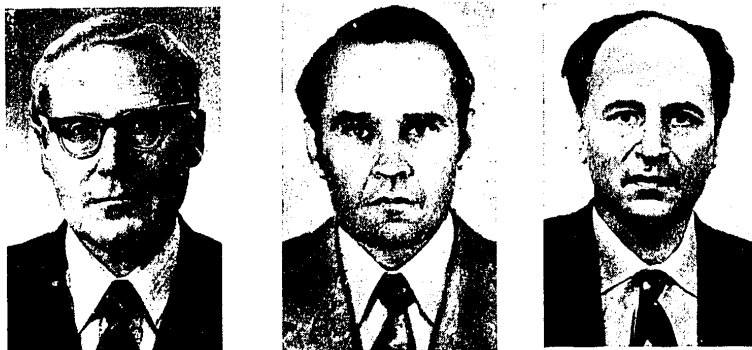
G. G. Devyatykh   Ye. M. Dianov   M. Ye. Zhabotinskiy

The Presidium of the USSR Academy of Sciences has awarded the A. S. Popov prize for 1980, in the amount of R 2,000, to Academician Grigoriy Grigor'yevich Devyatykh (Institute of Chemistry, USSR Academy of Sciences), Doctor of Physics and Mathematical Sciences Yevgeniy Mikhaylovich Dianov (Physics Institute imeni P. N. Lebedev, USSR Academy of Sciences) and Doctor of Technical Sciences Mark Yefremovich Zhabotinskiy (Institute of Radio Engineering and Electronics, USSR Academy of Sciences) for research in the development of low-loss fiber optical conductors for information transmission systems.

The series of works which was awarded the prize is a comprehensive study of the physical and information characteristics of fiber optical conductors, the development of the methodology and technology for manufacturing low-loss fiber optical conductors, including purification and analysis of the initial materials, as well as development of the metrics for fiber optical conductors and control over the manufacturing process.

54

Results of this work opened the practical possibility of creating wide-band
optical communications systems having the following significant advantages as
compared with existing ones: 1) Being wide-band in nature while maintaining
low losses (about 10 gigaHz/km) with losses of less than 1 dB/km;
2) Immunity to electromagnetic interference;
3) Small size and weight;
4) Replacement of scarce materials (copper, aluminum, lead) by glass; and
5) the Possibility of wide introduction of standardized digital information
transmission systems (because of the great wide-band nature).

The results have been introduced into industry. The fiber optical conductors
which have been developed will find broad application in telephone systems, in
cable television, in computer technology, in aircraft information transmission
systems, in systems for automating industry, transport and power engineering and
in a number of special devices.

COPYRIGHT: Izdatel'stvo "Nauka," "Vestnik Akademii nauk SSSR," 1980
[307-9194]

9194
CSO: 1860

FOR OFFICIAL USE ONLY

COMPONENTS AND CIRCUIT ELEMENTS, WAVEGUIDES,
CAVITY RESONATORS AND FILTERS

ASPECTS OF DESIGN OF NARROW-BAND FILTERS OF SURFACE ACOUSTIC WAVES

[Article by A. Ye. Znamenskiy, Ye. S. Muratov, V. N. Gulin]

[Text] In designing narrow-band filters of surface acoustic waves (PAV)
with relative bandpasses $\Delta f/f_0 < 5 \times 10^{-2}$, particular attention is given
to the choice of filter structure, methods of reducing spurious triple
passage signals (TP) and volumetric waves (OV), the need for accurate
realization of mean filter frequency, accounting for the effect of loads
and destabilizing factors on filter parameters. Let us examine each of
these problems based on the specifics of design of narrow-band filters in
particular.

Choice of filter structure

The primary material for sound guides of narrow-band filters is a quartz
slab of thermostable ST-section (xyl/42°45').

At the preset mean frequency, the lower limit of bandpass (PP) of the
filter is constrained by the possibilities of photolithography on large
surfaces (since the expanse of the interdigital transducer (VShP) is
inversely proportional to its PP), the increasing level of parasitic
signals in expanded VShP (reflection, diffraction on apodized structures,
signal attenuation in propagation) and the limited dimensions of existing
sound guides made from the ST-section of quartz.

Thus for relative PP $\Delta f/f_0$ about 10^{-2} and small intermediate frequencies
f_0, where long duration of pulsed filter response is necessary, it is more
advantageous to use a cascade connection of individual links with a
nonapodized VShP structure (Fig. 1c) instead of the traditional one-link
narrow-band filter PAV (Fig. 1a) consisting of apodized and nonapodized
VShP [1]. This makes it possible to greatly reduce the effect of the
aforementioned constraints. Figure 1c depicts a two-link filter structure
which theoretically permits production of a response curve of the type
$sinc^4$ x, where $x = \pi(f - f_0)T$, sinc x = (sin x)/x.

56

FOR OFFICIAL USE ONLY

With cascade connection of links of the type shown in Figure 1a, the overall dimensions of the device can be reduced somewhat by compactly arranging the apodized VShP. A natural bevel is produced on each slab which effectively reduces the level of signals reflected on the end face (Figure 1b).
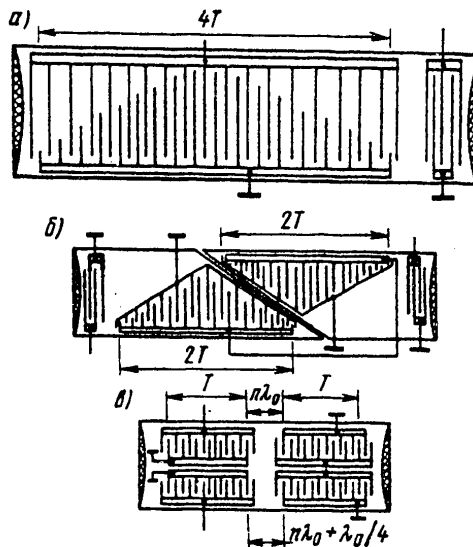
Figure 1

Spurious TP and OV signals

Existing methods of reducing TP signals, e.g. by arranging a metallized coating in the path of wave propagation resulting in a 180° phase shift of reflected waves with 1.6 dB power loss [2] or reduction in TP level (which, however, involves an increase in losses [3]), may be successfully used for the structure in Figure 1a.

For the structure in Figure 1c, in [1] a method of TP signal compensation is used with introduction of the appropriate shift between VShP in each link:

$$H_p = H_1 + (p-1)\lambda_s/2k.$$

where H_1, H_p are distances between the transmitting and receiving VShP in the first and p^{th} links of the filter, respectively; $p = 1,2 ..., k$; k is the number of links in the filter. This method does not introduce additional power losses.

For narrow-band filters PAV, the family of spurious OV signals situated in the direct proximity of the PP is the most hazardous; for example, for ST-quartz the nearest quasitransversal mode has a frequency which is 4.5 percent higher than the mean frequency of the filter f_0 [4]. The relative level of OV depends on the relationship of sound guide thickness t and surface wave length λ_0: thus for $t/\lambda_0 = 152/2\pi$, the relative level of these signals is no greater than -30 dB. Furthermore, a family of rapid quasitransversal and quasilongitudinal modes is excited with frequencies of 1.61 f_0 and 1.82 f_0 with relatively high levels (about 7 and 10 dB, respectively, below the primary signal). These spurious OV signals, aside from the methods of suppression noted above, can be effectively reduced by the filter's external matching circuits.

In [5] a method was considered for suppressing spurious OV signals by tapering the lower surface of the sound guide with respect to the upper one. Thus, in the example of a filter considered in [5] with a mean frequency of about 200 MHz and bandpass at a level of -3 dB of around 5 MHz, manufactured on a slab of ST-section quartz with a bevel of 3°, spurious OV signals were suppressed by more than 30 dB as compared to their initial level. Among the shortcomings of the method is the abrupt drop in effectiveness for relatively low frequencies 10-50 MHz. A method is also known for supressing spurious OV signals by construction of special two-channel receiving and transmitting VShP and a delay coating on one of the channels to support synphase reception of PAV and compensation of OV [6]. This method requires very precise parallelism between the surfaces of the sound guide and high precision of treatment of the lower edge to achieve effective suppression of OV: this makes manufacture of sound guides complicated. Furthermore, high identity of channels is required to achieve total compensation, and this is also difficult to do for expanded strutures.

In tests run on narrow-band filters of the structure shown in Figure 1a, the mean frequencys in the 40-90 MHz range, the level of spurious signals of the most hazardous OV (with frequency of about 1.045 f_0) was reduced 12-15 dB by putting notches on the bottom side of the sound guide. When the sound guide is 2 millimeters thick, the depth and spacing of the notch constituted 0.8 millimeter and 1 millimeter, respectively.
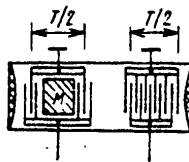

Figure 2

In combination with the absorptive coating applied to the notch which simultaneously is used for attachment of the sound guide to the housing, suppression of these spurious OV signals was greater than 45 dB.

For a two-link (cascade) structure of the filter shown in Figure 1b and 1c, spurious OV signals are no special problem, because with this design their relative levels in decibels are added. But when links are arranged on one sound guide to prevent OV transition from one link to another (due to overreflection on the bottom or side edges) it is necessary to use one of the methods considered. For example, in a two-link filter (Figure 1c) made from ST-section quartz slabs 5 millimeters thick, with a mean frequency of 12 MHz and bandpass of 62 kHz, application of the aforementioned notch on the bottom edge and an absorptive coating on the lower and side edges decouples the links by at least 45 dB.

Methods of adjusting mean filter frequency

Deviation of mean frequency of a narrow-band filter from the theoretical level is due to: straggling of the rate of propagation of PAV V_0 from specimen to speciemn on the order of $\pm$ 3 x 10^{-4}; change in the rate of propagation V on the metallized surface of the VShP due to technological scattering of the width of the digits and thickness of the coating; by the relationshp of the rate of propagation V as a function of the angle of misalignment of the piezocrystal and photomask during photolithography, etc.

Current methods for adjustment of mean filter frequency [7,8] are based on altering the rate of propagation of PAV in VShP by changing the thickness of the coating. This is achieved by etching an already existing coating or by applying a new dielectric coating by the vacuum method of deposition. Use of this methods for adjustment of the frequency of narrow-band filters with expanded VShP causes some problems related to the constrained technological possibilities of producing homogeneous and identically thick coatings on large areas.

A simple and accurate method for adjustment of the mean frequency f_0 of narrow-band filters represented by a combination of a comb filter (GF) and matched filter (SF) with double bandpass (Figure 2) was described in [9]. The essence of adjustment consists in changing the frequency of the "working" peak of the comb filter traveling inside a wider lobe of the SF with doubled bandpass. This is achieved by changing the delay between GF sections by means of elimination (application) of a section of metallization M. Therefore, in the case of narrow-band filters, the problem boils down to approximation of the required response curve by selecting SF with different bandpasses.

As illustrated by the resulting function sinc^4 (x), let us consider the process of synthesis of VShP ensuring f_0 adjustment of the entire filter.

1.   The function H(f) = sinc^4(x) is product of the response of four identical SF:

$$h(f) = \text{sinc}(x). \tag{1}$$

2.   Let us represent expression (1) in the form of a product of GF and doubled bandpass response:

$$\text{sinc}(x) = \frac{\sin x}{x} = \frac{\sin \pi (f - f_\bullet) T}{\pi (f - f_\bullet) T} = \frac{\sin \pi (f - f_\bullet) T/2}{\pi (f - f_\bullet) T/2} \cos \pi (f - f_\bullet) T/2. \tag{2}$$

Expression (2) coincides with the modulus of filter response as con-structed in Figure 2 to within a constant coefficient.

3.   Let us define the unknown pulsed filter response from AChKh:

$$H(f) = \text{sinc}^4(x).$$

For this purpose let us represent H(f) = H_1(f)H_2(f), where H_1(f) and H_2(f) are products of AChKh of GF and SF, respectively.

Let us then use the known theorem on the product of two functions [11]:

$$\int_{-\infty}^{\infty} g(\tau) f(t - \tau) d\tau = \frac{1}{2\pi} \int_{-\infty}^{\infty} F(\omega) G(\omega) e^{i\omega t} d\omega, \tag{3}$$

where F(ω) and G (ω) are spectra of two signals f(t) and g(t), respectively.

In this case, for pulsed reponse corresponding to H_1(f), F(ω) = G(ω) = cos π(f - f_0)T/2; for pulsed response corresponding to H_2(f), F(ω) = G(ω) = $\frac{\sin \pi (f - f_\bullet) T/2}{\pi (f - f_\bullet) T/2}$.

By alternately performing the geometric operation of convolution in accordance with the left side of expression (3), for all four comb filter structures, we find one apodized VShP. By carrying out convolution for two equidistant structures, we find another apodized VShP. As a result, together with the remaining two equidistant structures, we have four pulsed responses (four VShP) which we will combine into a two-link structure in Figure 3, where VShP 1 corresponds to convolution of pulsed responses of all four comb filters; VShP 2 corresponds to convolution of two equidistant structures; VShP 3 and 4 correspond to equidistant doubled-bandpass SF structures; M are sections of metallization, whose removal (application) ensures adjustment of meanfilter frequency; A_0 is an

60

FOR OFFICIAL USE ONLY

arbitrary unit of length.

Table 1 shows the theoretical values (in decibels) of change in levels of the first three side lobes of the function sinc^4 (x) as a function of frequency detuning of the "working" peak of function H(f) and mean frequency of the central lobe of function $H_2(f)$, in percents of the bandpass at a level of -3 dB. The tabular data show that this method of adjustment of the mean frequency in a very wide range of detuning has only a sli ;nt negative effect on the side lobe level; there is almost no change in reception efficiency at mean frequency.

Detuning, %	Designation of side lobes of function sinc^4 (x)					
	-3	-2	-1	+1	+2	+3
0	83.2	71.2	52.8	52.8	71.2	83.2
20	80.0	73.8	49.4	56.2	69.0	86.7
30	76.8	76.8	46	60	67.2	88
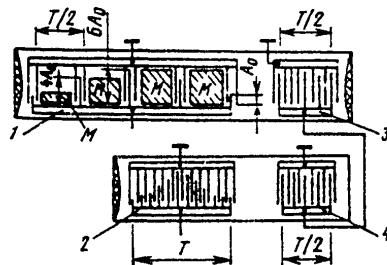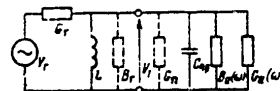
Fig. 3   Fig. 4

Effect of matching circuits on parameters of a narrow-band filter

To reduce the level of introduced losses of narrow-band filters, series or parallel inductances are used at the input and output of the filter to compensate for the static capacitance of the VShP at mean frequency f_0. Figure 4 shows the electrical equivalent circuit of a matched input VShP, where G_g and B_g are active and reactive conductances of the voltage generator V_g, respectively; $L = 1/\omega^2{}_0 C_{pr}$ is the compensating inductance; G_p is the conductance of ohmic losses in the metallized coating of the VShP; C_{pr} is static capacitance of the VShP; $G_a(\omega) =$

$$= (4/\pi) k^2 (\omega_e C_{np} N) \left(\frac{\sin x}{x} \right)^2 ; \qquad B_a(\omega) = (4/\pi) k^2 (\omega_e C_{np} N) \frac{\sin(2x) - 2x}{2x^2}$$

is the active and reactive conductance of VShP emission; $x = N\pi(\omega - \omega_e)/\omega_0$; k is the coefficient of electromechanical coupling of the sound guide

61

FOR OFFICIAL USE ONLY

material; N is the number of VShP electrode pairs.

The transmission coefficient H(f) of the input VShP based on the matching circuit

$$H(\omega) = \frac{V_1}{V_r} H_1(\omega) = \frac{G_r H_1(\omega)}{G_r + 1/i\omega L + i\omega C_{np} + i B_r + i B_s(\omega) + G_a + G_s(\omega)},$$ (4)

where $H_1(\omega)$ is the VShP response curve without matching circuit.

In [10] is cited analysis of expression (4) without consideration of B_g and G_p, while its basic conclusions are experimentally confirmed in [1]: under conditions close to matching ($1/\omega_0 C \approx \omega L$; $G_a(\omega_0) \approx G_g$), the level of side lobes of the amplitude-frequency curve of $H_1(\omega)$ double as compared to the case where there is no matching; and the bandpass of the primary lobe of the AChKh of $H_1(\omega)$ is expanded due to the frequency relationship of $G_a(\omega)$, leading to a reduction in the magnitude of the denominator of (4) with deviations from mean frequency.

Consideration of B_g (which may be conditioned by parasitic capacitance of assembly) in the denominator of (4) under nearly matched conditions results in a change in reactive conductances upon symmetrical detuning, i.e., asymmetrical expansion of the primary lobe of $H_1(\omega)$; this is equivalent to slight curvature of the AChKh (A-F response curve). For example, in experiments with a two-link filter of the structure in Figure 1c made on a slab of ST-quartz 100 x 20 x 5 millimeters in size, $f_0 = 12$ MHz with theoretical band neglecting matching circuits of 50 kHz and AChKh form $sinc^4(x)$ ($C_{pr} = 27$ pF, $1/G_a(\omega_0) = 3$ kohm, $1/G_g = 1.7$ kohm) the AChKh is shifted 2 kHz when parasitic capacitances of 5 pF are connected to the filter input and output; this is in good agreement with the estimate from (4). Consideration in (4) of the change in G_p during use (when exposed to destabilizing factors, for example) leads to a deviation in bandpass and introduced losses from the nominal rating.

The effect of temperature change on filter parameters

The chief destabilzing factor that affects filter parameters is wide temperature change. Experiments were run with mockups of a two-link filter described in the previous section in a temperature range from -50 to +65°C. Matching coils at the input, output and between links were mounted inside the housing and were teflon casings with dual-layer windings. Coil Q-factor $Q_L = 30$. The measured deviations in mean filter frequency due to temperature change are approximated by a parabolic function, i.e., they correspond to the known law of change of the temperature coefficient of delay in the ST-section of quartz. Maximum deviations of f_0 were 2 and 1 kHz, respectively, at t = -50°C and t = +65°C.

62

FOR OFFICIAL USE ONLY

In the course of the experiments deviation from nominal values of bandpass was observed within limits of 1 kHz and introduced losses within limits of 1 dB; this can be explained by the altered conductivity of ohmic losses in the metallized coating of the VShP which is obtained by chemical precipitation from a solution of silver film 0.08 microns thick.

These questions only touch upon some of the distinctive features of construction of narrow-band filters, an area which evidently has not been thoroughly investigated, but which affords interest for developers of surface-wave devices.

References

1. Bondarenko, V.S., Krylov, L.N., Muratov, Ye. S., Orlov, V.S., Voprosy radioelektroniki, seriya obshchetekhnicheskaya [Questions of radio engineering, general technical series], 1976, 7th ed.

2. Wauk, M., APPL. PHYS. LETT., vol 20, no 12, 1972.

3. Kheys, Khartman, TIIER, vol 64, no 5, 1976.

4. Wagers, R.S., TRANS. IEEE, v. SU-23, No 2, 1976.

5. Tanski, W., Acevedo, I., More R. A bulk mode suppression technique for surface wave devices. Ultrasonics Symposium, Proceed., Monterey, 1973.

6. Larosa, R., Vasile, C. ELECTR. LET. vol 8, No 19, 1972.

7. Haydl, W. Precision narrowband surface wave band pass filters. Ultrasonics Symposium. Proceeed., Milwaukee, 1974.

8. Nishikawa, K. An improved surface acoustic wave filters for a PCM timing tank. Ibid.

9. Znamenskiy, A. Ye., Muratov, Ye. S., ELEKTROSVYAZ' No 11, 1978.

10. Gonorovskiy, I.S., Radiotekhnicheskiye tsepi i signaly [Radio circuits and signals], Moscow: Sov. radio, 1971.

8617
CSO: 1860

63

FOR OFFICIAL USE ONLY

ELECTROMAGNETIC WAVE PROPAGATION, ELECTRODYNAMICS

UDC 621.371

EVALUATIONS OF THE EFFECTIVENESS OF DETERMINING PARAMETERS OF THE MARINE
SURFACE AND ATMOSPHERE BY SVCh (MICROWAVE) RADIOMETRY

Moscow RADIOTEKHNIKA in Russian No 5, 1980 pp 38-41 manuscript received
after revision 14 Aug 79

[Article by A. G. Grankov and A. M. Shutko]

[Text] Statement of the Problem

According to modern notions based on results of theoretical research and
measurement data, the field of intrinsic thermal radioemission of the
"ocean/atmosphere" system contains information on the nature of the
subincumbent surface and atmospheric parameters. The effect of individual
perturbation factors on the radiation properties of the system in various
sections of the spectrum is distinctive.

This feature determines the possibility of discrimination of perturbation
factors of surface Q^p and atmospheric Q^a origin, as well as evaluation of
their intensity [2, 3, 7, 8] according to data of measured radioluminescent
temperature T^{Ya} in specific sections of the spectrum λ_i:

$$T_{\lambda_i}^* = F_{\lambda_i}\left(Q_1^n, \ldots, Q_j^n, \ldots, Q_n^n, Q_1^*, \ldots, Q_i^*, \ldots, Q_m^*\right), \quad i = 1, \ldots, p; \quad p \geqslant n + m. \quad (1)$$

The accuracy of solution of the system of equations (1) is affected by the
following: (1) indeterminacy of initial data--values of T^{Ya}_i governed by
measurement error in radioluminescence as a result of calibration errors
ad fluctuating equipment noise; (2) indeterminacy of the operator F as a
result of imperfect notions about models of SVCh emission, the limited
amount of objective experimental data, and the wide natural diversity of
hydrometerological situations leading to ambiguity in the interrela-
tionship of radiation characteristics with characteristics of the ocean
and atmosphere.

To obtain reliable information on hydrometeorological parameters, it is
necessary to select spectral intervals of λ_i so that the solution is
resistant to the indeterminacies mentioned above.

64

In earlier studies by authors [7, 8] spectral intervals were defined as optimum for measuring perturbations of the surface type (surface temperature and wind velocity) under the assumption that atmospheric parameters (content of water vapor and water reserve of the clouds) are determined independently according to data of independent SVCh radiometry in the shortwave region and are considered to be allied perturbations.

A general solution is cited below, obtained by introducing four wavelengths into a standardized system of measurements. Spectral intervals are defined in the centimeter range of wavelengths 0.8-10 centimeters, optimum for measuring the temperature of the marine surface, intensity of swells (wind velocity), content of water vapor in the atmosphere and water reserve of clouds. Model estimates of analytic accuracy have been obtained for the characteristics in question under diverse hydrometeorological conditions.

Models and approximations

Underlying the choice of optimum wave lengths are the spectral features of formation of radiothermal emission of the water areas in the presence of various perturbing factors. In observation from artificial Earth's satellites, emission of the marine surface based on the effect of the atmosphere is described by the expression [1]

$$T_{\Sigma}^{s} = T_{M}^{a} e^{-\tau} + T^{*}(1 - e^{-\tau}) + T^{**}R(1 - e^{-\tau})e^{-\tau}, \qquad (2)$$

where $T^{ya}_{M} e^{-\tau}$ is the flux intensity of radioemission of the marine surface T^{ya}_{M}, attenuated in the atmosphere (coefficient $e^{-\tau}$); $T^{*}(1 - e^{-\tau})$ is intensity of direct flux of atmospheric emission; $T^{**}R(1 - e^{-\tau})$ is flux intensity of atmosheric emission reflected on the water surface; τ is the total integral absorption in the atmosphere composed of absorption in oxygen τ_{O2}, water vapor τ_{O} and droplet moisture of clouds τ_{W}: $\tau = \tau_{O2} + \tau_{O} + \tau_{W}$; R is the coefficient of reflection on the marine surface; T* and T** are effective (profile averaged) values of atmospheric temperature: approximately $T^{*} = T \approx T^{**} - T \approx 0.1T$; T is temperature of the marine surface.

The effect of temperature of radioluminescence of the calm marine surface is described by the expression $T^{ya}_{M} = \mathcal{H} T$, where $\mathcal{H}$ is the coefficient of emission of the marine surface defined by dielectric permeance of the water with parameters dependent on temperature, salinity and wavelength [1]. The spectral relationship of sensitivity of radioluminescence to variations in temperature $q_{\lambda}^{T} = \frac{\partial T^{a}}{\partial T}(\lambda)$ for various average values of T is shown in Figure 1 by the dotted lines. In calculations data were used on the relationshp of parameters $\mathcal{E}$ with temperature and wavelength from [6].

The effect of wind on radiation properties of the water areas in vertical sighting chiefly boils down to an increase in the coefficient of emission of the water surface due to the effect of foam formation (with wind velocity $V > V_{0} = 5-7$ meters per second). The interrelationship between V

and the increment in radioluminescence ΔT^{ya} is approximated by the linear relationship of the kind

$$\Delta T^s (V) = \begin{cases} 0, & 0 < V < V_*; \\ q_\lambda^v \cdot V, & V_* < V < 30 \text{ м/с} \end{cases}$$

(3)

The natural diversity of states of the surface of the world's oceans for the same wind velocities results in the ambiguity of radiation and wind relationships characterized by a dispersion of values $\tilde{q}_\lambda^v = q_\lambda^v + \delta q^v$. The spectral relationship of the slope coefficient q_λ^v obtained theoretically on the basis of the foam mechanism of brightening [2] and by systematization of data of experimental research [4, 5] is shown in Figure 1 by the solid lines.
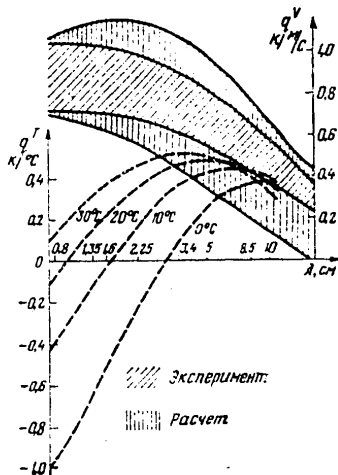
Figure 1
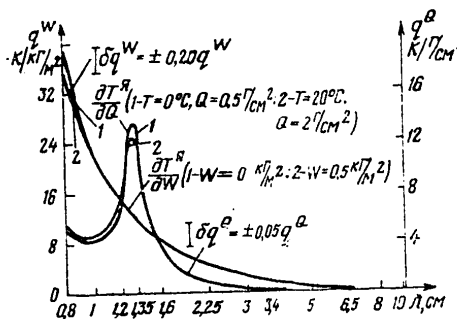
Figure 2

Integral characteristics of absorption of electromagnetic emission in the atmosphere T_Q and T_W are related, respectively, to atmospheric moisture content Q and water reserve of clouds W by linear relationships which are valid for W less than 0.5-1 kg/m^2: $T_Q = k_Q Q$; $T_W = k_W W$. The coefficients k_Q and k_W depend on wavelength. Figure 2 shows the spectral relationships of sensitivity of radioluminescence to variations in content of water vapor in the atmosphere $q_\lambda^Q = \frac{\partial T^s}{\partial Q} (\lambda)$ $q_\lambda^w = \frac{\partial T^s}{\partial W} (\lambda)$ (profiles of temperature, moisture content and pressure correspond to the model of standard

66

atmosphere). The dispersion of values of q^W and q^Q shown in the figure is due to changes in effective temperature of clouds within the limits of $-10 \leq T_{eff} \leq 30^\circ C$ and deviations of profiles of these characteristics from standard ones.

[Footnotes: 1. The effect of variations of salinity on radiation characteristics in the centimeter range is negligible and is not considered here.

In calculations, salinity was taken as equal to the average ocean value S = 35.7 promille. Possibilites of combined evaluation of temperature and salinity of the marine surface according to data of measurements in the decimeter range was considered in [8].

2. Calculation was done for a porous model of a homogeneous foam layer; the coefficient of porosity ranged from 0.95 to 0.99.

In the calculation the correlation relationship between the relative area of coverage with foam and the velocity of the wind was taken into account [4], and the frequency relationship of the increase in emissivity of sections covered with foam. In addition to the possible effect of model constraints, dispersion of theoretical values is explained by the constrained nature of data on the three-dimensional distribution of foam covers in thickness and concentration of air.]

Results of calculations

To determine optimum spectral intervals corresponding to the most stable solution of a system of radiation and geophysical relations (1) with respect to parameters T, V, Q, W, integral functions μ_T, μ_V, μ_Q, μ_W, are minimized; they characterize the transformation of errors of initial data into errors of analysis of said parameters. The sense of characteristics μ_{Q_j} is revealed by the vectorial interpretation of stability based on representation of the Jacobi matrix of a multiparametric relationship of (1) in the form of a system consisting of $\underline{n}$ vectors in $\underline{n}$-dimensional Euclidian space. The quantities μ_{Q_j} are expressed by parameters R_j and sin ϕ_j of the system $\mu_{Q_j} \sim 1/R_j \sin \varphi_j$,

where R_j is the length of the vector $q^{Q_j} = \{q_1^{Q_j}, ..., q_n^{Q_j}\}$

in n-dimensional space; $R_j = \sqrt{(q_1^{Q_j})^2 + (q_2^{Q_j})^2 + ... + (q_n^{Q_j})^2}$

ϕ_j is the angle between the vector q^{Q_j} and the hyperplane passing through remaining $n - 1$ vectors of the system. The quantity R_j describes the "effective" sensitivity of intensity of radioemission to variations of parameter Q_j in selected spectral intervals $\lambda_1, ... \lambda_n$. The quantity sin ϕ_j describes the degree of spectral distinctions, i.e., the degree of independence of measurements in spectral intervals $\lambda_1, ... \lambda_n$.

The solution of the problem is based on relationship (2) (vertical sighting) and relationships shown in Figures 1 and 2. Calculations were done at temperature $0 \leq T \leq 30°C$, wind velocity $0 \leq V \leq 20$ meters per second, content of water vapor $0.5 \leq Q \leq 3$ grams/centimeter^2, cloud water reserve $0 \leq W \leq 1$ kilogram per square meter.

Optimum sections of the spectrum were found in the range 0.8 to 10 centimeters and estimates of the critical nature of the solution to the criteria μ_T, μ_V, μ_Q, μ_W used, and also to values of the parameters T, V, Q, W themselves. Estimates of the effect of indeterminacy of spectra $q^V(\lambda)$, $q^W(\lambda)$, $q^Q(\lambda)$ on the accuracy of determination of the temperature of the marine surface and wind velocity were obtained in a wide range of hydrometeorological conditions.

Analysis of the solution showed that the position of optimum wavelengths weakly depends on the kind of goal function μ_{Qj} and more substantially on parameters T and V. In Table 1 are cited optimum spectral intervals obtained as a result of minimization of goal functions μ_{Qj} with respect to each of four parameters in the indicated limits of their variation.

Table 2 shows the root mean square errors of analysis of hydrometeorological parameters σ (T = 0°C, V = 0 m/s, Q = 0.5 g/cm^2, W = 0 kg/m^2) and their dispersion ν with change of λ_1, λ_2, λ_3, λ_4 within optimum spectral intervals, and also with change of parameters T, V, Q, W in the limits cited above (ν = 10 log $\frac{\sigma_{max}}{\sigma_{min}}$). In calculations it was accepted

that fluctuation error of measurement in each channel constitutes 0.2K.

Calculations show that minimization of the goal function μ_{Qj} with respect to parameter Q_j leads to minimum values of σ and ν for this parameter. With transition to the contiguous goal function μ_{Qk} (k ≠ j), deterioration of estimate accuracy does not exceed 5 percent, and ν increases 1-2 dB.

Accuracy of analysis of ocean and atmosphere parameters depends on hydrometeorological conditions. If the cloud water reserve does not exceed 1 kg/m^2, the deciding factor of variability is temperature of the ocean surface. For example, a rise in temperature from 0 to 20°C leads to an increase of errors σ_T and σ_V by a factor of two (Figure 3) [2].

[Footnotes: 1. The frequency of situations over the surface of water areas in which the parameter W varies within $0 \leq W \leq 1$ kg/m^2, constitutes 0.8-0.9.

2. Due to a decrease in spectral differences of emissive properties in variations of parameters T and V.]

FOR OFFICIAL USE ONLY

Table 1

λ_1, см	λ_2, см	λ_3, см	λ_4, см
0,8—0,85	1,35	1,6—2	8,5—10

Table 2

Q_j	T	V	Q	W
σ	0,6°C	0,5 м/c	0,04 г.см²	0,02 кг/м²
ч, дБ	5,3	6,7	4,7	5,2

Indeterminacy of the operator P_λ is a source of additional errors, dependent on measured local variations in hydrometeorological parameters T, V, Q, W. For example, indeterminacy of radiation and wind relationships governs the increase in error of analysis of temperature σ_T by 30 percent with local variations of wind velocity within ± 2.5 meters per second.

Figure 3 represents the relationship of σ_T as a function of T and V obtained on the basis of fluctuation errors of measurements and indeterminacy of spectra q_λ^V, Q_λ^W and q_λ^Q.
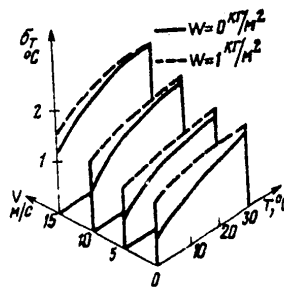
Figure 3

Table 1 shows that the optimum set of waves differs from that used aboard the "Kosmos-243" satellite by wave λ_3. Model estimates show that the use of λ = 1.6 centimeters instead of 3.4 centimeters makes it possible to raise accuracy of temperature analysis, water reserve of clouds and swell intensity by a factor of 1.5-2.

Conclusion

The presence of spectral features of interrelationship of radiation characteristics with hydrometeorological parameters of the ocean/atmosphere system makes it possible to find sections of the spectrum most effective for temperature analysis of the marine surface, wind velocity, atmospheric mosicure content and cloud water reserve. The position of the spectral intervals found is resistant to change of hydrometeorological conditions in wide limits. Accuracy of analysis of ocean and atmosphere parameters depends on values of the parameters themselves.

69

FOR OFFICIAL USE ONLY

FOR OFFICIAL USE ONLY

In addition to measurement errors for radioluminescence, an important component of errors of analysis of hydrometeorological parameters is the natural heterogeneity of the radiation and wind relationship and the indeterminacy of effective cloud temperature.

References

1. Basharinov, A.Ye., Gurvich, A.S., Yegorov, S.T. Radioizlucheniye Zemli kak planety [Radioemission of the Earth as a planet], Moscow: Nauka, 1974.

2. Shutko, A.M., Kutuza, B.G., Yakovlev, O.I. et al. Radiofizicheskiye issledovaniya planet. Itogi nauki, seriya Radiotekhnika [Radiophysical Moscow, VINITI, 1977.

3. Basharinov, A. ye., Shutko, A.M., Issledovaniye vzaimosvyazi kharakteristik polya teplovogo radiozilucheniya s sostoyaniyem poverkhnosti akvatoriy [Investigation of the interrelationship of characteristics of the field of thermal radioemission with the state of the surface of water areas], Preprint USSR Academy of Sciences' Institute of Radioelectronics, No 63, Moscow, 1971.

4. Soviet-American Experiment "Bering". Proceedings of Conclusive Symposium edited by K. Ya. Kondrat'yev, Yu. I. Rabinovich, V.L. Nordberg. Leningrad: Gidrometeoizdat, 1975.

5. Nordberg, W., Conaway, J., Thaddeus, P. QUART. J. ROY. METEOR. SOC. vol 95, No 404, 408, 1969.

6. Rabinovich, Yu. I., Melent'yev, V.V., TRUDY GGO vol 78, vyp 235, 1970.

7. Shutko, A.M., RADIOTEKHNIKA I ELEKTRONIKA vol XXIII No 10, 1978.

8. Grankov, A.G., Shutko, A.M., Theses of reports at XII All-Union Conference on Propagation of Radiowaves, vol 2, Moscow, 1978.

8617
CSO: 1860

70

FOR OFFICIAL USE ONLY

INSTRUMENTS, MEASURING DEVICES AND TESTERS, METHODS OF MEASURING
GENERAL EXPERIMENTAL TECHNIQUES

UDC 536.5.019.3:620.179

SCANNING DEVICE FOR CONTACT-FREE MEASUREMENT OF TEMPERATURE

Moscow IZMERITEL'NAYA TEKHNIKA in Russian No 7, 1980 pp 47-49

[Article by V. V. Aristov and F. I. Konzhukov]

[Text] The thermal method of non-destructive testing is now being more widely
introduced into various sectors of industry.

The structural irregularity and various defects of tested materials and items
governs the irregular distribution of thermal fluxes within a body which, in turn,
results in the appearance of temperature gradients on the surface. The heat
required for this may be liberated during the operation of the item or be
supplied from an external source. Recording of temperature differences, often
constituting fractions of a degree, is a rather complex problem, but the
knowledge of the temperature distribution along the surface of an item enables
us to solve the problem of defectoscopy and functional testing.

For quantitative processing of information contained in data on the distribution
of temperatures along the surface of an object of interest, the method of
thermal profiling is most suitable: it consists in producing curves whose points
are proportional to the temperature of the corresponding points on the surface.
This method is realized as follows: IR (inherent) emission of the specific section
of the test surface is focused by an optical system onto the sensitive area of
the emission sensor, at whose output is formed an electrical signal having an
amplitude proportional to the power of the IR emission striking the sensor. By
performing optico-mechanical scanning of the visual field of the sensor and
amplifying the electrical signal, an amplitude profile of IR emission of the
object is obtained along the scanning line.
This curve may be observed on the screen of an oscilloscope or be reproduced
by an automatic plotting device, be input into a computer or automatic control
system for processing.

This type of device enables us to measure the absolute temperature and
temperature differences along the scanning line at high speed; to dynamically
monitor the thermal field; and also to measure the temperature of moving
objects and large-scale items with high productivity.

71
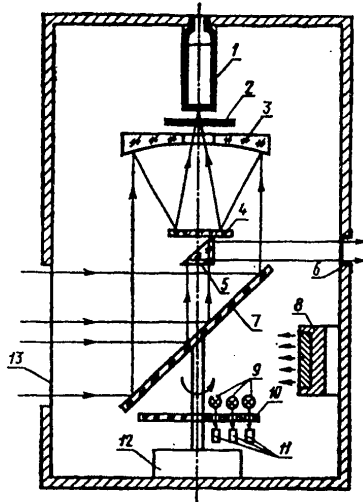
Figure 1

Because of the contact-free method, it is possible to monitor the quality of items at a considerable distance from the object.

Similar devices are used in automated control systems for production of glass sheet, plastics, to monitor rolling, high voltage power transmission lines, etc. With the active thermal method using this device, it is possible to monitor the quality of soldered, welded and glued joints. In these cases the instrument enables us to detect defects of the exfoliative, fracture, cracking, imperfect glueing type.

Figure 1 shows an optical arrangement of the base device IK-10T.

to oscillograph

Figure 2

72

IR emission from the object passes through the input window (13) and strikes the mirror (7) which is sloped at an angle of 45° to the optical axis. After being reflected on it, the emission flux enters the main spherical mirror (3) of the objective lens. The focused flux, being reflected on the counterreflector (4) and passing through a spectral filter (2), strikes the sensitive area of the receive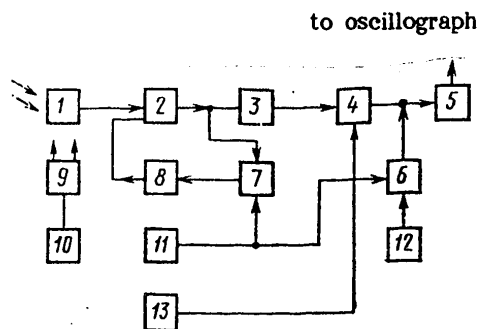r (1). The mirror (7) is rotated by an electric motor (12) and rotates the visual field of the lens from 0 to 360° at a frequency of 25 Hz. In the visual angle of 80°, the objective lens perceives emission from the object through the input window (13). Opposite the input window is the reference emitter (8), whose temperature is kept constant to within 0.2 $^{\circ}$C. The thermal emission from the reference emitter arrives at the receiver with a phase shift of about 90° with respect to the signal coming from the object of interest.

Some of the input flux enters the prism (5) and then strikes the aiming (6) eyepiece. Using this eyepiece it is possible to aim the instrument at the object of interest. On the axle of the electric motor is placed an opaque disk (10), synchronizer with specially shaped notches. On one side of the disk there are three lights (9) and on the other, three photocells (11). When the disk is rotated sync signals are received from the photodiodes. The emission receiver is a photoresistor of InSb with sensitive area 0.3 x 0.3 millimeters in size cooled by liquid nitrogen.

The signal recorded from the recevier is proportional to flux W of IR emission acting on the sensitive area based on the spectral characteristics of the receiver.

According to [1] we can write down

$$W = \frac{q_{пр} \cdot D_{вх}^2}{4 (f')^2} \int_0^{\infty} \tau_{оп}(\lambda) \cdot \varepsilon_{\lambda}(\lambda, T) \cdot s_{\lambda} \cdot W_{\lambda}(\lambda, T) \, d\lambda, \qquad (1)$$

where q_{pr} is the area of sensitivity of the receiver; D_{in} is the effective diameter of the objective lens; f' is the focal distance of the lens; $tau_{op}(\lambda)$ is the transmission coefficient of the optics; $\varepsilon_{\lambda}(\lambda, T)$ is spectral emissivity of the object of interest; s_{λ} is the adjusted spectral sensitivity of the receiver; $W_{\lambda}(\lambda, T)$ is the spectral density of emission power of an absolutely black body with the object's temperature; λ is the emission wavelength; T is the absolute temperature of the object.

The relationship of W as a function of the object's temperature is essentially nonlinear, and to obtain voltage which is linearly dependent on temperature, the signal must be appropriately processed. Figure 2 shows the block diagram of the IK-10T device. IR emission of the object strikes the emission receiver (1), is converted into an electrical signal and enters one of the inputs of a differential amplifier (2). With a shift in time, this same amplifier input receives a signal from a reference emitter (9). The amplified signal from this emitter passes through a block body pulse selector (7) and enters a level memory circuit (8). Continuous voltage, proportional to the signal from the reference emitter, is

73

sent from the level memory circuit to the second input of the differential amplifier (2). Therefore, the differential amplifier reacts to differences between the level of the reference signal and the signal from the object along the scanning line. This is a prerequisite for stable measurement of absolute temperature when the ambient temperature, receiver parameters, etc. undergo change. Then the amplified signal enters the linearizer (3) which linearizes the relationship of the output signal versus absolute temperature of the object. The form of the linearized function will change according to the types of spectral filter and receiver; thus the linearizer should be attuned to specific device.

From the output of the linearizer, the signal is fed to the working stroke selector (4) which only passes it when the input window is located in the visual field of the emission receiver. The selector is opened by pulses shaped in the synchronizer (13). A signal for the selector enters the input of the output amplifier (5). To the same input are fed two different voltage constants across the isotherm selector (6) in turns; their level can be controlled from the isotherm generating circuit (12). The isotherm selector is opened with a time shift as compared to the working stroke selector. Therefore, in one rotation of the scanner, the input of the output amplifier receives a signal from the object, a zero level (readout level) and pulse of constant amplitude (isotherm). During the next rotation of the scanner, everything is repeated except that the isotherm pulse already has another level. After the output amplifier, the signal is fed to the oscillograph which is synchronized from the IK-10T device to trigger two scanning lines in one rotation: one scan when the temperature profile is produced on the screen and a second one when the isotherm is reproduced. The signal from the output may also enter the input of the ASU and for processing on computer. The presence in the signal of two isotherms makes it possible to establish the boundaries of permissible deviations in temperature from the nominal. Measurement of absolute temperature and temperature differences are made on the oscillograph screen. Figure 1 also shows the automatic temperature control system (10) and synchronizer (11).

The IK-10T device has the following technical specifications: range of measured temperatures 100 to 800°C; basic error no more than 4 percent of measured value; minimum recorded difference no more than 0.5°C; instantaneous angle of visual field 3 mrad (i.e., instantaneous field of vision is 6 millimeters at a distance of 2 meters and 30 millimeters at a distance of 10 meters); the angle of the field of view is 80°; scanning rate at least 20 Hz; the instrument is powered by 220 VAC/50 Hz; the device weighs no more than 12 kilograms; the spectral range of the device depends on the type of spectral filter, and the spectral range of the emission receiver goes from one to 5.6 microns.

74

The device consists of two blocks: the receiving chamber unit which contains the emission receiver and scanning sytem; and the monitoring and control unit. Its calibration and testing should be done using a reference thermal emitter of the absolute black body (AChT) type, whose emissivity ε does not depend on the temperature of the AChT and wavelength of emission λ ; wherein ε is greater than or equal to 0.97. The angular dimensions of the output aperture of the AChT should be at least twice at great as the instanteous field of view of the device. In this instance, instrument readings do not depend on distance. When calibrating the device, the temperature of the AChT which is measured by thermoelectric thermomometer is smoothly varied in the working range of temperatures and the instrument readings read out on the oscillograph screen are compared with the thermometer readings.

When measuring the temperature of real objects it is necessary to consider that their emissivity, in contrast to AChT, is less than unity and depends on λ and temperature of the object; thus instrument readings will differ from the true temperature of the object. Consideration of emissivity and introduction of the proprer corrections is generally a difficult task, but many real objects in a limited range of temperatures can be considered as "gray" bodies: bodies whose emissivity differs from unity, but does not depend on λ and T [2]. For such objects, with reception of emission in a limited spectral range, the emission flux acting on the receiver can be written down as follows:

$$W = \varepsilon c T^q,$$

(2)

where ε is emissivity of the object; c is the coefficient of proportionality; q is the exponent depending on the spectral characteristics of the receiver ($3 \leqslant q \leqslant 5$).

At the output of the instrument, the voltage is proportional to temperature and consequently, in conformity with (2), is $\sqrt[q]{\varepsilon}$. Therefore, to introduce a correction for emissivity, output voltage should be multiplied by the constant . When emissivity is greater than or equal $\dfrac{1}{\sqrt[q]{\varepsilon}}$

to 0.9, additional error due to change in ε does not exceed the basic error (4 percent).

The IK-10T device has successfully passed state receiver tests and is recommended for series production.

References

1. Garrison, G.R., Radiatsionnaya pirometriya [Radiation pyrometry], Moscow, "Mir" 1964.

75

2. Kriksunov, L. Z. Spravochnik po osnovam infrakrasnoy tekhniki [handbook on infrared technique], Moscow, "Sov. radio" 1978.

COPYRIGHT: Izdatel'stvo standartov, 1980
[12-8617]

8617
CSO: 1860

76

UDC 681.7.064.63.089.6

LIGHT BEAM SPLITTER FOR CALIBRATING THE PHOTOMETRIC SCALE OF OPTICAL DEVICES

Moscow IZMERITEL'NAYA TEKHNIKA in Russian No 7, 1980 pp 25-26

[Article by V. N. Vatulev, P. L. Klimenko, A. I. Somsikov, O. V. Aleksandrov and N. S. Golyandin]

[Text] A method of calibrating the photometric scale of spectrophotometers by splitting the light beam into two yielding equal signals at the photometer output is described in [1, 2]. A device containing two independently traveling delicate, opaque shutters with contiguous edges was used. The independence of travel of the working shutters through the cross section of the light beam is not, however, a prerequisite for this method of calibration.   The use of a splitter with interconnected shutters offers advantages which will be discussed below.

In the figure is schematically depicted one possible version of such a device. The working shutters (1, 5) for splitting the luminous flux are attached to plates (2). For withdrawal (jointly or severally) of shutters (1) and (5) from the light beam (A), the plates (2) bearing the shutters are rotated around the axles (11) until they contact the stops (10). The axles (11) and stops (10) are attached to a common base (4) on which is also fixed a stop (3) which interacts with the plates (2): it locks the shutters (1,5) in working position. The connection of force between the plates (2) and the stop (3) (in working position of shutters 1, 5) or stop (10) (in withdrawn position) is effected by a spring (15). The position of the shutters (1, 5) with respect to the stop (3) must ensure contact of leading edges (16) of the shutters along their entire length.   The shutter micro-adjustment mechanism in the plane of cross section of the light beam (A) consists of guides (14), micrometer screw (6) and reversing spring (12). The macroadjustment shutter mechanism contains guides (8) mounted in the housing (7) of the calibrated instrument, for the slide block (13). The locking device (9) assures attachment of the slide block (13) on the guides (8): coarse locking of shutter (1,5) position with respect to beam (A). The functions of the shutter microlock are fulfilled by the micrometer screw (6) which interacts directly with the base (4). The presence of two base traveling mechanisms assures rapid and precision establishment of any coefficient of light division.

77

FOR OFFICIAL USE ONLY
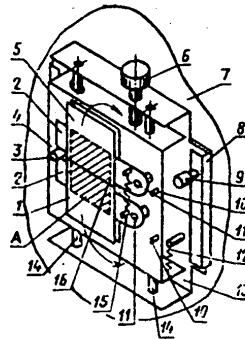
It was emphasized in [1] that the main requirement for calibration by the method of splitting of light flux is satisfaction of the condition of geometric complementability and intensity of the portions of luminous flux produced with the aid of the shutters. It is therefore important that the shutters close without gaps or overlaps. In the design in question, control of the juxtaposition of the shutters upon closure is performed once when the device is assembled, and it may therefore be done more carefuly than in a design in which there is no connection between the shutters. The spring (15) guarantees high reproducibility of shutter position upon reintroduction into the beam. Therefore the closeness of shutter closure is reliably assured and it becomes unnecessary to continously monitor the alignment of the shutters' leading edges: this greatly facilitates and speeds up of the calibration process.

ИКС-14		ИКС-14 A	
T, %	Δ, %	T, %	Δ, %
6.25	0.1	6.25	0.3
12.5	0.15	9.375	0.25
18.75	0.25	12.5	0
25	0.35	18.75	0.1
31.25	0.05	25	0.3
37.5	0	31.25	0.25
43.75	0.15	37.5	0.1
50	0.05	40.625	0
56.25	0.05	43.75	0
62.5	0.05	50	0.1
68.75	0.15	56.25	0.1
75	0.2	59.375	0.15
81.25	0.05	62.5	0.05
87.5	0.15	68.75	0.1
93.75	0.15	75	0.2
		81.25	0.3
		87.5	0.1

This splitter was manufactured at LOMO and has been used to test IR transmission scales of the IKS-24 spectrophotometer [3]. Transmission scale error was determined with the aid of two devices: a set of rotating sector disks (PKS-731 device) and the aforementioned splitter. It was found that the discrepancy of results did not exceed 0.3 percent. In contrast to the PKS-731,

78

FOR OFFICIAL USE ONLY

FOR OFFICIAL USE ONLY

which permits testing the scale of the instrument being calibrated only at ten points (in conformity with the number of standard disks it contains), the splitter makes it possible to produce any number of points in any field of the scale and cover those sections of the scale which are not covered by the PKS-731 device.

The table shows the discrepancies (delta) in transmission scale between calibration curves obtained by splitting luminous flux and using the sector disks (PKS-731 device). The tabular data enable us to assess the convergence of results in calibration of the IKS-14 and IKS-14A spectrophotometers.

The splitter under consideration also enables us to rapidly test the linearity of the photometric scale. For this purpose, using the coarse adjustment mechanism, the dividing line of the plates (16) is moved along the cross section of the light beam, it locked in several arbitrary positions and in each of them it is determined whether or not therre is equality between the instrument readings when both shutters (1) and (5) are withdrawn from the luminous flux (transmission T = 100 percent), and the sum of instrument readings $T_1 + T_2$, when only shutter (1) (T_1) or shutter (5) (T_2) is in working position.

References

1. Klimenko, P.L., Vatulev, V.N., ZhPS vol 19 iss 4 1973.

2. Klimenko, P.L., Vatulev, V.N., Patent description No 374570, "BYULL. IZOBRET. No 15 1973.

3. Golyandin, N.S. et al., ZhPS vol 23 iss 4 1975.

8617
CSO: 1860

79

FOR OFFICIAL USE ONLY

FOR OFFICIAL USE ONLY

OPTOELECTRONICS, QUASI-OPTICAL DEVICES

UDC 389.14:681.785.57:62-503.5

PRECISION SERVO SYSTEM FOR OPTICAL INTERFEROMETERS

Moscow IZMERITEL'NAYA TEKHNIKA in Russian No 7, 1980 pp 26-27

[Article by M. N. Dubrov]

[Text] The accuracy of determining the position of poles in optical inter-
ferometers is of great value for measurements of length, travel, optical density
of matter, and when interferometers are used as highly sensitive transducers of
small forces, displacements and deformations. The highest indicators have been
obtained using photodetectors which have a measurement sensitivity of up to
10^{-5} within a single interference band [1-3].

The results are shown below of tests run on a device which operates on the
principle of photocompensation measurement systems with degenerative feed-
back [4]. The servo system enables us to continuously record displacements of
the pattern with a resolution of 10 interference bands with a sensitivity of 10^{-4}
periods or 0.03 nanometers at a wavelength of 0.63 microns.

The scheme of the device (Figure 1) in highly analogous to the servosystem of
a laser seismograph in [5]. The interference pattern (1) is focused by a lens (2)
on the moving mirror of the galvanometer (3) and is then projected onto an
optical discriminator (4) which is a transparent/reflective grating whose lines are
applied on the glass plate as parallel interference bands and whose spacing
coincides with the period of the pattern. The portions of luminous flux passing
through and reflected on the discriminator enter the photodetectors (5)
connected via a differential circuit to the input of the D.C. amplifier (6) whose
output is connected to the mirror galvanometer. At the point of equilibrium of
the system, the interferogram is situated with respect to the discriminator so
that the optical signals entering both photodetectors are equal. When the in-
terference bands (1) are moved in any direction, an imbalance of the
appropriate sign appears in the system and the galvanometer mirror (3) moves
the interferogram image with respect to the discriminator (4) to compensate for
the displacement of bands. The signal (current or voltage) which controls the
galvanometer is proportional to the shift in the pattern and part of its is used
for recording by device (7).

The range of measurable displacements N_{max} is defined by the number of lines
of the discriminator, but can not exceed
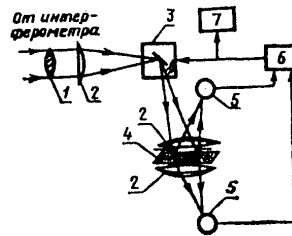
$$N_{max} < \beta d/\lambda,$$

80

FOR OFFICIAL USE ONLY

Figure 1

where beta is the maximum angle of deflection; d is the diameter of the galvanometer mirror; lambda is wavelength. The speed of the servo system is limited only by the time lag of the mirror galvanometer. When using the galvanometer from a CRT oscillograph it is easy to realize a band of frequencies from 0 to 1 kHz. An important aspect of this compensation system is that the actuator is not directly connected to the optical interferometer and does not disturb its operation.

The block diagram of a device for testing the servo system is shown in Figure 1. The interferometer (2) is assembled on a vibration-damped table. It is a Michaelson interferometer with equal arms about 10 centimeters long. One of its mirrors is attached to a piezoceramic transducer with a range of travel of several micrometers. For protection against convective air flows and other thermal oscillations, the interferometer is screened by a metal housing. The light source is a He-Ne laser (1) (wavelength = 0.63 micron). The total power of the interfering beams at the input of the servo system (3) is about one milliwatt. The device is calibrated by measuring, using a diagram tape of an automatic recorder (5,6), the distances between neighboring points of equilibrium of the system with a stationary interference patttern; this corresponds to displacement of the pole by exactly one period: 0.316 micron. The block diagram also shows a photocompensation microvoltmeter (4) and the control unit (7) of the interferometer piezotransducer.

To measure piezoelectric characteristics, a linearly fluctuating voltage with an amplitude of + 500 V is fed to the transducer and simultaneously the displacement of the interference pattern is recorded. On the diagram of the dual-coordinate automatic recording device were obtained hysteresis loops typical for the given material. The range of motion was two microns: more than six interference bands.

When rectangular voltage pulses with an amplitude of 50 millivolts are fed to the piezotransducer, the servo system establishes the mirror displacement on the
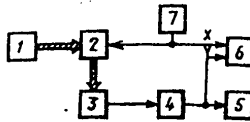
81

Figure 2

order of 0.1 nanometer. The noise, whose level is roughly 1/3 of the mirror displacements, can be explained by the instability of the optical density of air in the arms of the interferometer; the mean quadratic amplitude of fluctuations of the index of refraction corresponds to a value on the order of 10^{-10} [6]. It should be mentioned that the maximum sensitivity definable by the quantum nature of light [2] for the chosen power of interfering beams in the frequency band of one Hz is on the order of 10^{-7} of the period of the pattern. Thereby exists the principal possibility of increasing the sensitivity of the servo system by two to three orders. The device under consideration may also be used in interference measurements in the IR, UV and other regions of the spectrum.

References

1. Kartashev, A.I., Etsin, I.Sh., UFN vol 106 iss 4 1972.

2. Moss, G.E. et al. APPL. OPT. vol 11 No 11 1971.

3. Zakharov, V.P. et al., PTE No 6 1976.

4. Dubrov, M.N., Karmaleyeva, R.M., IZV. AN. SSSR. FIZIKA ZEMLI No 7 1976.

5. Veli, V., Bostrom, R. PRIBORY DLYA NAUCHNYKH ISSLEDOVANIY No 9 1968

6. Dubrov, M.N. RADIOTEKHNIKA I ELEKTRONIKA vol 21 No 10 1976.

8617
CSO: 1860

PHOTOCELL WITH HIGH TIME RESOLUTION FOR THE VACUUM ULTRA-
VIOLET

[Article by L. I. Andreyeva, V. V. Demin, P. M. Lozovskiy, Z. M. Semichastnova,
S. P. Chernov and A. I. Yuzhin]

[Text] Until recently in the region of the vacuum ultraviolet (VUF) there were
not receivers with sufficient time resolution. We developed a coaxial photocell
(FEK) based on phototcells to record VUF pulses of emission of nanosecond
length [1].

A copper disk mounted on the central rod of the coaxial output is used as the
FEK cathode; a grid made of finely structured fabric with a mesh of 500 microns
serves as the anode; it is connected to the outer sheel of the coaxial output.
The distance between the anode and cathode is 0.8 millimeters. Cesium iodide,
which has high quantum output and is resistant to oxygen when the photocathode
travels through the air, was selected as the emission layer. The latter is very
important with today's manufacturing technology. An important parameter is the
thickness of the cesium iodide layer which has high specific resistance. The
optimum thickness is 200 to 320 angstroms. An FEK with cesium iodide
photocathode is barely sensitive to emission with a wavelength of more than 200
nanometers; the photoemission threshold is 6.4 eV.

For the section of VUF from 105 to 200 nanometers there are transparent
materials for input windows and sealed designs are preferable to designs with an
open input. Plane parallel disks 25 millimeters in diameter and 1 to 1.5
millimeters in thickness cut from single crystals of lithium, magnesium or
calcium fluoride were used as windows. The short-wave boundary of passage of
these windows was 105, 110 and 120 nanometers. The window for the thermal
compensation ring made of silver foil 0.2 nanometers thick and the rings for the
support washer made of sintered glass are sealed by pre-cleaning in a salt
vacuum of silver chloride which does not react with the noble metals. The
active additive to provide good adhesion of the solder to the crystals of alkaline
and alkaline-earth fluorides was ammonium hexafluorotitanate based on a
calculation of 0.2 to 1 milligram of activator per square centimeter of crystal
contact surface. The photocells were thermocycled in a temperature range of
20 to 320°C. The transparency of the crystal in VUF after soldering and heat

83

treatment did not change.

The instruments passed the mechanical and climatic tests conducted in conformity with [2].

To study the time characteristics of FEK, emission of hydrogen VUF of a laser with wavelength 1651 nanometers   was used. The laser pulse has a width on the order of several nanoseconds, because the lifetime of the upper laser level is less than one nanosecond, and the junction used for generation is self-limited. The recording system consisted of the FEK, a section of RK-75-9-12 coaxial cable 1.5 meters long, a TBPD-16 coupling capacitor, a section of RK-75-9-12 coaxial cable 2.5 meters long, the 12-7 oscillograph. The measured width of the advancing pulse front was 0.4 nanosecond. The time constant of the entire recorded system, defined by the pulse drop, was 0.9 nanosecond.

References

1.   Andreyeva, L.I., Stepanov, B. M.   IZMERITEL'NAYA TEKHNIKA No 8 1965.

2.   GOST 22261-76 "Devices for measuring electrical quantities.   General technical specifications".

8617
CSO: 1860

._____

UDC 535.854:621.325.29

DYNAMIC HOLOGRAPHIC MONITORING OF INTERNAL HETEROGENEITIES OF SEMICONDUCTOR MATERIALS IN THE NEAR INFRA-RED REGION

Moscow IZMERITEL'NAYA TEKHNIKA in Russian No 7, 1980 pp 23-25

[Article by L. N. Gnatyuk, M. L. Gurari, S. V. Mamakina and S. N. Marchenko]

[Text] The measurement of phase distortions of optical elements which are not transpaᵣent in the visible part of the spectrum using holography was reported in [1]. Measurements were made at a wavelength of 1.06 microns; the emission sensors were IAE-6 photodetector chips sensitive to ੭e near IR-region. In theory, however, the use of photodetectors does not solve the problem of designing dynamic quality control devices for objects in the visible and near IR-region. The need is particularly urgent for dynamic means of holographic quality control in cases where we must carry out rapid defectoscopy of many elements of complex form.

The most suitable recording medium in dynamic systems of holographic quality control of materials are magnetic MnBi films. Their sure advantages over photodetectors is that they are not selective to the wavelength of recorded emission; they do not require additional processing to reconstruct the image after recording; and they permit repeated recording and erasure on a single piece of film. Furthermore, MnBi films have high resolution up to 2,000 lines per millimeter. In [2, 3] are cited hologram recordings of diffusely scattering objects with radiation of the near-IR on MnBi films, and methods are described for making repeated recording of holograms on these films.

Let us consider the method of dynamic monitoring of phase irregularities at a wavelength of 1.06 microns with the aid of real-time holography on MnBi films.

As we know, in real-time holography, the hologram of the object of interest is produced with the aid of reference and object beams; then the recorded image is reconstructed from the hologram; the object of interest is illuminated by the object beam and we observe the real-time interference pattern between the wave reconstructed from the hologram and the wave coming directly from the object. However, when optically active recording media (e.g., magnetooptic films) are used as holograms, it is necessary to take into account the direction of polarization of the light used in the reconstruction stage, which is a considerable complement to the traditional method of real-time holography.

85

Let us consider the factors affecting the visibility of the interference pattern with real-time holography using optically active recording media. Reference and object beams having parallel directions of polarization in the plane of the hologram are usually used to produce a hologram, because only parallel vector wave components interfere with each other.

In Figure 1 is shown a diagram of the direction of the electrical vector for the object and reconstructed waves. Let the direction of polarization of the reference and object beams ue parallel to axis OY. Let us also consider that when the image is reconstructed from the hologram recorded on MnBi film, the direction of polarization of the reconstructed wave in the first order of diffraction is perpendicular to the direction of polarization of the reconstructing wave [4-6]. When the object beam illuminating the object passes through the hologram recorded on MnBi film, the beam in the 0th order changes the direction of polarization through an angle psi. The value of the angle psi may be obtained by considering the shape of the diffraction grating recorded on the hologram. A plane wave polarized along axis OY falling on a binary magnetooptic diffraction grating has an amplitude along the x-axis (see Figure 1):

$$E_x = 0; \quad E_y = E_0. \tag{1}$$

After interaction with the holographic medium in its direct proximity, the wave has amplitude values in the zero order of diffraction

$$\left. \begin{aligned} E_{nx} &= \xi E_0 \frac{2s - d}{d} \sin\theta; \\ E_{ny} &= \xi E_0 \cos\theta, \end{aligned} \right\} \tag{2}$$

where ksi is a coefficient characterizing light energy losses in interaction with the recording medium (for a Kerr effect grating, ksi = R, the Fresnel coefficient of reflection; for a Faraday effect grating, ksi = e^{-al}, where a is the coefficient of absorption, l is the film thickness); θ is the angle of rotation of the displacement vector of the wave after interaction with the magnetized medium; d is the period of the diffraction grating; s is the size of the section which has changed direction of magnetization in recording of the diffraction grating in a single period.

The angle of rotation of the direction of polarization of a wave after passage through a binary diffraction grating in the 0th order may be defined as:

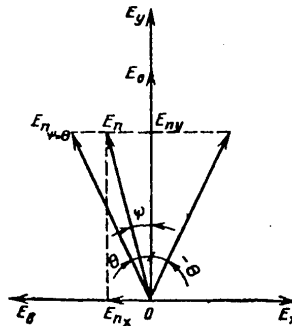$$\mathrm{tg}\,\psi = \frac{E_{nx}}{E_{ny}} = \frac{2s - d}{d}\,\mathrm{tg}\,\theta. \tag{3}$$

Figure 1

The angle psi depends on the shape of the diffraction grating and varies from −θ to +θ. If a symmetrical sirusoidal diffraction grating is recorded on the film, then psi = 0.

Therefore, in holographic investigation of an object in real time, behind the hologram is propagated the reconstructed wave with amplitude E_r, polarized along axis OX; and the object wave, whose direction of polarization forms an angle of 90° − psi with the axis OX. The object beam passing through the hologram generates a high level of noise in the receiver, because only the horizontal component, proportional to sin psi interferes with the reconstructed wave. On the display screen, this appears as a bright image of the object without the superimposed interference pattern, carrying information on the change which has occurred with the object.

Let us define the visibility factor [7] of the interference pattern in real time. Let us designate the amplitude of the reconstructed wave E_r. Then

$$ V = \frac{2E_{\text{в}} \cdot E_{nx}}{E_{\text{в}}^2 + E_n^2} = \frac{2E_{\text{в}} \, |E_n \sin \psi|}{E_{\text{в}}^2 + E_n^2}, \qquad (4) $$

i.e., visibility V is proportional to the quantity sin psi = $\dfrac{2s - d}{d}$ sin θ.

If, for example, a very simple bina y diffraction grating is recorded in the MnBi film, where s = 2/3d; θ = 12°; E_r = E_p, then psi is approximately equal to 4°, and V is approximately equal to 0.07. With this value of visibility, the interference bands are very hard to distinguish.

87

FOR OFFICIAL USE ONLY

But if the plane of polarization of one of the beams (reconstructing or object) is turned, after the hologram is recorded, to match the plane of polarization of the object beam passing through the hologram with that of the beam reconstructed from the hologram, the visibility of the interference pattern becomes equal to unity.

Let us examine another factor which also reduces the visibility of the interference pattern (4). Because of the low diffraction efficiency of holograms recorded on MnBi films, scattering of the reconstructing beam on hetero-geneities of the recording material is a substantial source of noise which greatly exceeds the useful signal in some instances.

But this undesirable effect can easily be eliminated after matching the plane of polarization of the object beam passing through the hologram and the reconstructed wave. If we consider that the plane of polarization of the scattered emission causing the background noise coincides with the plane of polarization of the reconstructing beam, this means that it is perpendicular to the plane of polarization of the reconstructed and object waves passing through the hologram. By installing an analyzer after the hologram, we can reduce the intensity of noise caused by scattering of the reconstructing beam to 1/10 or 1/20 and eliminate its negative effect on the visibility of the interference pattern.

Therefore, the use of the method of holographic interferometry in real time with an optically active recording medium requires the introduction of an additional step: rotation of the plane of polarization of one of the beams to match the plane of polarization of the object beam passing through the hologram to that of the reconstructed beam.

Figure 2 shows an arrangement where it is possible to implement dynamic quality control of objects of interest by real-time holography on MnBi films.

The emission source (wavelength = 1.06 microns) consists of a master oscillator (1), in this case the industrial laser LTIPCh-7 using YAG-Nd^{3+}, operating in the frequency mode; and an amplifier (3) using an active element made of glass and neodymium. When recording the hologram, the first pulse of the master oscillator is amplified. Subsequent laser pulses used to reconstruct the image pass at a frequency of 12.5 or 2.5 Hz through the amplitude along the same optical pathway without amplification.

For real-time holography, it is necessary to have a prism with which the intensity ratio of the reference and object beams could be changed [8]. This is because the optimum ratio of beam intensities is different in producing holograms and reconstructing the wave front. In the diagram, the laser beam is split using an LiNbO$_3$ (2) electrooptical crystal and a birefringent prism (4).

To improve the operation of the polarization prism, an electrooptical crystal 6x4x20 millimeters is placed between the oscillator and amplifier. The one millimeter diameter laser beam is propagated in a very uniform electrical field in the crystal and promotes efficient pumping of the beam's energy from the reference beam into the object beam. The polarization prism employed assures

88

FOR OFFICIAL USE ONLY

a change in the ratio of energies of the reference and object beams within the limits of $1/50 \leq E_{ref}/E_{obj} \leq 50$.

The vertically polarized reference beam is directed by the mirror (5) onto the MnBi film (6). The horizontally polarized object beam is directed into a second electrooptical $LiNbO_3$ crystal (7) which is used to alter the direction of polarization of the beam. The object beam, reflected by the mirror (8) and expanded by the collimator (9), illuminates the diffusely scattering object of interest (10) and strikes the MnBi film (6). The analyzer (11) transmits emission having a horizontal direction of polarization. The reconstructed virtual image of the object of interest and of the object itself, illuminated by the object beam, are projected by the lens (12) onto the input screen of an UM-93 electronic optical transducer. Filters KS-15 and IKS-5 (13) eliminate EOP flare spots by irradiation of the oscillator excitation lamp.

The spot recorded on the MnBi film must be carefully stopped down so that when reconstructing the image, the emission propagating from the object of interest passes only through those sections of film on which the hologram is recorded.

By regulating the voltage on the electrooptical crystal (2) during recording of the hologram, the energy ratio of the reference and object beams is controlled at

$$E_{ref}/E_{obj} = 1/7 \text{ to } 1/20;$$

and in the reconstruction stage
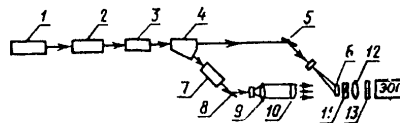
$$E_{ref}/E_{obj} = 30 \text{ to } 50.$$

Figure 2

A change in voltage on the electrooptical crystal (7) ensures vertical polarization of the object beam during hologram recording and rotates the direction of polarization of this beam through an angle psi in the reconstruction mode, i.e., it provides the greatest visiblity of interference patterns in real time on the EOP screen. If the direction of polarization of the object beam is not altered during the reconstruction phase, the interference pattern can not be observed in real time on the EOP screen due to low visibility.

89

FOR OFFICIAL USE ONLY

This arrangement also makes it possible to realize the popular method of dual-exposure holography on MnBi films. For real-time quality control of elements, the method of shift holography with strips of finite width was used [1] according to which in the reconstruction mode, the object of interest is shifted and the object beam striking the object is rotated through a small angle in the plane perpendicular to the direction of shift. Dynamic quality control of optical elements, lenses, plane parallel plates, etc. made of silicon, IKS-24 glass and GaAs, was carried out using this arrangement; these substances are opaque in the visible region of the spectrum, but are transparent in the near-IR. The interferogram contains information on the irregular distortions of the wavefront emanating from the material of the object of interest. Qualitative assessment of phase distortions of optical elements, which generally emit plane or spherical wavefronts, may be implemented immediately after obtaining the interferogram, without computer processing [1].

This method of real-time holography using MnBi films makes it possible to dynamically obtain interferograms of objects of interest in a form convenient for analysis. It can be used for dynamic diagnosis and non-destructive testing of phase objects and materials (especially ISK glass, semiconductors of Si, GaAs, etc.) which are transparent in the near-IR region.

<div align="center">References</div>

1. Gnatyuk, L.N. et al. IZMERITEL'NAYA TEKHNIKA No 7 1975.

2. Abakumov, B.M. et al., KVANOVAYA ELEKTRONIKA No 7 1975.

3. Abakumov, B.M. et al., IZMERITEL'NAYA TEKHNIKA No 6 1977.

4. Merrich, R.S., APPL. PHYS. LETT. Vol 15 1979

5. Haskall, H.M., IEEE TRANSACTIONS ON MAGNETICS Vol 6 No 3 1970.

6. Kitovich, V.V., Magnity i magnitoopticheskiye operativnyye zapominayu-chiye ustroystvr [Magnets and magnetooptical dynamic memories], Moscow, "Energiya" 1975.

7. Landsberg, G.S., Optika [Optics], Moscow, "Nauka" 1976.

8. Kol'yer, R. et la., Opticheskaya golografiya [Optical holography], Moscow, "Mir" 1973.

COPYRIGHT: Izdatel'stvo standartov, 1980
[12-8617]

8617
CSO: 1860

POTENTIAL DIRECTION-FINDING ACCURACY OF TRACKING GONIOMETERS USING
AMPLITUDE AND PHASE TECHNIQUES

[Article by B. S. Rybakov]

[Text] Based on the general theory of radar measure-
ments an investigation is made of the potential ac-
curacies with which tracking goniometers of amplitude
and phase type determine the bearing of signal emission
sources with space-time distortions in the presence of
white noise.

The potential accuracy of direction finding by tracking goniometers using
amplitude and phase methods of instantaneous signal comparison was in-
vestigated in Ref. 1. The signals in the different channels of the
goniometer were taken as completely correlated (harmonious fluctuations)
and consequently the synthesis and analysis of the goniometers took into
consideration only the time fluctuations of the input waveforms and noise.
The present paper generalizes the results of Ref. 1 to the case where the
signal at the reception point has a random space-time structure. For the
sake of simplicity, the study was done on two-channel goniometers.

The aggregate of signals at the output of the antennas forms a two-
dimenisonal normal process characterized by a matrix of correlation func-
tions with elements

$$R_{ij}(t_1, t_2, \alpha) = \sqrt{P_{ci}P_{cj}}\rho_{ij}(t_2 - t_1)\,\mathrm{Re}\,U_i(t_1, \alpha)\,U_j^*(t_2, \alpha) \times$$

$$\times u(t_1)u^*(t_2)\exp[j\omega(t_2 - t_1)] + \delta_{ij}\sqrt{N_{0i}N_{0j}}\delta(t_2 - t_1).$$

Here and below we retain the notation of Ref. 1: P_{ci} -- average signal
power; N_{0i} -- spectral noise density; δ_{ij} -- Kronecker delta; $U_i(t,\alpha) =$
$U_{ai}(t,\alpha)\exp[j\phi_i(t,\alpha)]$ -- complex directional pattern of the goniometer
antenna; $u(t) = u_a(t)\exp[j\phi(t)]$, $u_a(t)$, $\phi(t)$ -- laws of amplitude and
phase modulation of the signal; $\delta(t_2 - t_1)$ -- delta function; ω -- carrier

frequency; $\rho_{ij}(t_2 - t_1)$ -- autocorrelation and crosscorrelation functions of quadrature components of the signals, i, j = 1, 2; $\tau = t_2 - t_1$ -- time separation; α -- true bearing, the value $\alpha = 0$ corresponding to the equi-signal direction.

The potential accuracy of angle measurement for direction finders of this type, according to Ref. 1, can be characterized by spectral density

$$S_{opt} = \Delta t \left[-\frac{1}{2} \int_{t-\Delta t}^{t} \int_{t-\Delta t}^{t} \sum_{i,j=1}^{2} \frac{\partial W_{ij}(t_1, t_2)}{\partial \alpha} \frac{\partial R_{ij}(t_1, t_2)}{\partial \alpha} dt_1 dt_2 \right]_{/\alpha=0}^{-1} \tag{1}$$

$$\text{where } W_{ij}(t_1, t_2) = \frac{\sqrt{P_{ci}P_{cj}}}{N_{0i}N_{0j}} v_{ij}(t_1, t_2) \operatorname{Re} U_i(t_1, \alpha) U_j^*(t_2, \alpha) \times$$

$$\times u(t_1) u^*(t_2) + \frac{\delta_{ij}}{N_{0i}N_{0j}} \delta(t_1, t_2)$$

are elements of the matrix of so-called backward correlation functions that satisfy integral equation 10.3.9 [Ref. 1]. By analogy with Ref. 1, it is also assumed here that the range of integration $[t - \Delta t, t]$ is considerably greater than the time of correlation of signal fluctuations, but for time Δt that the angular coordinate α of the target can be taken as constant.

Generalizing the results of Ref. 1, by calculating the slowly varying functions $v_{ij}(t_1, t_0)$ and their derivatives $v_{ij}'(t_1, t_2)$ at $\alpha = 0$, we easily get from (1):

a) for the phase method (ΦMC)

$$S_{opt}^{\Phi MC} = \frac{2\pi}{\left(\frac{\pi D}{\lambda}\right)^2 h_\Sigma^2} \left[\int_{-\infty}^{\infty} \frac{k S_{12} S_{2}^* i\omega}{(1 + h S_{11})(1 + h S_{22}) - h^2 k S_{12} S_{21}^*} \right]^{-1} ; \tag{2}$$

b) for the amplitude method (AMC)

$$S_{opt}^{AMC} = \frac{2\pi}{\mu^2 h_\Sigma^2} [B_{12} + B_{21}]^{-1}, \tag{3}$$

$$\text{where } B_{12} = \int_{-\infty}^{\infty} \frac{S_{11}^2 (1 + h S_{11})^2 - h^2 k S_{11} S_{12} \times S_{12} S_{21}^*}{(1 + h S_{11})(1 + h S_{22}) - h^2 k S_{12} S_{21}^*} d\omega, \tag{4}$$

D is the spatial separation of the antennas; λ is wavelength; μ is the slope of the direction-finding characteristic with angular separation of antennas; $h_i = P_{ci}/2\Delta f_{ii}N_{0i}$ is the signal-to-noise ratio in the i-th

FOR OFFICIAL USE ONLY

channel, $h_\Sigma = h_1 + h_2$, $h_1 = h_2 = h$; Δf_{ii} is the band of the energy spectrum $S_{ii}(\omega)$ of time fluctuations of the signal; $S_{ij}(\omega)$ are the mutual energy spectra of signal with band Δf_{ij}; the expression for B_{21} is derived from (4) by reversing subscripts. For the sake of brevity, the symbol ω has been omitted in writing the $S_{ij}(\omega)$ in (2) and (4). The spectra have been normalized so that $S_{ij}(0) = 1$ when i, $j = 1$, 2, and consequently

$$\Delta f_{ij} = 1/\int_{-\infty}^{\infty} \rho_{ij}(\tau)\, d\tau, \text{ with } \rho_{ii}(0) = 1; \; k = \Delta f_{11}\Delta f_{22}/\Delta f_{12}\Delta f_{21}.$$

Let us assume that the space-time correlation function of the signal is factorized, i. e. that it is represented as a product of correlation functions with respect to separate variables:

$$\rho(D, \tau) = \rho(D)\, \rho(\tau). \tag{5}$$

Relations (2), (3) with consideration of (5) are transformed to

$$S_{opt}^{\Phi MC} = \frac{2\pi}{\left(\frac{\pi D}{\lambda}\right)^2 h_\Sigma^2} \left[\int_{-\infty}^{\infty} \frac{\rho^2(D)\, S^2(\omega)}{1 + h_\Sigma S(\omega) + h^2\{1 - \rho^2(D)\}S^2(\omega)}\, d\omega \right]^{-1}, \tag{6}$$

$$S_{opt}^{AMC} = \frac{2\pi}{\mu^2 h_\Sigma^2} \left[\int_{-\infty}^{\infty} \frac{S^2(\omega)}{1 + h_\Sigma S(\omega) + h^2\{1 - \rho^2(\mu)\}S^2(\omega)}\, d\omega \right]^{-1}, \tag{7}$$

where $\rho(D)$, $\rho(\mu)$ are the correlation coefficient and the quadrature component coefficient of the signal respectively for spatial and angular separation. Assumption (5) is not stringent, and is applicable to a broad class of propagation channels.

In the special case of completely correlated signals $\rho(D) = \rho(\mu) = 1$, relations (6), (7) are reduced to the results [Ref. 1]:

$$\mu^2 S_{opt}^{AMC} = \left(\frac{\pi D}{\lambda}\right)^2 S_{opt}^{\Phi MC} = \frac{2\pi}{h_\Sigma^2} \left| \int_{-\infty}^{\infty} \frac{S^2(\omega)}{1 + h_\Sigma S(\omega)}\, d\omega \right|^{-1}.$$

In another special case of independent signal fluctuations, we have from (6), (7):

$$\lim_{\rho(D) \to 0} S_{opt}^{\Phi MC} \to \infty$$

$$\lim_{\rho(\mu) \to 0} S_{opt}^{AMC} = \frac{2\pi}{\mu^2 h_\Sigma^2} \left[\int_{-\infty}^{\infty} \frac{S^2(\omega)}{[1 + hS(\omega)]^2}\, d\omega \right]^{-1}. \tag{8}$$

The unbounded increase in $S_{opt}^{\Phi MC}$ as $\rho(D) \to 0$ means that it is impossible to take a bearing on a source of emission that sets up a spatially uncorrelated field. From the physical standpoint, this can be attributed to the fact that the distribution of phase difference of signals at the output of the spaced antennas will be uniform in this case, and hence the readout of the bearing will be uncertain. In direction finding by the amplitude method, as can be seen from (8), S_{opt}^{AMC} is finite since the bearing can be tracked with respect to the ratio of powers of signal fluctuations in each of the channels.

Relations (6), (7) contain uncomputed integrals. Quantitative evaluations can be made by introducing specific approximations of the spectrum of time fluctuations $S(\omega)$. We will restrict ourselves to the exponential form of $\rho(\tau)$ for which

$$S_{opt}^{\Phi MC} = \frac{1}{\left(\frac{\pi D}{\lambda}\right)^2 \Delta f h_\Sigma^2}\left[\frac{\rho_0^2}{\sqrt{(1+h)^2 - \rho_0^2 h^2}\,\{\sqrt{(1+h(1+\rho_0)} - \sqrt{1-h(1-\rho_0)})\}}\right]^{-1}, \quad (9)$$

$$S_{opt}^{AMC} = \frac{1}{\mu^2 \Delta f h_\Sigma^2}\left[\frac{1}{\sqrt{(1+h)^2 - \rho_0^2 h^2}\,\{\sqrt{1+h(1+\rho_0)} - \sqrt{1-h(1-\rho_0)}\}}\right]^{-1}. \quad (10)$$

In expressions (9), (10) for the sake of brevity $\rho(D) = \rho(\mu)$ are replaced by ρ_0. The results of calculations from (9), (10) are shown in Fig. 1, a and b respectively.
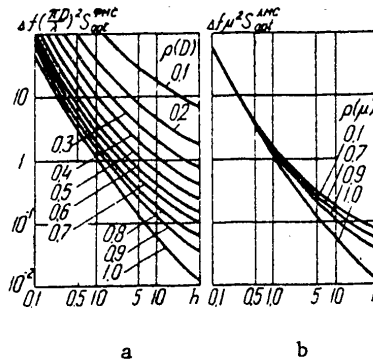

a   b

Fig. 1

It was concluded by a comparative analysis in Ref. 1 that the potential accuracy of the phase method is the same as that of the amplitude method if the overall powers in both cases are the same, and if $\mu = \pi D/\lambda$. However

94

this conclusion remains valid only in the case of completely correlated signals (Fig. 1, a and b). In the case of signals partly correlated in space, comparison of these methods entails difficulties in connection with the fact that the relation between $\rho(D)$ and $\rho(\mu)$ remains unclear unless the type of antenna system is assigned when $\mu = \pi D/\lambda$.

Let us restrict ourselves to examination of the case of linear apertures. Fig. 2, a and b show the results of calculation of the correlation coefficients of quadrature components ρ_0 for spatial and angular separation respectively. In view of the single-valued relation between ρ_0 and the correlation coefficient of envelopes K_E that has frequently been measured in experiments, these figures carry the scale for K_E on the left
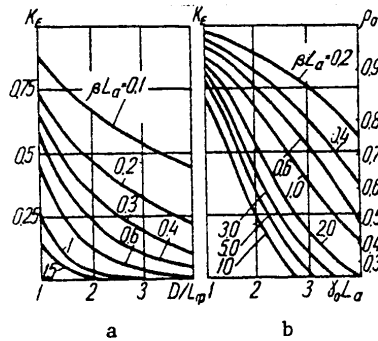

a   b

Fig. 2

and the scale for ρ_0 on the right. The calculations were done in accordance with Ref. 3, assuming that the field is normal, uniform with correlation function in the plane of the apertures of the reception antennas: $B_c(\Delta x) = \sigma_c \exp(-\beta|\Delta x| + j\gamma\Delta x)$. Here $\beta = 1/d_0$, d_0 is the radius of spatial correlation of the field; $\gamma = 2\pi l/\lambda$, $l = \sin\alpha$, α is the angle of arrival; Δx is the spatial separation; D/L_ϕ is the spatial separation with respect to aperture length L_ϕ; $\gamma_0 L_a = 2\pi(L_a/\lambda)\sin\alpha_0$, α_0 is the angle of folding of the directional pattern of the antenna from the normal to the aperture. The angle of arrival α was assumed to be coincident with the equisignal direction of the antenna systems $\alpha = 0$. To ensure the conditions under which the direction finding methods were compared in Ref. 1, we set $D/L_\phi = 1$, $D = L_\phi$, $L_a = 2L_\phi$, $\gamma_0 L_a = \pi$ (corresponding to the optimum level for intersection of directional patterns with respect to voltage [Ref. 3]). As we can readily see, on Fig. 2, a and b, the correlation coefficients of the quadrature components for angle and space separation can be assumed to be practically the same.

Thus, other things being equal, the amplitude method as compared with the phase method realizes a smaller or equal (in the case of completely correlated signals) direction-finding error. A similar conclusion was drawn from analysis of direction-finding errors in Ref. 3 with consideration of only the spatial distortions of the field (instantaneous readout of the bearing).

95

The amplitude and phase methods of direction finding can be compared for other parameters of antenna systems in each specific case from the results of calculations of Fig. 1 and 2.

REFERENCES

1. G. P. Tartakovskiy (general editor), "Voprosy statisticheskoy teorii radiolokatsii" [Problems of the Statistical Theory of Radar], Moscow, Sovetskoye radio, Vol 2, 1964.

2. D. D. Klovskiy, V. A. Soyfer, "Obrabotka prostranstvenno-vremennykh signalov" [Space-Time Signal Processing], Moscow, Svyaz', 1967.

3. N. P. Krasnenko, B. S. Rybakov, "Potential Accuracy of Direction Finding by Monopulse Methods," IZVESTIYA VUZov: RADIOELEKTRONIKA, Vol 18, No 4, 1975, p 30.

6610
CSO: 1860

YU. B. KOBZAREV AWARDED A. S. POPOV GOLD MEDAL

Moscow VESTNIK AKADEMII NAUK SSSR in Russian No 8, 1980 p 134

[Article: "The Gold Medal imeni A. S. Popov to Yu. B. Kobzarev"]

[Text] The Presidium of the USSR Academy of Sciences
has awarded the gold medal imeni A. S. Popov for 1980
to Academician Yuriy Borisivich Kobzarev for basic work
in the area of theoretical radio engineering, radio
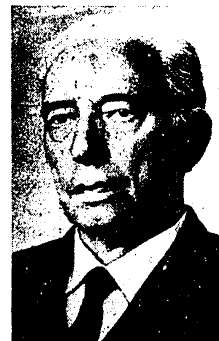physics and radar.

Academician Kobzarev is one of the most important
scientists in the area of radio engineering and radio
physics and the founder of the Soviet school of
specialists in radar and interference resistance in
radio equipment.

He developed the quasi-linear oscillation theory which
permitted the processes of oscillation generation and
transformation to be efficiently described for a broad
class of radio engineering devices and which opened new
paths to the solution of problems of frequency stabilization
in electron generators.

Yu. B. Kobzarev developed the scientific bases for radar technology and a number
of effective methods for detecting and determining the coordinates of aircraft
using radar. An experimental model for a radar station, on the basis of which
the first industrial models of radar stations were produced for the PVO [Anti-
aircraft Defense] system for aircraft detection, was created under his direction.

Kobzarev developed a number of principles and devices to improve the interference
resistance of radar systems.

The development of a statistical theory for detecting radar signals in noise
and methods for synthesizing optimal and sub-optimal devices for isolating the
signals being sought from all interference, as well as the development of new
trends in the study of fluctuations in the earth's electromagnetic field on a
global scale and in research on the natural environment using radio physics
methods are among the most important services of Yu. B. Kobzarev.

FOR OFFICIAL USE ONLY

The work of Yu. B. Kobzarev has played a substantial role in the development of radio engineering, radio physics and radar.

COPYRIGHT: Izdatel'stvo "Nauka," "Vestnik Akademii nauk SSSR," 1980
[307-9194]

9194
CSO: 1860

A. V. RZHANOV AWARDED ORDER OF LENIN

Moscow VESTNIK AKADEMII NAUK SSSR in Russian No 8, 1980 p 133

[Article: "Corresponding Member of USSR Academy of Sciences A. V. Rzhanov is 60 Years Old"]

[Text]

Corresponding Member of the USSR Academy of Sciences Anatoliy Vasil'yevich Rzhanov was awarded the Order of Lenin for great service in the development of science, preparation of scientific cadres and in connection with his 60th birthday by order of the Presidium of the USSR Supreme Soviet 8 Apr 80.

A. V. Rzhanov is a scientist known in the area of semiconductor physics and semiconductor electronics.

He has been engaged in the study of important theoretical and experimental problems since his first years of his work at the Institute of Physics imeni P. N. Lebedev of the USSR Academy of Sciences. Models for transistors have been developed by Rzhanov, recombination processes in semiconductors have been studied and their surface properties have been investigated. Rzhanov has devoted much effort and energy to the development of science in Siberia, being the permanent director of the Institute of Semiconductor Physics, Siberian Branch of the USSR Academy of Sciences for almost 2 decades. Under his direction, research in the areas of the physics of semiconductor surfaces, ellipsometric inspection methods, optical electronics and molecular epitaxy are successfully being developed at the Institute.

FOR OFFICIAL USE ONLY

The active scientific-organizational work of Rzhanov as director of the Institute
and mem er of the Presidium of the Siberian Branch of the USSR Academy of Sciences
promotes improvement in the effectiveness of scientific research and the resolution
of important national economic problems.

In a salutory address to the celebrant, the Presidium of the USSR Academy of
Sciences wished him health and new successes to the good of Soviet science.

COPYRIGHT: Izdatel'stvo "Nauka," "Vestnik Akademii nauk SSSR," 1980
[307-9194]

9194
CSO: 1860

- END -

100

FOR OFFICIAL USE ONLY